Pyrazole and Pyrazolyl Copper and Zinc Complexes in Ring Opening Polymerization of ε-Caprolactone and D,L-Lactide

By

DIVAMBAL APPAVOO

Submitted in fulfillment of the requirements for the degree

MASTER OF SCIENCE

in

CHEMISTRY

at the

UNIVERSITY OF JOHANNESBURG

MAY 2011

SUPERVISOR: PROFESSOR JAMES DARKWA

DEDICATION

Dedicated to my mom Anjeela Rookmani Appavoo

ABSTRACT

Six pyrazole and pyrazolyl compounds, 3,5-dimethylpyrazole (**L1**), 3,5-diphenylpyrazole (**L2**), 3,5-di-*tert*-butylpyrazole (**L3**), bis(3,5-dimethylpyrazol-1-yl)methane (**L4**), bis(3,5-diphenylpyrazol-1-yl)methane (**L5**) and bis(1,2-bis{(3,5-dimethylpyrazol-1-yl)methyl}benzene (**L6**), were reacted with Zn(II) and Cu(II) benzoates to form pyrazole and pyrazolyl metal benzoates. The complexes are $[Zn(C_6H_5COO)_2(\mathbf{L1})_2]$ (**1**), $[Zn(3,5\text{-}NO_2\text{-}C_6H_3COO)_2(\mathbf{L1})_2]$ (**2**), $[Zn(4\text{-}OH\text{-}C_6H_4COO)_2(\mathbf{L1})_2]$ (**3**), $[Zn(2\text{-}Cl\text{-}C_6H_4COO)_2(\mathbf{L1})_2]$ (**4**), $[Zn(C_6H_5COO)_2(\mathbf{L2})_2]$ (**5**), $[Zn(3,5\text{-}NO_2\text{-}C_6H_3COO)_2(\mathbf{L2})_2]$ (**6**), $[Zn(4\text{-}OH\text{-}C_6H_4COO)_2(\mathbf{L2})_2]$ (**7**), $[Zn(2\text{-}Cl\text{-}C_6H_4COO)_2(\mathbf{L2})_2]$ (**8**), $[Zn(3,5\text{-}NO_2\text{-}C_6H_3COO)_2\mathbf{L4}]$ (**9**), $[Zn(4\text{-}OH\text{-}C_6H_4COO)_2\mathbf{L6}]$ (**10**), $[Zn_2(C_6H_5COO)_4\mathbf{L6}]_n$ (**11**), $[Zn(3,5\text{-}NO_2\text{-}C_6H_3COO)_2\mathbf{L6}]$ (**12**), $[Zn(2\text{-}Cl\text{-}C_6H_4COO)_2\mathbf{L6}]$ (**13**), $[Cu(C_6H_5COO)_2(\mathbf{L1})_2]$ (**14**), $[Cu(3,5\text{-}NO_2\text{-}C_6H_3COO)_2(\mathbf{L1})_2]$ (**15**), $[Cu(4\text{-}OH\text{-}C_6H_4COO)_2(\mathbf{L1})_2]$ (**16**), $[Cu(2\text{-}Cl\text{-}C_6H_4COO)_2(\mathbf{L1})_2]$ (**17**), $[Cu(C_6H_5COO)_2(C_6H_5COOH)]_2$ (**18**), $[Cu(2\text{-}Cl\text{-}C_6H_4COO)_2(\mathbf{L3})_2]$ (**19**), $[Cu(C_6H_5COO)_2\mathbf{L4}]$ (**20**), $[Cu(2\text{-}Cl\text{-}C_6H_4COO)_2\mathbf{L4}]$ (**21**), $[Cu(C_6H_5COO)_2DMSO]_2$ (**22**), $[Cu(C_6H_5COO)_2\mathbf{L6}]_2$ (**23**), $[Cu(2\text{-}Cl\text{-}C_6H_4COO)_2\mathbf{L6}]_{2n}$ (**24**), $[Cu(4\text{-}OH\text{-}C_6H_4COO)_2\mathbf{L6}]_2$ (**25**) and $[Cu(3,5\text{-}NO_2\text{-}C_6H_3COO)_2\mathbf{L6}]_n$ (**26**). The molecular structures of the Zn(II) and Cu(II) complexes **6**, **9**, **11**, **14**, **17**-**19**, **22**-**26** were determined by X-ray diffraction studies that revealed four types of geometries adopted by these complexes: (i) 4-coordinate tetrahedral (**6**, **9**, **14**), (ii) 6-coordinate octahedral (**17**), (iii) paddle wheel (**18**, **19**, **22**, **23**, **25**) and (iv) polymeric structures (**11**, **24**, **26**). Catalysis studies performed with selected complexes (**1**-**4**, **9**-**17**, **23**-**26**) revealed that they initiate the ring opening polymerization (ROP) of ε-caprolactone (ε-CL) and D,L-lactide at elevated temperatures, and under solvent-free conditions and in toluene respectively. Polycaprolactone (PCL) and poly(D,L-lactide) (PLA) produced were of moderate molecular weights (858-4 757 Da for PCL and 602-3 185 Da for PLA) and polydispersity indices (1.36-2.16 for PCL and 1.42-2.35 for PLA). End group of the

polymers, determined by MALDI-TOF MS, were benzoates, hydroxyl, methoxy groups and cyclic. From the $^{13}C\{^{1}H\}$ NMR spectra of polymers synthesized, the stereochemistry of PLA was predominantly isotactic.

TABLE OF CONTENTS

LIST OF FIGURES

LIST OF TABLES

LIST OF SCHEMES

ABBREVIATIONS

PLA	Polylactide
PCL	Polycaprolactone
ROP	Ring opening polymerization
ε-CL	ε-Caprolactone
M_n	Number molecular weight
M_w	Weight molecular weight
PDI	Polydispersity index
[M]/[I]	[Monomer]/[Initiator]
DP_n	Degree of polymerization
IR	Infra red
NMR	Nuclear magnetic resonance
SEC	Size exclusion chromatography
MALDI-TOF	Matrix-Assisted Laser Desorption Ionization Time-of-Flight
ESI-MS	Electrospray ionization mass spectrometry
Pz	Pyrazole
μ_{eff}	Effective magnetic moment
$CDCl_3$	Deuterated chloroform
DMSO	Deuterated dimethylsulphoxide
J	Coupling constant
k_{app}	Apparent rate constant
Me	Methyl
Et	Ethyl
Bz	Benzoate

Ph	Phenyl
Pz	Pyrazole or pyrazolyl
^{t}Bu	Tertiary butyl
^{i}Pr	Isopropyl
Mr	Molecular weight
M	Molecular ion
s	Singlet
d	Doublet
t	Triplet
b	Broad
m/z	mass/charge
DSC	Differential scanning calorimetry
TGA	Thermogravimetric analysis

ACKNOWLEDGEMENTS

I would like to thank the following people without whom the work in this dissertation would not have been achieved. Firstly my sincere appreciation and gratitude goes to my supervisor Professor James Darkwa for his professional guidance throughout this research work. I also wish to thank Dr Archana Bhaw-Luximon (University of Mauritius) and Prof Selwyn Mapolie (University of Stellenbosch) for their professional input and advice on the work. Dr Ilia Guzei (University of Wisconsin) and Dr Bernard Owaga (University of Johannesburg) are greatly thanked for their services in the X-ray molecular structural elucidation of the compounds described in this work that proved very useful in understanding the coordination chemistry of the compounds. I am grateful to Dr Marietjie Stander (University of Stellenbosch) for MS analysis, Dr Edith Antunes (Rhodes University) for elemental analysis and Prof Fumio Sanda (Kyoto University), Prof Kyoko Nozaki (University of Tokyo) and Prof Ravin Narrain (University of Alberta) for SEC and MALDI-TOF MS analysis of samples. My gratitude also goes to the Chemistry department and the entire University of Johannesburg community for providing a friendly environment fundamental for this research work. I feel highly indebted to my Dr Juanita van Wyk, Dr Bernard Owaga and Dr Stephen Ojwach for their advice throughout this project. I wish to express my appreciation to my friends and colleagues, who helped with advice, smoothed my path during this research with their good humour and with whom I spent cherished moments. I am particularly grateful to Khuphukile Sithole and Afag Elkhadir for their constant support. I want to thank my mom, dad and sister for their constant encouragement. Last but least, I thank the Lord for His spiritual protection and guidance throughout the dissertation.

INTRODUCTION

Biodegradable polymers are synthetic polymers that have excellent water resistance and at the same time are biodegradable (like most natural polymers). This unique combination of properties makes biodegradable polymers ideal ingredients in the development of a variety of products for use in manufacturing, household and medical applications. Examples of such polymers include polycaprolactone (PCL) and polylactide (PLA). PCL is a tough, aliphatic semicrystalline thermoplastic polyester with low tensile strength[1] but an extremely high elongation at breakage (4 700%). PCL displays the rare property of being miscible with many other polymers and is mechanically compatible with others. Polylactide (PLA) is also a crystalline polymer, with good tensile strength, low extension and a high modulus and hence has been considered an ideal biomaterial for load bearing applications.[2] PLA is a versatile aliphatic polymer having good mechanical properties, hydrolyzability, and biocompatibility and is synthesized from agricultural-based renewable sources like starch-containing resources. PLA is attractive in the long term as degradable substitutes for petrochemical-based materials. Hence, the commercial production of poly(lactide) has recently been scaled-up for a variety of film and fibre applications.[3] Their good mechanical properties, hydrolyzability, biodegradability, biocompatibility, and permeable properties that make them a leading candidate in several industries including: (i) biomedical as orthopaedic fixation devices (screws, plates, rods, and pins), wound closure (resorbable sutures and surgical staples), wound dressing (artificial skin), prosthetics, dental implants, vascular grafts, stents,

[1] Kamber, N. E.; Jeong, W.; Gonzalez, W.; Hedrick, J. L.; Waymouth, R. M. *Macromolecules* **2009**, *42*, 1634.

[2] Nair, L. S.; Laurencin, C. T. *Prog. Polym. Sci*. **2007**, *32*, 762.

[3] Darensbourg, D. J.; Choi, W.; Karroonnirun, O.; Bhuvanesh, N. *Macromolecules* **2008**, *41*, 3493.

and erodible polymer vehicles for controlled drug delivery[4,5] and (ii) agricultural and packaging (trash bags, wrapping and food containers). Cargill has developed processes that use corn and other feedstock to produce different PLA grades (NatureWorks®). For this company, the actual production is estimated to 50–60 Ktons per year although the production capacity is given at 140 Ktons.[6]

Many research groups around the world are working on the development of an efficient system that can initiate the polymerization of the cyclic monomers to the polyesters. Consequently, many systems, including enzymatic,[7] organic compounds,[8] inorganic acids[9] and most importantly metal complexes.[10] This system comprises of complexes of almost all the metals on the periodic table. Compounds that have been employed as ligand for this system are numerous. Among the list of complexes used as initiator for the polymerization of lactides and ε-caprolactone, two compounds stand out: aluminium isopropoxide [$Al(O^iPr)_3$], and tin octanoate, [$Sn(Oct)_2$]. These compounds have been used extensively as initiators because they have shown many advantages over the other complexes. Yet, there are some drawbacks associated with these initiators as well, and as a means of overcoming these problems, research continues in finding the best initiator system that is highly active, cheap, non-toxic, biocompatible and that produces polyesters of high stereoselectivity.[10,11]

[4] Dubois, P.; Jacobs, C.; Jérôme, C.; Teyssié, P. *Macromolecules* **1991**, *24*, 2266.

[5] Albertsson, A. C.; Varma, I. K. *Biomacromolecules* **2003**, *4*, 1466.

[6] Bordes, P.; Pollet, E.; Avérous, L. *Prog. Polym. Sci.* **2009**, *34*, 125.

[7] Nobes, G. A. R.; Kazlauskas, R. J.; Marchessault, R. H. *Macromolecules* **1996**, *29*, 4829.

[8] Pratt, R. C.; Lohmeijer, B. G. G.; Long, D. A.; Waymouth, R. M.; Hedrick, J. L. *J. Am. Chem. Soc.* **2006**, *128*, 4556.

[9] Chuma, A.; Horn, H. W.; Swope, W. C.; Pratt, R. C.; Zhang, L.; Lohmeijer, B. G. G.; Wade, C. G.; Waymouth, R. M.; Hedrick, J. L.; Rice, J. E. *J. Am. Chem. Soc*. **2008**, *130*, 6749.

[10] Labet, M.; Thielemans, W. *Chem. Soc. Rev*. **2009**, *38*, 3484.

[11] Platel, R. H.; Hodgson, L. M.; Williams, C. K. *Polym. Rev*. **2008**, *48*, 11.

CHAPTER 1

LITERATURE REVIEW ON METAL COMPLEXES USED AS INITIATORS FOR POLYMERIZATION OF POLYESTERS AND ON METAL CARBOXYLATES AND PYRAZOLES

1.1 Introduction

As the depletion of petrochemical feedstock continues and carbon dioxide emissions from the formation and disposal of conventional plastics reach epic levels, there is an urgent need to use renewable and environmental friendly polymers.[12] The complete substitution of petroleum-based feedstock for plastics by renewable feedstock would lead to reduced land pollution, since biodegradable polymers won't stay in the environment as long as polyolefins.[13] There is limitless number of sectors where biodegradable polymer materials may find use, such as agriculture, medicine and packaging. Since the extent of biodegradability of a polymer may be tailored to meet specific requirements, each industry is able to create its own ideal materials such as polyhydroxyalkanoates, polyesteramides and polyesters: polycaprolactone (PCL) and polylactide (PLA). These polyesters are synthesized by different methods including polycondensation and ring opening polymerization (ROP) with metal-coordinated catalysts. ROP has been commonly accepted as the most efficient synthetic route for industrial production of polyesters. However, it is ludicrous to expect a full replacement of conventional polymers by their biodegradable counterparts any time soon primarily because the latter is currently more expensive to manufacture than polyolefins.

[12] Wu, J.; Yu, T. L.; Chen, C. T.; Lin, C. C. *Coord. Chem. Rev*. **2006**, *250*, 602.

[13] Kolybaba, M.; Tabil, L. G.; Panigrahi, S.; Crerar, W. J.; Powell, T.; Wang, B. Paper Number: *RRV03-0007*, American Society of Agricultural Engineers (ASAE) Meeting Presentation in **2003** in USA.

Developing catalysts that are effective and inexpensive for producing these biodegradable polymers would aid in reducing costs.

Since the biopolymer, on its own, can be derived from renewable feedstock, such as animal sources (collagen and gelatine), marine sources (chitin) and agricultural feedstock (wheat, corn, rice, beans and potatoes), it has a low cost.[13] Finding a cheap catalytic pathway of manufacturing the biopolymers would cause a marked rise in interest in these materials for use in many areas. Worldwide research efforts to explore effective catalysts for the synthesis of biodegradable polymers are ongoing in various academic and industrial laboratories.[14] The focus of these undertakings is specifically to develop improved methods of producing biodegradable polymers in a controlled manner as a means of tuning their mechanical properties and degradation profiles. The catalyst, also known as the initiator, is the one responsible for the type of polymer formed, in terms of the molecular weight of the polymer and the stereochemistry of polymers with chiral centres. It controls the properties of the polymer at the initiation stage of the polymerization as well as during the chain growth, whereby side reactions might occur. In this respect, all researchers working in this area aim in synthesizing polyesters with controlled architecture and tailor-made properties by careful selection of the initiator.

1.2 Metal complexes used as initiators for lactide and lactone polymerization

Polyesters can be synthesized by two main pathways, namely condensation polymerization and ring opening polymerization (ROP) of cyclic esters. ROP is the preferred synthetic route as it circumvents the disadvantages of the former method, examples of which are high temperatures, long reaction time, low molar mass and side reactions, although, ROP requires

[14] Darensbourg, D. J.; Choi, W.; Karroonnirun, O.; Bhuvanesh, N. *Macromolecules* **2008**, *41*, 3493.

a catalyst. Depending on the catalyst used, ROP proceeds via four different reaction mechanisms. These are: (i) cationic, (ii) anionic, (iii) monomer-activated and (iv) coordination-insertion. Coordination-insertion ROP of lactides and ε-caprolactone have been extensively investigated. A large variety of compounds such as alkyls, oxides, carboxylates and alkoxides of metals are effective initiators for the controlled ring opening of lactones as they synthesized polymers of low molecular weight distribution.[15] The most widely used initiators for polymerization of cyclic esters are various tin[16] and aluminium alkoxides,[17] which are used industrially and more recently rare earth metal compounds,[18] zinc[19] and copper[20] that are used in research. The subsequent sections will provide a brief literature review on the activities of these initiators towards ROP of cyclic esters and the microstructure of synthesized PLA.

1.2.1 Aluminium-based initiators for ROP of lactides and lactones

Aluminium-based initiators are widely investigated for ROP of lactides and ε-caprolactone because good control over the polymerization process is achieved, even though the initiators produced are less active than the catalysts based on other metals like tin.[11] Aluminium(III) triflate, [$Al(OTf)_3$], was found to be a very good catalyst for ε-caprolactone (ε-CL) ROP, giving PCL with molecular weight (M_n) of 18 400 $gmol^{-1}$ and a polydispersity index (PDI) of

[15] Cayuela, J.; Bounor-Legaré, V.; Cassagnau, P.; Michel, A. *Macromolecules* **2006**, *39*, 1338.

[16] (a) Sawhney, A.; Pathak, C. P.; Hubbell, J. A. *Macromolecules* **1993**, *26*, 581. (b) Han, D. K.; Hubbell, J. A. *Macromolecules* **1996**, *29*, 5233.

[17] Duda, A.; Florjanczyk, Z.; Hofman, A.; Slomkowski, S.; Penczek, S. *Macromolecules* **1990**, *23*, 1640.

[18] (a) Li, S. M.; Rashkov, I.; Espartero, L.; Manolova, N.; Vert, M. *Macromolecules* **1996**, *29*, 57. (b) Rashkov, I.; Manolova, N.; Li, S. M.; Espartero, J. L.; Vert, M. *Macromolecules* **1996**, *29*, 50.

[19] Cheng, M.; Attygalle, A. B.; Lobkovsky, E. B.; Coates, G. W. *J. Am. Chem. Soc.* **1999**, *121*, 11583.

[20] John, A.; Katiyar, V.; Pang, K.; Shaikh, M. M.; Nanavati, H.; Ghosh, P. *Polyhedron* **2007**, *26*, 4033.

1.94.[21] However, for the polymerization of lactides, [Al(OTf)$_3$] showed poor polymerization control, producing polymers of broad molecular weight distribution.[22] Furthermore, one of the most studied aluminium-based catalysts, aluminium(III) isopropoxide, which showed promising results for the ROP of lactones, was also found to be active for ROP of lactide, but with very low conversions. An advantage of aluminium-based catalysts in lactide ROP is the high degree of stereocontrol, affording well-controlled polymers in terms of microstructure (syndiotacticity, isotacticity or atacticity). So, in an effort to improve activity while maintaining selectivity, a number of new aluminium catalysts have been investigated. The best known are aluminium alkoxides and aluminium Schiff base compounds.

1.2.1.1 Aluminium isopropoxide initiators

Teyssié[23] and Kricheldorf[24] worked with aluminium alkoxides of the type [$R_{3-n}Al(OR)_n$] (R = alkyl or aryl groups) as initiators for the polymerization of lactides and lactones. Aluminium isopropoxide (n = 3) and dialkyl aluminium alkoxide (n = 1) have been studied, the latter showing reduced activities compared to the former.[25] Kowalski has worked on the mechanism of polymerization with [Al(O^{i}Pr)$_3$][26] and established that the complex exists as a mixture of two different aggregated forms in toluene: trimer (**A$_3$**) and tetramer (**A$_4$**).[27] These species coexist in equilibrium with the tetramer being more stable than the trimer (Scheme 1.1).

[21] Wang, Y.; Kunioka, M. *Macromol. Symp.* **2005**, *224*, 193.

[22] Kunioka, M.; Wang, Y.; Onozawa, S. Y. *Macromol. Symp.* **2005**, *224*, 167.

[23] Dubois, P.; Deghe, P.; Jérôme, R.; Teyssié, P. *Macromolecules* **1992**, *25*, 2614.

[24] Kricheldorf, H. R.; Berl, M.; Scharnagl, N. *Macromolecules* **1988**, *21*, 286.

[25] Ropson, N.; Dubois, P.; Jérôme, R.; Teyssié, P. *Macromolecules* **1995**, *28*, 7589.

[26] Kowalski, A.; Duda, A.; Penczek, S. *Macromolecules* **1998**, *31*, 2114.

[27] Dubois, P.; Ropson, N.; Jérôme, R.; Teyssié, P. *Macromolecules* **1996**, *29*, 1965.

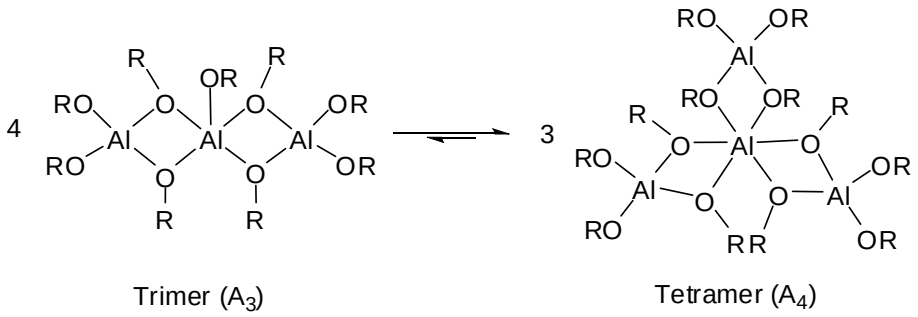

Scheme 1.1. Equilibrium between $[Al_3(OR)_5(\mu\text{-}OR)_4]$ trimer (**A_3**) and $[Al_4(OR)_6(\mu\text{-}OR)_6]$ tetramer (**A_4**) adapted from Ropson.[27]

Their activities differ towards ε-CL and lactides in that all three aluminium alkoxides bonds are active in polymerizing L- and D,L-lactides as compared to only one for ε-CL. It is interesting to note that polymerization of lactide in toluene at 70 ^{o}C using a monomer to initiator ([M]/[I]) ratio of 1 600:1 takes several days to reach completion. Polymerization of the lactides at this temperature starts after an induction period, probably due to the association of the $[Al(O^{i}Pr)_3]$ in solution. The polymerization proceeds via a coordination-insertion mechanism, a general scheme of which is illustrated in Scheme 1.2. Firstly, there is complexation of the carbonyl oxygen of the cyclic ester to the metal in the initiator, followed by insertion of the monomer into the metal-oxygen bond. This involves the cleavage of the acyl-oxygen bond. The dead end of the polymer chain is an ester group, while the active end contains the metal-oxygen bond. The termination step involves hydrolysis of the metal-oxygen bond.

During ROP, both intermolecular and intramolecular transesterifications occur. These side reactions are generally encountered during the later stages of polymerization, particularly at high temperature and results in broadening of the PDI and loss of control of polymerization. In this case, the limited monomer conversion could be due to the occurrence of transesterification reactions; firstly by intramolecular transesterification process, also known

as back-biting that could be the cause of the low conversions. In addition, intramolecular transesterification reactions are responsible for the broadening of the molecular weight distribution and hence for the decrease in the average number molecular weight. Secondly, intermolecular transesterification reaction could be responsible for the increase in PDI with polymerization time.[4]

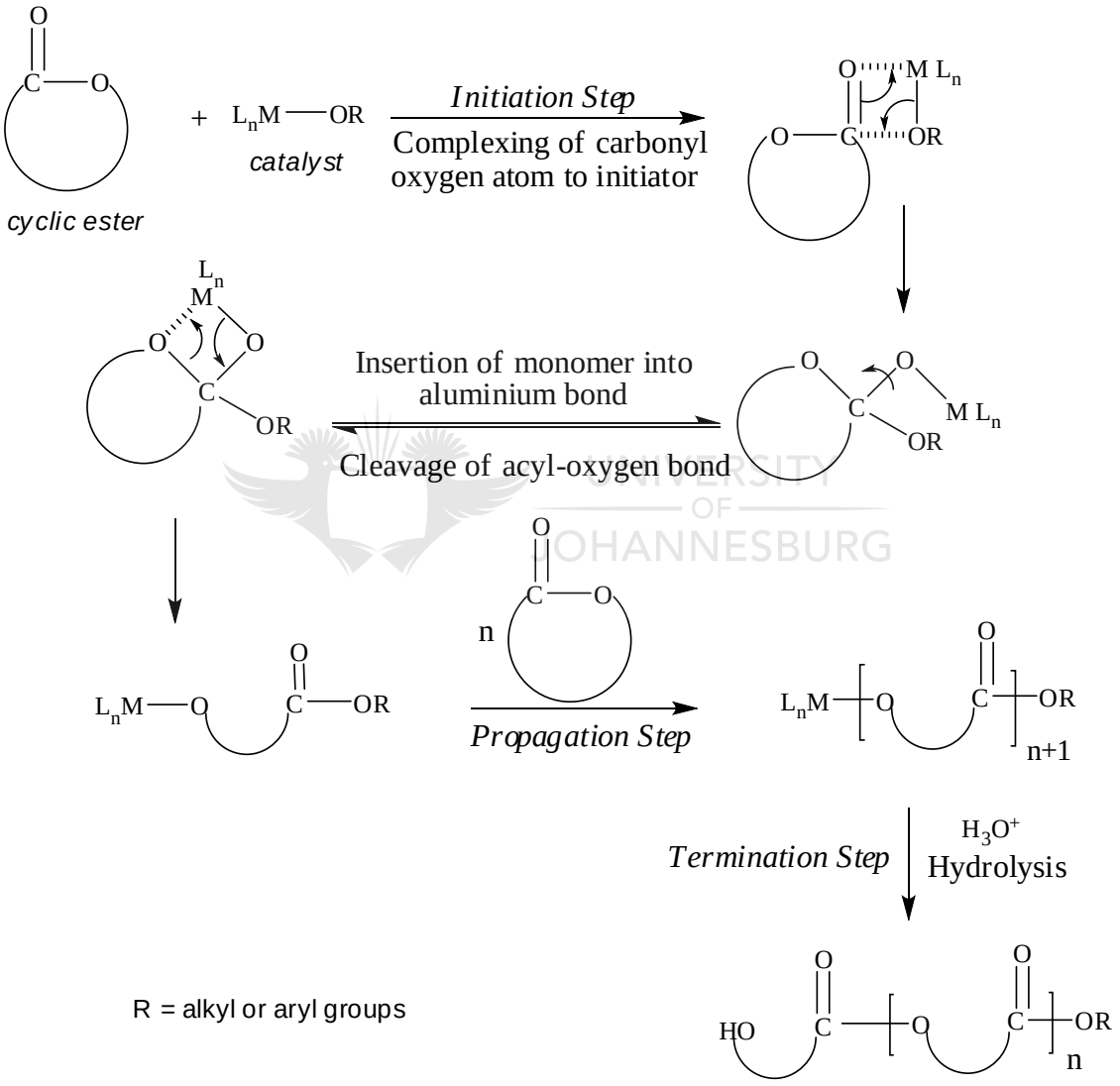

Scheme 1.2. Coordination-insertion mechanism for ROP of a cyclic ester initiated by a metal complex with a metal-oxygen bond.

While lactide ROP require temperatures of 70 ^{o}C to proceed efficiently, [Al($O^{i}Pr$)$_3$] is more reactive towards the ROP of ε-CL, with this polymerization commonly achieved at 0 ^{o}C. When dissolved in ε-CL, **A_3** disaggregates to a single intermediate species, which then forms a single six-coordinated aluminium complex, [Al($O^{i}Pr$)$_3$.3ε-CL],[27] the actual initiator for the ROP of ε-CL.[28] The rate of polymerization is much higher when using [Al($O^{i}Pr$)$_3$.3ε-CL] than the interconversion rate between **A_3** and **A_4**. A consequence of which is the faster and more controlled polymerization using **A_3** compared to **A_4**.[29] Polymerization of ε-CL (7-membered ring) is reported to occur faster than for lactide (6-membered ring). Hence, ε-CL polymerization in toluene at room temperature using a [M[/[I] ratio of 500:1 is 90% complete in 1 h. PCL obtained from this reaction had M_n of 41 800 gmol^{-1} and a PDI of 1.66.[29]

In order to solve the problem of low conversions associated with polymerization of these cyclic esters, lactide in particular, other aluminium compounds were investigated. Among them, aluminium Schiff base complexes are the most extensively studied.

1.2.1.2 Aluminium Schiff base initiators

The most commonly examined heteroleptic aluminium alkoxide initiators are those with Salen ligands, N,N`-bis(salicylidene)ethylenediamine, some of which afford excellent stereocontrol of lactide polymerization. A few examples of the Salen aluminium complexes are illustrated in Figure 1.1.

[28] Ropson, N.; Dubois, P.; Jérôme, R.; Teyssié, P. *Macromolecules* **1993**, *26*, 6378.

[29] Duda, A.; Penczek, S. *Macromolecules* **1995**, *28*, 5981.

Spassky showed that Salen aluminium methoxide complexes initiate controlled polymerization of *rac*-lactide to moderately isotactic PLA in 125 h.[30] Thus, the chiral aluminium complex **1** was used to selectively polymerize *rac*-lactide to give optically active poly(R-lactide) up to 50% conversion.[10] A structurally related complex, **2**, was used by Coates to make other stereoselective PLA. Complex **2** successfully gave syndiotactic PLA from *meso*-lactide, with an enantiotropic selectivity of 96%.[31] With similar objectives, complex **3**, which was produced by the coordination of Jacobsen's ligand to aluminium, was used as initiator for lactide polymerization. The complex showed moderate activity with excellent M_n of 8 600 $gmol^{-1}$ and end-group control.[32]

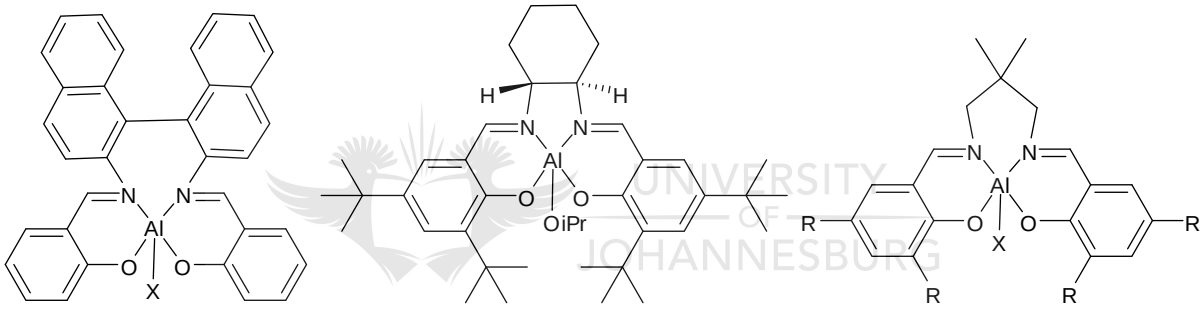

Figure 1.1. Salen aluminium alkoxide initiators used for lactide ROP.[10]

Achiral Salen aluminium complexes were also employed as initiators for lactide polymerization. Good isoselectivity was shown by these complexes in *rac*-lactide polymerization,[33] which was further enhanced by bulky *ortho*-phenoxy substituents, like

[30] Jhurry, D.; Bhaw-Luximon, A.; Spassky, N. *Macromol. Symp*. **2001**, *175*, 67.

[31] Ovitt, T. M.; Coates, G. W. *J. Am. Chem. Soc.* **1999**, *121*, 4072.

[32] Chisholm, M. H.; Patmore, N. J.; Zhou, Z. P. *Chem. Commun*. **2005**, 127.

[33] Du, H.; Pang, X.; Yu, H. Y.; Zhuang, X. L.; Chen, X. S.; Cui, D. M.; Wang, X. H.; Jing, X. B. *Macromolecules* **2007**, *40*, 1904.

initiator **5**. The cause of the enhanced activity was the presence of flexible backbone substituents and the electron withdrawing groups like chlorine, in the *ortho* and *para*-phenoxy positions, like in initiator **4**.[33] It was observed that the backbone on the ligand changes from binaphtyl in **1** and **2** to cyclohexanyl in **3** and a C-3 linker in **4** and **5**. Comparing the initiator system of binaphtyl backbone to the C-3 linker, the activities of **4** and **5** were found to be higher than **1** and **2**, showing that a more flexible backbone leads to improved activity.[34]

Polymerization of ε-CL was also carried out using different aluminium Schiff base complexes, such as [HapenAlO^{i}Pr] (Hapen = N,N`-ethylenebis(*o*-hydroxyacetophenone imine)) and aluminium Salen. Different aluminium Schiff bases have been used by Arbaoui that led to good control of the reaction at low temperatures (25 and 40 ^{o}C), producing PCL with narrow molecular weight distribution.[35] Increasing the temperature, however, resulted in loss of control upon polymerization and slightly broadening in the molecular weight distribution due to transesterification reactions. Control of polymerization could only be maintained at low temperatures, which also implied long polymerization reactions that can take several days for completion. Alternatively, changing the substituents on the two phenyl rings of the ligand of salicylaldimine aluminium complexes resulted in changing activities of the initiator.[36] Bulky substituent on the imine moiety enhanced the polymerization while bulky substituents on the salicylidene moiety seem to slow it down. The most efficient Schiff base reported contained a 2,4,6-tri-*tert*-butylphenylimine moiety and a methyl substituent on

[34] (a) Tang, Z. H.; Chen, X. S.; Pang, X.; Yang, Y. K.; Zhang, Z. F.; Jing, X. B. *Biomacromolecules* **2004**, *5*, 965. (b) Tang, Z. H.; Chen, X. S.; Yang, Y. K.; Pang, X.; Sun, J. R.; Zhang, X. F.; Jing, X. B. *J. Polym. Sci., Polym. Chem.* **2004**, *42*, 5974.

[35] Arbaoui, A.; Redshaw, C.; Hughes, D. L. *Chem. Commun.* **2008**, 4717.

[36] Nomura, N.; Aoyama, T.; Ishii, R.; Kondo, T. *Macromolecules* **2005**, *38*, 5363.

the 3-position of the salicylidene moiety and complete conversion of monomer happened within 2 h.[37]

Despite the good selectivity and good control of polymers obtained by the polymerization of these cyclic esters using aluminium-based catalysts, the major drawback remains their low catalytic activities. Moreover, these aluminium complexes are air sensitive and hence have to be kept under inert atmosphere to prevent their decomposition. To counteract the shortcomings of the aluminium catalysts and produce polymers with high activity, good control and selectivity, other metal complexes were investigated as initiators.

1.2.2 Tin octanoate initiator for ROP of lactides and ε-caprolactone

Stannous(II) ethylhexanoate (or tin octanoate), [$Sn(Oct)_2$], is the most commonly used catalyst in industries for the ROP of cyclic esters. The catalyst is very effective, commercially available, easy to handle and soluble in most commonly used organic solvents.[38] In order to achieve controlled synthesis of the polymer, the tin catalyst must be used together with a nucleophilic compound, which is generally an alcohol. Usually a primary alcohol is used and it not only allows control of the molecular weight, but also accelerates the polymerization process. Among many researchers who worked on the use of [$Sn(Oct)_2$] as initiator for polymerization, Kowalski was able to prove the livingness of the polymerization of ε-CL using this complex by the linear increase the molecular weight as measured by size exclusion chromatography (SEC), with the monomer conversion.[39] The influence of reaction conditions on the rate of polymerization was also studied by the same research group; the observations showed that the concentration of the growing species remains constant throughout the process

[37] Libiszowski, J.; Kowalski, A.; Duda, A.; Penczek, S. *Macromol. Chem. Phys.* **2002**, *203*, 1694.

[38] Möller, M.; Kange, R.; Hedrick, J. L. *J. Polym. Sci., Part A: Polym. Chem*. **2000**, *38*, 2067.

[39] Duda, A.; Penczek, S.; Kowalski, A.; Libiszowski, J. *Macromol. Symp*. **2000**, *153*, 41.

and that adding alcohol (in particular butanol) increases the number of active sites, resulting in higher polymerization rate. During this process, carboxylic acids (hexanoic acid mainly) temporarily convert the growing species into dormant molecules, resulting in a decrease in polymerization rate. The alcohol plays the role of an initiator when it is used in concentrations as much as twice the amount of catalyst. When introduced in excess, the alcohol also plays the role of a transfer agent. However, without the nucleophilic compound, the polymerization is not controlled. In addition to the alcohol, high temperature is required for the optimum activity of tin octanoate. The high temperature in turn encourages intermolecular and intramolecular transesterification reactions leading to the broadening of the polydispersity index of the polymer.[39]

Bhaw-Luximon and co-workers contributed a lot to understanding the effect of solvent on the activity of [$Sn(Oct)_2$] as initiator. Polymerization of ε-CL was carried out in dioxane and toluene at 110 ^oC using tin octanoate-ethanolamine system and it was observed that in dioxane, only 40% conversion is obtained after 42 h and gives a low molecular weight polymer (M_n = 2 400 $gmol^{-1}$). In toluene, complete conversion of monomer to polymer was reached within 24 h, leading to a medium molecular weight polymer (M_n = 5 700 $gmol^{-1}$).[40]

Lactide polymerization using [$Sn(Oct)_2$] with/without alcohol has been studied for more than 20 years and is observed to occur via a coordination-insertion mechanism especially when alcohols are added and at moderate temperature (less than 100 ^oC).[41] When alcohol is omitted, [$Sn(Oct)_2$] produces PLA with high M_n reaching 10^6 $gmol^{-1}$ and attaining completion in about 100 h, but polymerization does not seem to occur by coordination-insertion

[40] Bhaw-Luximon, A.; Jhurry, D.; Motala-Timol, S.; Lochee, Y. *Macromol. Symp*. **2005**, *231*, 60.

[41] Kowalski, A.; Duda, A.; Penczek, S. *Macromolecules* **2000**, *33*, 7359.

mechanism because anhydride PLA end groups are not observed. Furthermore, the polymerization shows a non-linear relationship between the M_n and the $[Sn(Oct)_2]$ concentration.[42] The independence of M_n on $[Sn(Oct)_2]$ has been mentioned in some papers without any conclusive results because $[Sn(Oct)_2]$, if not sufficiently purified, may contain impurities acting as coinitiators.[43] In addition, this initiator system suffers some limitations, an important one being the lack of selectivity of the PLA produced.

Since this tin initiator as well as the previous aluminium systems cannot achieve good stereoselectivity and activity respectively, there was a need to find a system with the important features of selectivity and activity. One system that has been used to address the shortcomings of aluminium and tin initiators are organolanthanides.

1.2.3 Organolanthanide initiators for ROP of lactides and lactones

Lanthanide-based systems are the most recent initiators developed for the polymerization of cyclic esters. Several research teams have used organolanthanide complexes for polymerization of lactides and ε-caprolactone because these complexes display moderate Lewis acidity, good polymerization activity and have no known toxicity.[10] McLain was the first to report the use of yttrium and lanthanide alkoxides for L-lactide polymerization. The complex $[Y(OCH_2CH_2NMe_2)_3]$ proved to be an efficient initiator in CH_2Cl_2 at ambient temperature, reaching complete conversion in 15 min. Molar mass of polymers produced by this yttrium initiator increased linearly with conversion and low polydispersity indices (around 1.2) were exhibited by the polymers.[10]

[42] Kricheldorf, H. R.; Kreiser-Saunders, I.; Stricker, A. *Macromolecules* **2000**, *33*, 702.

[43] Kricheldorf, H. R.; Kreiser-Saunders, I.; Boettcher, C. *Polymer* **1996**, *36*, 1253.

Spassky has also examined a series of lanthanide clusters of general formula $[Ln_5(\mu\text{-}O)(OR)_{13}]$ (R = alkyl or aryl groups), which showed that their activity decreased with the ionic radius of the lanthanide.[10] For example, $[Ln_5(\mu\text{-}O)(O^iPr)_{13}]$ was used for the living ROP of D,L-lactide in CH_2Cl_2 at ambient temperature. The general order of reactivity of these lanthanide initiators was found to be La >> Sm > Y > Yb, which agrees with a decrease of reactivity as the size of the lanthanide atom increases. Polydispersities are also low for the polymers, except when La is used due to transesterification reactions. For all the initiator systems, a linear relation between $\ln[M]_o/[M]_t$ and time was observed, indicating the livingness of these systems.

Rare earth metal-based catalysts are good initiators for ε-CL polymerization as well. An example is triphenyl yttrium that gives high molecular weight of 89 000 $gmol^{-1}$ and yield of 91% conversion after 30 min of bulk polymerization of ε-CL at 100 ^oC. However, rare earth metal phenyl compounds not only catalyze the polymerization of ε-CL but also the decomposition of PCL. Consequently, the polymerization needs to be stopped early enough to prevent the decomposition of the polymer formed.[44] Thus, in general, the rare earth metal-based complexes present good activities towards ROP of lactides and ε-caprolactone but also have limitations. Besides the drawbacks mentioned, another disadvantage is the handling of these complexes as they are air and moisture sensitive. Hence, researchers have to work on finding complexes that can be easily handled and at the same time show good activity and selectivity in polymerization. This search has led to employing zinc complexes as initiators.

[44] Deng, X.; Yuan, M.; Xiong, C.; Li, X. *J. Appl. Polym. Sci.* **1999**, *73*, 1401.

1.2.4 Zinc initiators for ROP of lactides and lactones

Zinc(II) complexes for cyclic ester polymerizations have been motivated largely by advantageous features such as lack of colour, low cost and low toxicity, all of which are important for many applications of the polymers, especially in the biomedical field. One compound that has been used as initiator is zinc oxide which successfully catalyzes the ROP of ε-CL in the ionic liquid ([bmim][BF_4]) under microwave treatment. The combination of ionic liquid and microwave increases the efficiency of the ROP, resulting in polymers with average molecular weight between 2 260 $gmol^{-1}$ and 11 060 $gmol^{-1}$ with PDI between 1.30 and 2.50.[45] On the other hand, when used for lactide ROP, zinc oxide showed slow polymerization and suffered from epimerization.[14]

Diol supported zinc complexes have also been employed as initiators for ROP of lactide. A diol derived zinc complex (Figure 1.2a) was employed as initiator for lactide polymerization, which proceeded up to 90% conversion within 40 h at room temperature, giving polymers with PDI of 1.41. Polymerization using the same initiator was completed in 4 h when the temperature was raised to 80 ^oC, however, the polymer formed had a broader PDI of 2.2.[46]

[45] Liao, L.; Liu, L.; Zhang, C.; Gong, S. *Macromol. Rapid Commun.* **2006**, *27*, 2060.

[46] Chisholm, M. H.; Lin, C. C.; Gallucci, J. C.; Ko B. T. *Dalton Trans.* **2003**, 406.

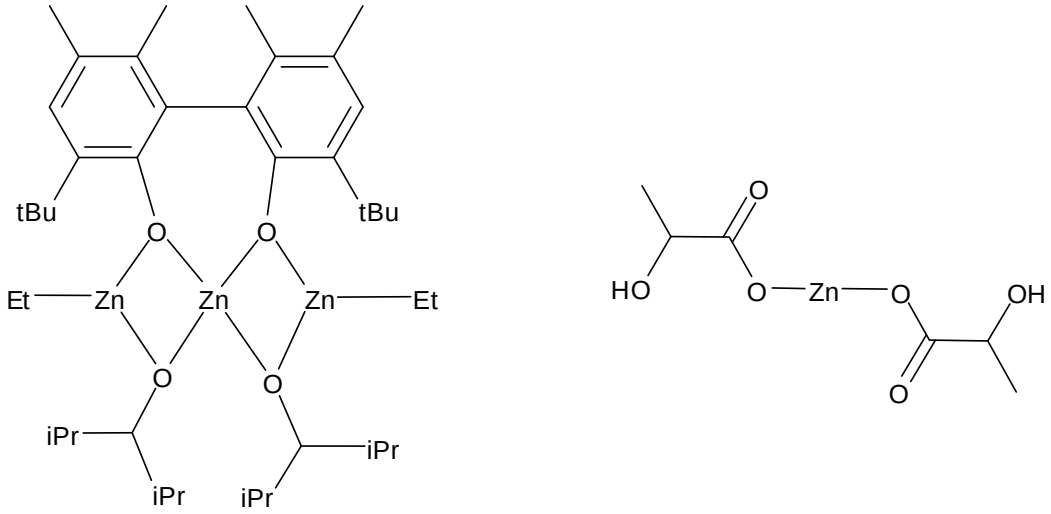

(a) **(b)**

Figure 1.2. **(a)** Diol derived zinc complex for lactide ROP;[46] **(b)** zinc lactate.

An attempt to improve on the PDI for the diol system was made using zinc lactate (Figure 1.2b) as initiator for the ROP of lactides. The polymerization reaction of D,L-lactide was carried out using a [M]/[I] ratio of 2 870:1 at 150 ^{o}C under vacuum. After 96 h of reaction, 97% conversion of monomer to polymer with a degree of polymerization (DP_n) of 646 and a PDI of 1.6, determined by SEC, were obtained. The rate of polymerization using this initiator system was found to be lower compared to the use of zinc diol as initiator and in addition higher temperature is required for the lactate system.[47] Since these zinc complexes discussed so far did not give any promising results, there was a need to look into other zinc complexes of different ligands that would be more efficient in initiating ROP of lactides and lactones.

Consequently, Chishlom used trispyrazolyl and trisindazolyl-hydroborate ligands as tripodal monoanionic tridentate ligands, which can confer the required steric hindrance around the metallic centre to prevent aggregation. Three zinc alkoxide complexes (**6**, **7** and **8**) with these

[47] Schwach, G.; Coudane, J.; Engel, R.; Vert, M. *Polym. Bull*. **1996**, *37*, 771.

ligands have been synthesized (Figure 1.3).[48] Polymerizations of L-lactide employing **6** were controlled with evidence of a linear relationship between M_n and the percentage conversion and low PDIs (1.1-1.2). The kinetics of ROP was shown to be first order in lactide as well as in metal complexes in CD_2Cl_2 and $CDCl_3$. But low activity was observed for initiator **6** as the results showed that **6** took 60 days at [M]/[I] ratio of 500:1 in CH_2Cl_2 and at 25 ^oC to achieve 90% conversion. Similarly, complex **7** has low activity for ROP of lactide because of electron-withdrawing effect of the CF_3 groups. The evaluation of chiral zinc complex **8** towards copolymerization of a 1:1 mixture of *meso* and *rac*-lactide in CD_2Cl_2 revealed that *meso* and *rac*-lactides were polymerized at essentially the same rate during the initial phase of the polymerization (> 30%), then the *meso*-lactide was consumed faster.[47]

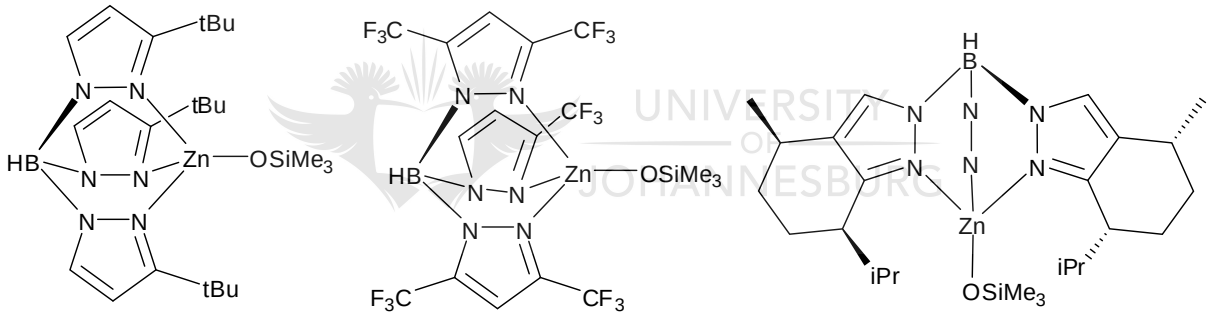

6 **7** **8**

Figure 1.3. Trispyrazolyl and trisindazolyl-hydroborate ligands supported zinc complexes.[48]

These results show that the use of tris(pyrazolyl)borate zinc alkoxides as single-site catalysts for lactide polymerization was successful, except for the very slow activity of the catalysts. In order to improve on this system, sterically bulky β-diketiminate (BDI) ligands were used to access many zinc(II) complexes (**9**–**12**) (Figure 1.4) for ROP of lactide in the past several years.

[48] Chisholm, M. H.; Eilerts, N. W. *Chem. Commun*. **1996**, 853.

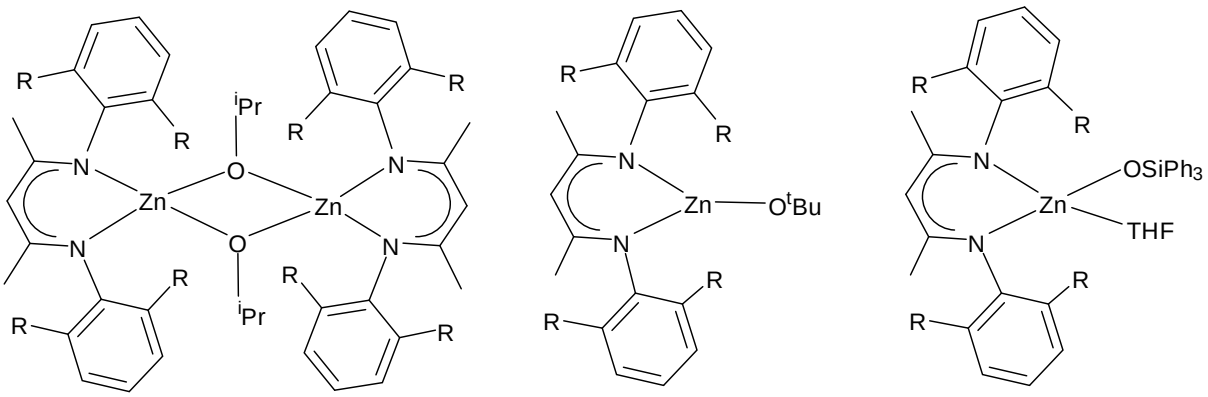

Figure 1.4. β-Diiminate supported Zn complexes.[49]

Complex **9** catalyzed the ROP of *rac*-lactide, yielding highly heteroatactic microstructures with stereoselectivity up to 90% at room temperature and 94% at 0 °C, affording syndiotactic PLA. Using complex **9** as catalyst, polymerization of *rac*-lactide was 50% faster than that of *meso*-lactide and seven times faster than the polymerization of L-lactide.[50] Changing the substituent groups on the β-diketiminate ligand significantly affects its stereoselectivity. For instance, changing the substituents from isopropyl to ethyl groups (complex **10**) result in decreasing heterotacticity. Comparing complexes **9** and **10**, it is interesting to note that polymerization of *meso*-lactide with **9** affords syndiotactic PLA, while **10** yields moderately heterotactic PLA.[49] Since the bimetallic system showed good activity and selectivity, the monometallic zinc system was studied using complex **11**. The latter initiates polymerization of *rac*-lactide with [M]/[I] ratio of 100:1 in CH_2Cl_2 at 20 °C in 10 min. Different initiating

[49] Cheng, M.; Attygalle, A. B.; Lobkovsky, E. B.; Coates, G. W. *J. Am. Chem. Soc.* **1999**, *121*, 11583.

[50] Chamberlain, B. M.; Cheng, M.; Moore, D. R.; Ovitt, T. M.; Lobkovsky, E. B.; Coates, G. W. *J. Am. Chem. Soc.* **2001**, *123*, 3229.

groups also affect the rate of polymerization. For instance, when using complex **12**, the polymerization proceeds up to 90% completion in 40 min.[51]

Despite the few disadvantages of the zinc initiators, their overall performances towards ROP of cyclic esters are good, making zinc a very attractive metal for this type of polymerization.

1.2.5 Copper initiators for ROP of lactides and lactones

Although very few studies have been carried out on copper complexes as potential initiators for polymerization of cyclic esters, the reports to date show that some copper complexes (Figure 1.5) are able to catalyze the ROP of L-lactide efficiently at elevated temperatures under solvent-free conditions, producing polylactides of moderate molecular weights with narrow molecular weight distributions. For example, ROP of lactide using complex **13** at [M]/[I] ratio of 100:1 and 160 ^{o}C for 4 h resulted in 25% conversion of monomer to PLA of M_n = 14 100 gmol^{-1} and PDI of 1.14. When R^1 was changed to CH_3, complex **14** catalyzed the ROP of lactide under the same conditions as **13** to give rise to higher conversion of 72% but lower M_n of 8 200 gmol^{-1} and unchanged PDI. A further change in R^1 to C_2H_5 to form complex **15** gave lower conversion of 51%, a lower M_n (6 200 gmol^{-1}) as well as narrower PDI (1.08). So, from these complexes, it is obvious that there is a big future for copper complexes as initiators for ROP of cyclic esters.[20]

[51] Chisholm, M. H.; Gallucci, J.; Phomphrai, K. *Inorg. Chem*. **2002**, *41*, 2785.

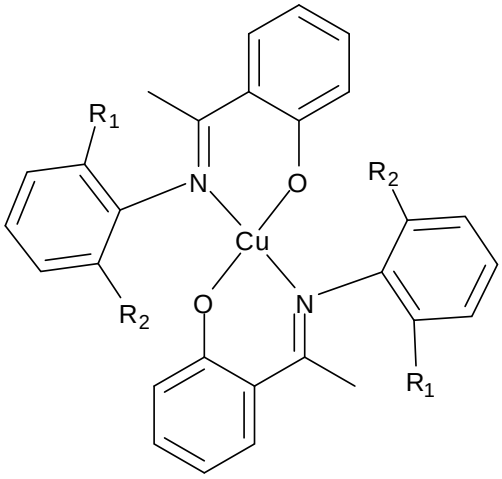

R_1 = H, R_2 = Me (**13**)
R_1 = R_2 = Me (**14**)
R_1 = R_2 = Et (**15**)

Figure 1.5. Cu(II) complexes of a series of phenoxy-ketimine ligands.[20]

From the examples discussed, it can be noted that several studied have been conducted on this area of research. On one hand, $[Al(O^iPr)_3]$ and $[Sn(Oct)_2]$ are the two main initiators currently in use because of their attractive features, which are good selectivity and activity, respectively. Yet, none of these two systems possess both features, leading to either high selectivity or activity. On the other hand, organolanthanide complexes have also been used and were found to possess both excellent selectivity and activity, but one major drawback of these initiators is their instable nature. Other initiators based on transition metals, such as zinc and copper, have shown that they also have some of the required features as well as the shortcomings.

The mains features of the existing initiators were combined in designing a new catalytic system that will circumvent their shortcomings. Hence, the choice of the metal and the ligands becomes crucial in making the initiator that will show good activity and high stereoselectivity. For the purpose of this project, zinc and copper were chosen based on the

success of their previous compounds as initiators. Additional characteristics of these two metals are low cost, tolerance, abundance and low toxicity and also lack of colour in the case of zinc. Since the presence of a metal-oxygen bond is important in ROP, carboxylates are chosen to be the primary ligands. In order to enhance the activity of the metal complex, pyrazole and pyrazolyl compounds are the chosen N donor, secondary ligands.

1.3 Metal carboxylates structures

Carboxylates have been used for the construction of motifs of inorganic materials that have interesting properties.[52] The success in designing target metal carboxylates depends on the modulation of various coordination modes of carboxylates for synthetic[53] and biologically occurring molecules.[54] Among the different coordination chelating modes, monodentate and bridging generally decide the structural features of inorganic carboxylate complexes.[55] Bridging through two oxygen atoms of the carboxylato group (bidentate) generally leads to paddle wheel or polymeric structures.[56] Some examples of the coordination of carboxylates to zinc and to copper that have been reported in literature are summarized in the following sections.

1.3.1 Zinc carboxylates

Various zinc carboxylates are known to possess mild antiseptic and fungal properties. They have also been used as catalysts, wood preservatives, waterproofing agents, auxiliary drying agents in paints, hardeners in varnishes and as processing lubricants and anti-stick agents in

[52] Mellot-Draznieks, C.; Ferey, G. *Prog. Solid State Chem*. **2005**, *33*, 187.

[53] James, S. L. *Chem. Soc. Rev*. **2003**, *32*, 276.

[54] Wilkox, D. E. *Chem. Rev*. **1996**, *96*, 2435.

[55] Robert, V.; Lamercier, G. *J. Am. Chem. Soc*. **2006**, *128*, 1183.

[56] Gutchke, S. O. H.; Price, D. J.; Powell, A. K.; Wood, P. T. *Eur. J. Inorg. Chem*. **2001**, 2739.

the rubber and plastic industries.[57] In particular, zinc salicylate, approved by US Food and Drug Administration (FDA), is used as an anti-oxidant and stabilizer for polymers. Brownless synthesized some zinc complexes to investigate the nature of the products formed between zinc salicylates and ligands like 3,5-di-*tert*-butyl derivative.[57] One of the complexes formed is a tetrahedral $[Zn(salH)_2(bipy)]$, where salH is salicylato and bipy is 2,2`-bipyridine. The salicylates are bonded through the carboxylate oxygen, the most common mode of coordination for mono-deprotonated salicylic acid. While growing the crystals in methanol, the alcohol reacted with the complex to generate octahedral $[Zn(salH)_2(bipy)CH_3OH]$ (Figure 1.6). This distorted octahedral array was achieved by coordination of a methanol molecule and the conversion of one of the monodentate salicylate ligands into a bidentate chelating carboxylate.[57]

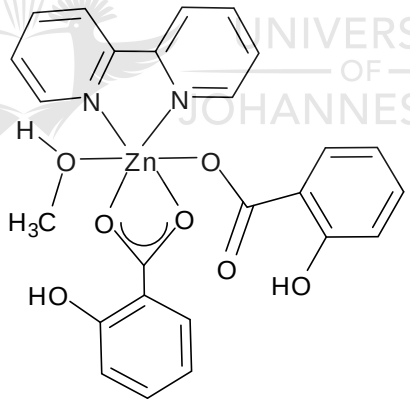

Figure 1.6. Molecular structure of $[Zn(salH)_2(bipy)CH_3OH]$.[57]

Besides this monometallic complex, zinc carboxylates are also known to adopt polymeric structures, which in turn have several applications. Metal-organic coordination polymers in general have attracted considerable attention in recent years because they can be used for gas

[57] Brownless, N. J; Edwards, D. A.; Mahon, M. F. *Inorg. Chim. Acta* **1999**, *287*, 89.

storage,[58] sensing,[59] molecular recognition,[60] molecular magnetism,[61] catalysis[62] and nonlinear optics.[63] Among these frameworks, coordination polymers based on zinc carboxylates play a special role because of the large number of possible building units, varying from Zn(II) monomers to small di-, tri- or tetranuclear clusters or even infinite chains, assembled into robust porous frameworks. In such structures, zinc atoms adopt coordination numbers 4, 5 or 6 for tetrahedron, tetragonal pyramid and octahedron respectively. Hence, the options of having several binding modes in different zinc carboxylate complexes make them versatile.[64] Thus, the synthesis of two such compounds has been reported by Fedin *et al.* and the luminescent properties of the polymers were investigated as well.[65] The structure comprises of two crystallographically-independent Zn(II) atoms forming a trinuclear zinc carboxylate with two distorted tetrahedral and one distorted octahedral zinc centres of formula $[NH_2(CH_3)_2]_2[Zn_3bdc4].DMF.H_2O$, where (bdc4 = 1,4-benzenedicarboxylate) (Figure 1.7).

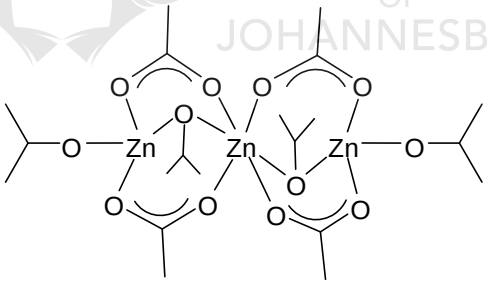

Figure 1.7. Structure of $[NH_2(CH_3)_2]_2[Zn_3bdc4].DMF.H_2O$.[65]

[58] Dybtsev, D. N.; Chun, H.; Yoon, S. H.; Kim, D.; Kim, K. *J. Am. Chem. Soc.* **2004**, *126*, 32.

[59] Zhao, B.; Chen, X. Y.; Cheng, P.; Liao, D. Z.; Yan, S. P.; Jiang Z. H. *J. Am. Chem. Soc.* **2004**, *126*, 15394.

[60] Venkataraman, D.; Gardner, G. F.; Lee, S.; Moore, J. S. *J. Am. Chem. Soc*. **1995**, *117*, 11600.

[61] Fujita, W.; Awaga, K. *J. Am. Chem. Soc*. **2001**, *123*, 3601.

[62] Fujita, M.; Kwon, J. Y.; Washizu, S.; Ogura, K. *J. Am. Chem. Soc.* **1994**, *16*, 1151.

[63] Meng, X. R.; Song, Y. L.; Hou, H. W.; Fan, Y. T.; Li, G.; Zhu, Y. *Inorg. Chem.* **2003**, *42*, 1306.

[64] Cotton, F. A.; Lin, C.; Murillo, C. A. *Acc. Chem. Res*. **2001**, *34*, 759.

[65] Sapchenko, S. A.; Dybtsev, D. N.; Samsonenko, D. G.; Fedin, V. P. *New J. Chem*. **2010**, *34*, 2445.

Zinc carboxylates are not the only carboxylates that show such interesting structures. The chemistry of copper carboxylates has also been extensively studied and examples of these complexes are given in the section below.

1.3.2 Copper carboxylates

Copper(II) carboxylates are the commonly used forms of the metal in constructing copper carboxylate with other ligands. They are structurally a very diverse group of coordination compounds due to the various coordination modes of the carboxylato ligands. In general, most compounds contain a tetracarboxylato $[Cu_2(OOCR)_4]$ core (where R = alkyl or aryl groups), which in turn has a typical dimeric paddle wheel structure, where the two oxygen atoms of the RCOO group coordinate to two different copper centres. A large number of such complexes have been reported, all having the polymeric structure $[Cu_2(OOCR)_4]_n$ in which dimeric units are linked into chains by the interaction of a copper atom from one unit with the carboxylate oxygen of a neighbouring dimer.[66] Copper(II) carboxylates react with additional (in most cases nitrogen and oxygen donors) ligands to form complexes that have been shown to have diverse stereochemistry. By breaking the polymeric structure with the coordination of an additional ligand in the axial position, distinct dimers of the acetate hydrate type, of general formula $[Cu_2(OOCR)_4L_2]$, where R = benzyl group and L = pyrazolyl compound, are obtained.[59] By increasing the concentration of L, monomeric complexes of composition $[Cu(OOCR)_2L_2]$ are often formed with either monodentate or bidentate coordination modes for the carboxylate ligands.[67] Low molecular weight Cu(II) carboxylato compounds have

[66] Doyle, A.; Felcman, J.; do Prado Gambardella, M. T.; Verani, C. N.; Bragança Tristao, M. L. *Polyhedron* **2000**, *19*, 2621.

[67] Lah, N.; Giester, G.; Lah, J.; Segedin, P.; Leban, I. *New J. Chem*. **2001**, *25*, 753.

frequently been used to mimic the active site in metalloenzymes, since many metalloprotein active sites have been recognized to have carboxylate rich coordination environments.[68]

The coordination modes of carboxylato ligand are dramatically sensitive to ligand steric effects, solvent effects, participation of counter ions and other factors. It is therefore important to establish strategies leading to desired architectures in order to isolate mononuclear, dinuclear and polymeric carboxylates. Dinuclear copper(II) carboxylates with a pair of copper atoms held by carboxylato-O,O` bridges are of interest towards understanding intramolecular magnetic exchange phenomena.[69] Studies have been carried out on N-carbazolylacetic acid with Cu(II) and d^{10} ions as a means of understanding the modes of binding of the carboxylates. A Cu(II) complex $[Cu_2(Cabo)_4(DMF)_2].2DMF$ where Cabo = N-carbazolylacetate (Figure 1.8), which consists of centrosymmetric dinuclear unit with each Cu(II) ion having four O atoms of RCOO groups in equatorial positions and a DMF molecule bound *trans* to the Cu-Cu vector at the apex is one such example. The magnetic susceptibility of this complex is typical of a dinuclear copper(II) complex exhibiting intramolecular antiferromagnetic exchange.[69]

[68] Holz, R. C.; Bradshaw, J. M.; Bennett, B. *Inorg. Chem.* **1998**, *37*, 1219.

[69] Casanova, J.; Alzuet, G.; Latorre, J.; Borras, J. *Inorg. Chem*. **1997**, *36*, 2052.

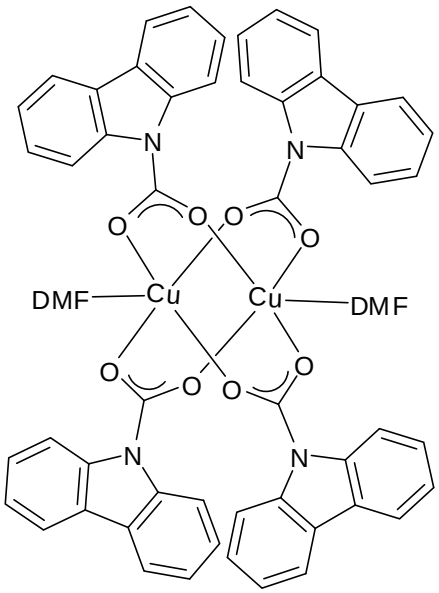

Figure 1.8. Structure of $[Cu_2(Cabo)_4(DMF)_2].2DMF$.[69]

Another example of a paddle wheel is the copper(II) N-oxide complex (Figure 1.9a), which has been of interest because of its biological activity and also for the study of the antiferromagnetic properties. This geometry is preferred by copper(II) carboxylates and the axial positions are commonly occupied by solvents or by ancillary ligands. Thus, if bidentate spacer ligands are used to connect the paddle wheel units, the distance of separation between the paddle wheel cores may be controlled. For instance, using two different dipyridyl linkers (Figure 1.9) produces distances, d1 and d2 if the dipyridyl is 4,4`-bipyridine and 2,2`-bipyridine respectively. The different linkers give different distances and changes the magnetic properties of the complexes significantly. Interactions within the paddle wheel moieties were found to be strongly antiferromagnetic with values typical of Cu(II) carboxylates. However, inter-dinuclear interactions between these moieties were too weak to be detected, suggesting that magnetic exchange is via the bipyridyl linkers.[70]

[70] Sarma, R.; Boudalis, A. K.; Baruah, J. B. *Inorg. Chim. Acta* **2010**, *363*, 2279.

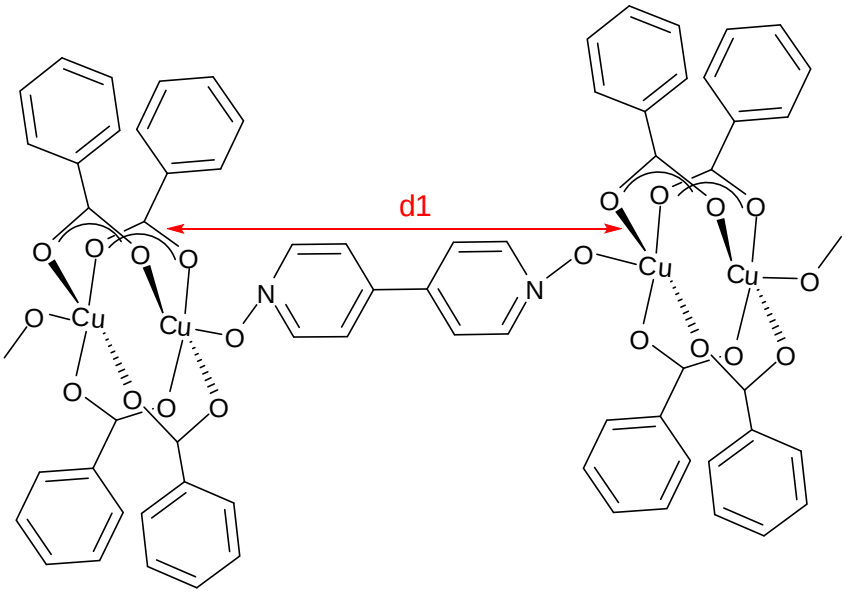

(a)

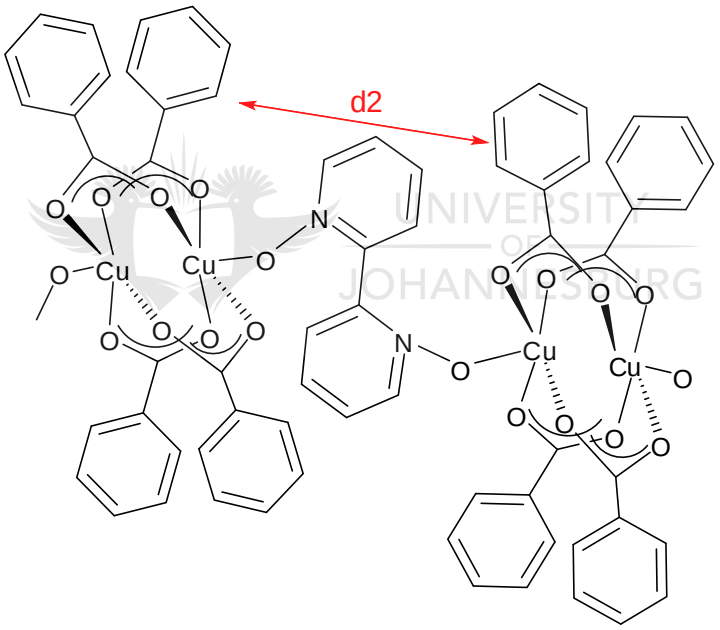

(b)

Figure 1.9. The separation of paddle wheel units by N-oxide connectors.[70]

Since the monocarboxylate Cu complex shows interesting structure, it was conceivable that the presence of more than one carboxylate group on the benzyl ring could bring even more interesting features to the structure of the complex. Thus, multicarboxylate benzene ligands were investigated and have been found to be good building blocks in designing new materials

due to their rich coordination modes. The syntheses of interesting polymeric copper complexes have been reported not only because of their intriguing structural diversity but also because of their potential functions as microporous solids for molecular adsorption, ion-exchange and heterogeneous catalysis. The complex obtained from the assembly of copper(II) ions and 1,2,4,5-benzenetetracarboxylic acid in the presence of auxillary ligands of 4,4`-bipyridine, is a tetranuclear neutral 2D polymer. The complex constitutes a basic building block composed of one Cu_2 paddle wheel secondary building block and two mononuclear Cu(II) motifs (Figure 1.10).[71]

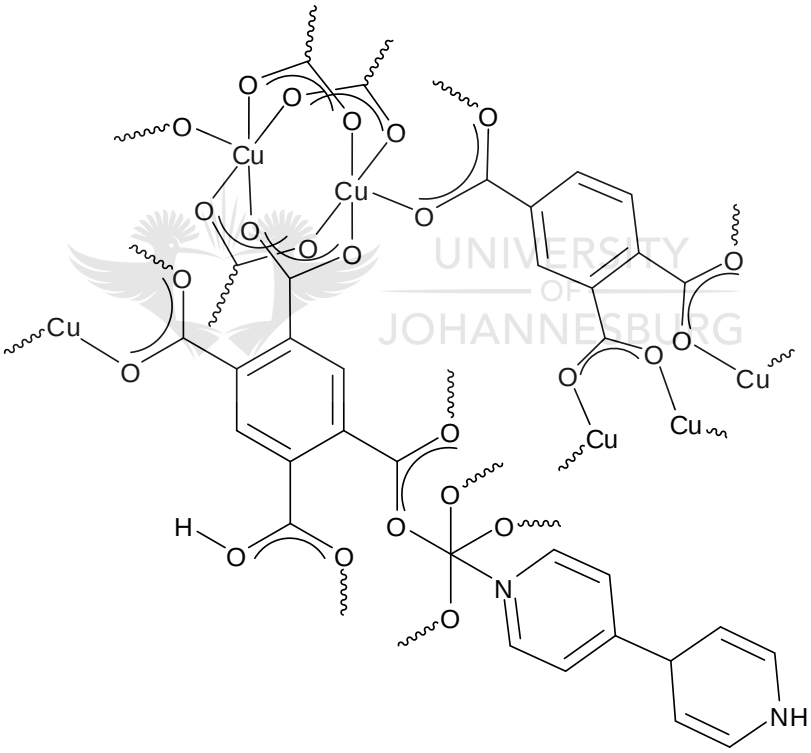

Figure 1.10. Structure of polymeric Cu(II) complex.[71]

A variant to the chemistry of carboxylates of zinc and copper is the introduction of pyrazole as ancillary ligands, recently reported by Baruah's group.

[71] Cao, R.; Shi, Q.; Sun, D.; Hong, M.; Bi, W.; Zhao, Y. *Inorg. Chem*. **2002**, *41*, 6161.

1.4 Metal carboxylates with pyrazoles in their structures

Pyrazole and its derivatives are known to possess important biological and pharmaceutical activities, such as antimicrobial, antiviral, antitumor, anti-inflammatory,[72] antifungal and antidepressant activities. The coordination chemistry of pyrazole and its derivatives has been investigated in detail during the 1960s. The pyrazole nucleus is thermally and hydrolytically very stable and coordinates to metals and metalloids, as a ligand, through the 2-N (Figure 1.11). A substituent in position 3 introduces steric hindrance to the system.[73] Thus, many researchers have studied zinc and copper complexes of this ligand, primarily through introduction of substituents and a brief review in the subsequent sections illustrates this.[73]

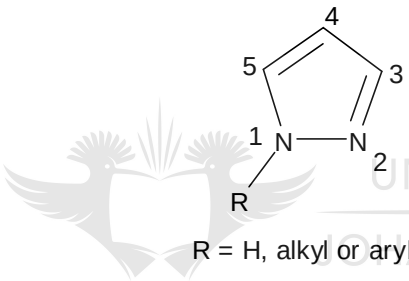

Figure 1.11. Structure of pyrazole.[73]

1.4.1 Zinc carboxylates with pyrazoles

Zinc complexes containing pyrazole ligands are known to mimic the biological activity of carbonic anhydrase.[74] Baruah has reported the formation of a number of mononuclear and binuclear zinc(II) carboxylate complexes with monodentate 3,5-dimethylpyrazole (pz) and bidentate 3,5-dimethylpyrazolato (bpz) ligand respectively, which were prepared in one pot reactions using different solvents (Scheme 1.3).

[72] Badawey, E.; El-Ashmawey, I. M. *Eur. J. Med. Chem.* **1998**, *33*, 349.

[73] Trofimenko, S. *Chem. Rev.* **1972**, *72*, 497.

[74] Walz, R.; Ruf, M.; Vahrenkamp, H. *Eur. J. Inorg. Chem.* **2001**, 139.

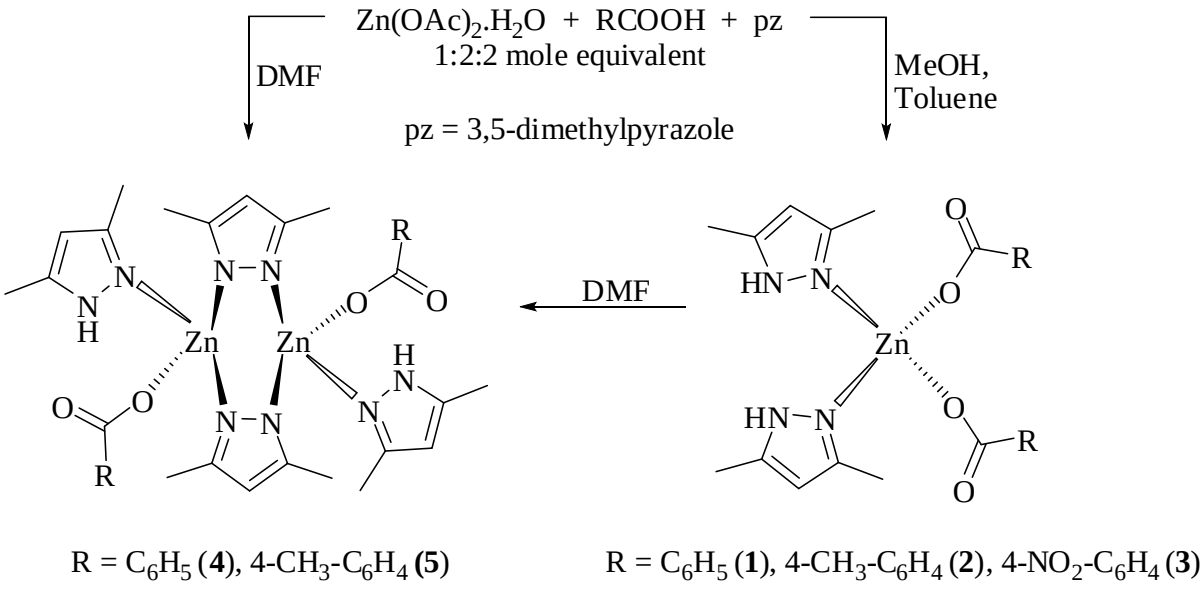

Scheme 1.3. Formation of mono and dinuclear complexes from two different solvents.

The zinc complex prepared from benzoic acid in the presence of 3,5-dimethylpyrazole from a mixed solvent (methanol:toluene = 3:1) is a mononuclear complex, having composition $[Zn(C_6H_5COO)_2(pz)_2]$ (**1**). Complex **1** has a near tetrahedral geometry around the metal centre with both pz units in *cis*-orientation to each other. The same reaction in dimethylformamide (DMF) results in the formation of a binuclear species, **4**, having composition $[Zn_2(C_6H_5COO)_2(bpz)_2(pz)_2]$, in which case also the two zinc centres adopt a near tetrahedral geometry. The pair of pz as well as the pair of benzoato ligands across the metal centres are in *trans* geometry to each other. The bridging dimethylpyrazolate anions and the two zinc centres adopt a planar arrangement, which generates a hexagonal geometry at the core. Also, conversion of mononuclear complexes to binuclear in dimethylformamide is observed, suggesting that during the transformation, the solvent molecule plays an important role.[75] Hence, the choice of solvent is crucial in determining the structure of the

[75] Sarma, R.; Kalita, D.; Baruah, B. *Dalton Trans.* **2009**, 7428.

zinc complex formed. Moreover, in order to study the effect of changing the pyrazole ligand on its coordination to Zn, a tripodal pyrazole ligand was used.

Another series of zinc complexes containing the tripodal ligand bis(5-*tert*-butyl-3-methylpyrazol-2-yl)acetic acid (HBMPA), which is designed to model the 2-his-1-carboxylate facial triad observed in the active sites of various metalloenzymes such as carboxypeptidase A (CPA) and thermolysin (TLN) have also been reported. This particular pyrazolyl ligand was chosen to get a better understanding of the structure and function relationship of CPA and TLN, specifically the ability of zinc to activate coordinated water molecule. Complex [Zn(BMPA)(CH_3)] and methane were produced when Zn(CH_3) and HBMPA were reacted (Figure 1.12) and room temperature protonolysis of [Zn(BMPA)(CH_3)] with either PhSH or acetohydroxamic acid yielded [Zn(BMPA)(Ph)] and [Zn(BMPA)(AH)] respectively as white solids, although treatment with alkyl thiols, phenols, or water resulted in no reaction even after extended periods of time at elevated temperatures.[76]

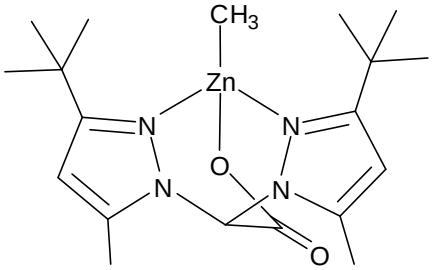

Figure 1.12. Structure of [Zn(BMPA)(CH_3)].[76]

[76] Hammes, B. S.; Kieber-Emmons, M. T.; Letizia, J. A.; Shirin, Z.; Carrano, C. J.; Zakharov, L. N.; Rheingold, A. L. *Inorg. Chim. Acta* **2003**, *346*, 227.

This study was further extended to copper complexes of this type of ligand system and fascinating structures were found, as exemplified in the following section.

1.4.2 Copper carboxylates with pyrazoles

Baruah studied the preparation of structurally important copper(II) complexes from copper(II) actetate monohydrate, 3,5-dimethylpyrazole and benzoic acid. One of the products of this one pot reaction is a regular paddle wheel structure, in which the axial positions are occupied by two 3,5-dimethylpyrazole molecules (Figure 1.13).[77]

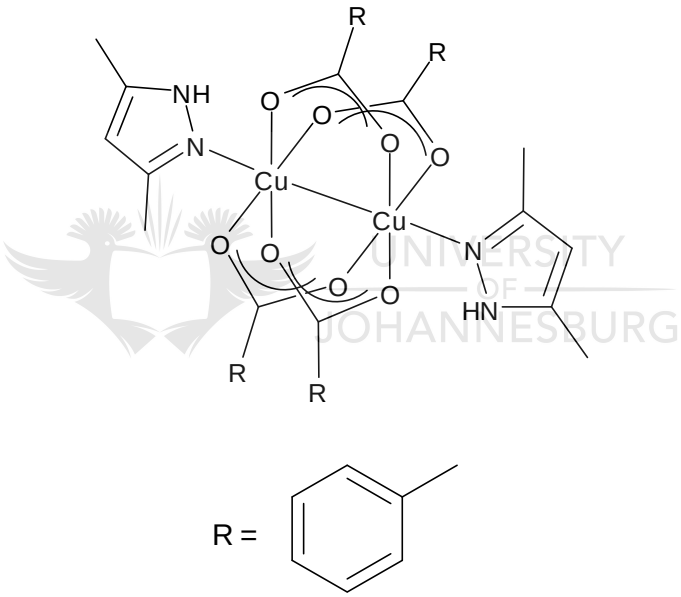

Figure 1.13. Structure of the paddle wheel Cu(II) complex.[77]

Even if paddle wheel binuclear copper(II) carboxylates are very common, there are some mononuclear ones that are also formed. When N-benzoyl 3,5-dimethylpyrazole and copper(II) nitrate trihydrate were made to react in a 2:1 molar ratio in aqueous methanol at 25 ^{o}C for three days, an interesting mixed copper(II) benzoate complex was formed. The

[77] Casarin, M.; Corvaja, C.; Nicola, C. D.; Falcomer, D.; Franco, L.; Monari, M.; Pandolfo, L.; Pettinari, C.; Piccinelli, F. *Inorg. Chem.* **2005**, *44*, 6265.

complex has composition *cis*-$(pz)_2Cu(C_6H_5COO)_2$ and *trans*-$(pz)_2Cu(C_6H_5COO)_2H_2O$ (where pz = 3,5-dimethylpyrazole), which is structurally important as it has a unique lattice in which both *cis* and *trans* coordination of 3,5-dimethylpyrazole are present around two independent copper(II) centres (Figure 1.14).[78]

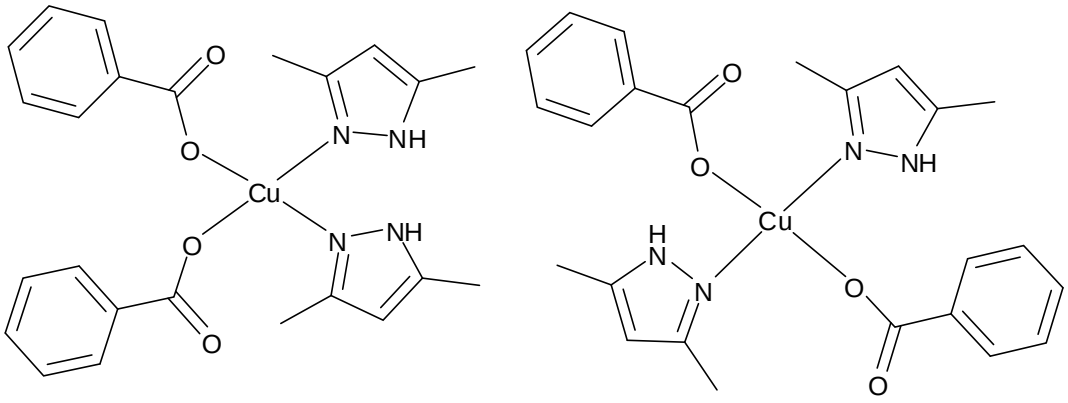

Figure 1.14. Structure of *cis*-$(pz)_2Cu(C_6H_5COO)_2$ and *trans*-$(pz)_2Cu(C_6H_5COO)_2H_2O$.[78]

1.5 Scope and objectives of dissertation

The aims of this research were: (i) synthesize a range of pyrazole and pyrazolyl Zn(II) and Cu(II) benzoates and characterize these complexes using several analytical techniques and X-ray diffractometer and (ii) evaluate the catalytic activities of the complexes in initiating ROP of D,L-lactides and ε-caprolactone, and characterize the PLA and PCL obtained to determine the type of polymer produced by these systems. In pursuit of these aims, Zn(II) and Cu(II) complexes were synthesized with the ligand system comprising of benzoates and pyrazolyl compounds. These complexes were then used as initiators for ROP of D,L-lactide and ε-caprolactone at elevated temperatures in toluene and in bulk respectively.

[78] Deka, K.; Laskar, M.; Baruah, B. *Polyhedron* **2006**, *25*, 2525.

CHAPTER 2

SYNTHESIS AND CHARACTERIZATION OF LIGANDS AND METAL COMPLEXES

2.1 Introduction

Most of the metal complexes used as initiators for the ROP of lactides and ε-caprolactone possess a common feature, which is a metal-oxygen bond. This bond is of primary importance because it is conceivable that the coordination-insertion mechanism, undergone by polymerization systems employing these complexes, takes place at the metal-oxygen bond. It has also been observed that the presence of other chelate ligands that act as ancillary ligand normally enhances the activity of the complex. This secondary ligand is not directly involved in the polymerization, but it does tune the properties of the metallic centre, such as electronegativity of the metal and the accessibility of the monomer to the metal centre.[79]

Nitrogen donor ligands are the most commonly used ancillary ligands. Metal complexes featuring Salen and Salan-type N^O ligands have been known to exhibit excellent stereocontrol in lactide ROP.[80] Pyrazole and its derivatives constitute another important group of N donor compounds that have been used because of their attractive coordination chemistry. Darkwa has shown that pyrazole-based complexes could be used as catalysts in several reactions, examples of which are the oligomerization and polymerization of phenylacetylene catalyzed by [Pd(Pz1)Cl_2] (where Pz1 = 2,6-bis(3,5-dimethylpyrazol-1-yl methyl)pyridine) and silver triflate, producing polyphenylacetylene.[81] Compounds like [Ni(Pz2)$_2$$Br_2$] (where Pz2 = 2-(3,5-dimethylpyrazol-1-yl)-ethanol) has been found to be an

[79] Roman, L. M. A.; O'Keefe, B. J.; Hillymer, M. A.; Tolman, W. B. *Dalton Trans*. **2003**, 3082.

[80] Hormnirun, P.; Marshall, E. L.; Gibson, V. C.; White, A. J. P.; Williams, D. J. *J. Am. Chem. Soc*. **2004**, *126*, 2688.

[81] Ojwach, S. O.; Guzei, I. A.; Darkwa, J.; Mapolie, S. F. *Polyhedron* **2007**, *26*, 851.

active catalyst in ethylene oligomerization.[82] Therefore, metal complexes of these ligands have potential use in material chemistry and catalysis because of the ease of functionalizing the ligands to desirable electronic and steric effects as well as improved solubility.[83]

Hence, for this project, the ligand systems chosen include pyrazole and pyrazolyl compounds coordinated to zinc and copper through the nitrogen atoms and a range of benzoic acids, which coordinate via the carboxylate oxygen to the metal to form a metal-oxygen bond. Therefore, in this chapter the syntheses of zinc(II) and copper(II) pyrazolyl benzoate complexes are described. Benzoic acids, with different substituents on the phenyl ring, were employed as primary ligands because of their interesting coordination chemistry and their ability to form metal-oxygen bonds that are needed for ROP of lactide and ε-caprolactone.

2.2 Materials

All reactions were performed under a dry nitrogen atmosphere using standard Schlenk techniques. $[Zn(OAc)_2]$, $[Cu(OAc)_2]$, benzoic acid (C_6H_5COOH), 3,5-dinitrobenzoic acid (3,5-NO_2-C_6H_3COOH), 4-hydroxybenzoic acid (4-OH-C_6H_4COOH), 2-chlorobenzoic acid (2-Cl-C_6H_4COOH), 3,5-dimethylpyrazole (**L1**), tetrabutylammonium bromide, tetrabutylammonium hydrogen sulfate, α,α`-dibromo-o-xylene, dibenzoylmethane, hydrazine and 2,2`,6,6`-tetramethylheptane-3,5-dione were used as received from Sigma Aldrich. All solvents were of analytical grade and were dried and distilled prior to use. Toluene and dichloromethane were dried and distilled from sodium and benzophenone, and P_2O_5

[82] Ainooson, M. K.; Ojwach, S. O.; Guzei, I. A.; Spencer, L. C.; Darkwa J. *J. Organomet. Chem*. **2011**, *696*, 1528.

[83] Reger, D. L.; Brown, K. J.; Gardinier, J. R.; Smith, M. D. *Organometallics* **2008**, *22*, 4973.

respectively. 3,5-Diphenylpyrazole (**L2**),[84] bis(3,5-dimethylpyrazol-1-yl)methane (**L4**),[85] bis(3,5-diphenylpyrazol-1-yl)methane (**L5**)[85] and bis(1,2-bis{(3,5-dimethylpyrazol-1-yl)methyl}benzene) (**L6**)[81] were prepared according to literature procedures.

2.3 Instrumentation

^{1}H NMR and $^{13}C\{^{1}H\}$ NMR spectra were recorded in chloroform-d ($CDCl_3$) and dimethylsulphoxide-d_6 (DMSO) on a Varian Gemini 2 000 instrument (300 MHz for ^{1}H NMR and 75 MHz for $^{13}C\{^{1}H\}$ NMR) and a Bruker Ultrashield 400 instrument (400 MHz for ^{1}H NMR and 100 MHz for $^{13}C\{^{1}H\}$ NMR) at room temperature. ^{1}H and $^{13}C\{^{1}H\}$ NMR chemical shifts were referenced to the residual signals of the protons or carbons of the NMR solvents and are quoted in δ: $CDCl_3$ at 7.24 and 77.0 ppm for ^{1}H and $^{13}C\{^{1}H\}$ NMR spectra respectively; DMSO at 2.45 and 39.5 ppm for ^{1}H and $^{13}C\{^{1}H\}$ NMR spectra respectively. Coupling constants are measured in Hertz (Hz). Infrared spectra were recorded on a Bruker FR-IR Tensor27 spectrometer fitted with an ATP-IR probe. Elemental analyzes were performed on a Vario Elementar IIImicrocube CHNS analyzer at Rhodes University, South Africa. ESI-MS spectra were recorded on a Waters API Quattro Micro spectrophotometry at the University of Stellenbosch, South Africa. The magnetic moments of the copper complexes were measured using a Magway MSB MK1 magnetic susceptibility balance. The effective magnetic moments, μ_{eff}, are calculated in Bohr magnetons (BM) using the equation: $\mu_{eff} = [(3kT\chi_A)/(N\beta^2)]^{1/2}$ (where k = Boltzmann's constant; N = Avogadro's number; β = Bohr magneton; χ_A = molar susceptibility of the paramagnetic atom).

[84] Kitajima, N.; Fujisawa, K.; Fujimoto, C.; Morooka, Y.; Hashimoto, S.; Kitagawa, T.; Toriumi, K.; Tatsumi, K.; Nakamura, A. *J. Am. Chem. Soc.* **1992**, *114*, 1277.

[85] Tolman, W. B.; Tokar, C. J. *Biomimetic and Special Property Ligands*, 51.

2.4 Synthesis of 3,5-ditertiarybutylpyrazole (L3)

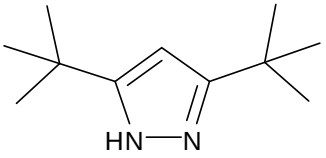

A mixture of 2,2`,6,6`-tetramethyl-3,5-heptanedione (0.22 g, 1.00 mmol) and hydrazine monohydrate (0.05 g, 1.00 mmol) was heated in a round bottom flask under nitrogen for 2 h. The liquid mixture started to solidify after 1 h of reaction and at the end of 2 h, the whole mixture was a white solid. After cooling to room temperature the solid product was removed from the flask without any purification.

Yield: 0.16 g (89%).

^{1}H NMR ($CDCl_3$): δ 1.29 (s, 18H, C(C<u>H</u>$_3$)$_3$); 5.88 (s, 1H, Pz-<u>H</u>).

$^{13}C\{^{1}H\}$ NMR ($CDCl_3$): δ 30.5; 31.4; 97.3.

2.5 General synthesis of zinc and copper complexes

Zinc and copper complexes were synthesized using two methods: A and B.

Method A involves a one pot, overnight reaction between the metal(II) acetate, the pyrazolyl compound and the benzoic acid in methanol. The metal(II) acetate and the appropriate benzoic acid, in a 1:2 mole ratio, were refluxed in methanol (50 mL) for 5 h. A solution of the pyrazolyl compound in methanol (2 mL) was then added dropwise with constant stirring and heating. The mole ratio of the pyrazolyl to the metal(II) actetate was 1:1 for bidentate pyrazolyl ligands (**L4** and **L6**). After 16 h of refluxing, the solution was allowed to cool to room temperature and slow evaporation of the solvent resulted in the formation of crystals. Zinc products were characterized by NMR, IR, elemental analysis and mass spectrometry,

while their copper counterparts were characterized by IR, elemental analysis, mass spectrometry and magnetic moment measurements.

Method B is an adaptation of the procedure used by Baruah[75] to synthesize carboxylate complexes with pyrazoles. The method of preparation is a one pot, room temperature reaction between the metal(II) acetate, benzoic acid and pyrazolyl compound. The metal(II) acetate was stirred with the benzoic acid, in a 1:2 mole ratio, in methanol (15 mL) for 30 min at room temperature, after which a solution of the pyrazole in toluene (5 mL) was added to the mixture and stirred for a further 30 min. The ratio of the metal(II) acetate to pyrazole was dependent on the type of pyrazole used. For **L1**, **L2** and **L3**, the metal(II) acetate and the pyrazole ratio was 1:2, whereas the ratio was 1:1 for **L4**, **L5** and **L6**.

2.5.1 Synthesis of zinc(II) complexes

Method B was used to prepare complexes **1**-**8**.

*[Zn(C_6H_5COO)$_2$(**L1**)$_2$] (**1**)*

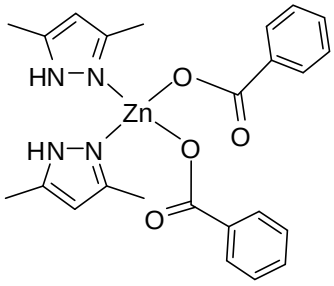

Reaction of [Zn(OAc)$_2$] (0.18 g, 1.00 mmol), C_6H_5COOH (0.24 g, 2.00 mmol) and **L1** (0.19 g, 2.00 mmol) was carried out in a methanol (15 mL) and toluene (5 mL) mixture. Filtration

and subsequent slow evaporation of the filtrate resulted in white crystals that were analyzed as follows:

Yield: 0.40 g (80%).

^{1}H NMR ($CDCl_3$): δ 2.24 (s, 12H, C<u>H</u>$_3$-Pz); 5.91 (s, 2H, C<u>H</u>-Pz); 7.36 (t, $^{5}J_{HH}$ = 14.8 Hz, 4H, 3,5-Bz); 7.43 (t, $^{5}J_{HH}$ = 14.8 Hz, 2H, 4-Bz); 8.14 (d, $^{3}J_{HH}$ = 7.2 Hz, 2,6-Bz).

$^{13}C\{^{1}H\}$ NMR ($CDCl_3$): δ 11.9; 105.8; 127.8; 130.1; 131.2; 135.0; 173.6.

ESI-MS m/z (%): 379 $[M - C_6H_5COO]^+$, 50.

IR: 1 609 cm^{-1} ($\nu_{C=O}$).

Anal. Calcd for $C_{24}H_{26}N_4O_4Zn$: C, 57.66%; H, 5.24%; N, 11.21%. Found: C, 57.60%; H, 5.39%; N, 11.24%.

*[Zn(3,5-NO_2-$C_6H_3COO)_2$(**L1**)$_2$] (**2**)*

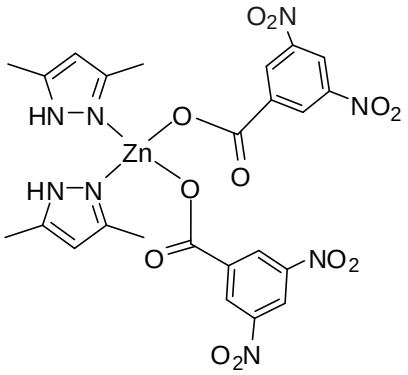

Complex **2** was prepared using $[Zn(OAc)_2]$ (0.18 g, 1.00 mmol), 3,5-NO_2-C_6H_3COOH (0.43 g, 2.00 mmol) and **L1** (0.19 g, 2.00 mmol). Compound **2** was isolated as a white solid after filtration and evaporation of the solvent from the filtrate.

Yield: 0.40 g (59%).

^{1}H NMR (DMSO): δ 2.12 (s, 6H, C<u>H</u>$_3$-Pz); 5.76 (s, 2H, C<u>H</u>-Pz); 8.91 (s, 6H, 2,4,6-Bz).

^{13}C{^{1}H} NMR (DMSO): δ 11.8; 103.8; 120.6; 129.0; 138.5; 148.1; 166.5.

IR: 1 625 cm^{-1} ($\nu_{C=O}$).

Anal. Calcd for $C_{24}H_{22}N_4O_{12}Zn$: C, 42.40%; H, 3.26%; N, 16.48%. Found: C, 42.18%; H, 3.24%; N, 16.44%.

*[Zn(4-OH-C_6H_4COO)$_2$(**L1**)$_2$] (**3**)*

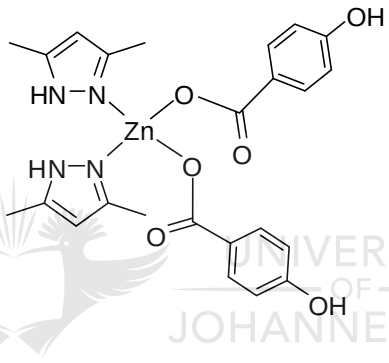

Reaction of [Zn(OAc)$_2$] (0.18 g, 1.00 mmol), 4-OH-C_6H_4COOH (0.28 g, 2.00 mmol) and **L1** (0.19 g, 2.00 mmol) gave **3** as a white solid, which was isolated in a similar manner as **1**.

Yield: 0.32 g (60%).

^{1}H NMR (CDCl$_3$): δ 2.12 (s, 6H, 5-C<u>H</u>$_3$-Pz); 2.43 (s, 6H, 3-C<u>H</u>$_3$-Pz); 6.01 (s, 2H, Pz-<u>H</u>); 9.12 (s, 4H, 3,5-Bz); 9.25 (s, 4H, 2,6-Bz).

^{13}C{^{1}H} NMR (CDCl$_3$): δ 11.7; 12.4; 105.2; 115.0; 123.8; 131.8; 145.0; 149.3; 161.1; 170.0; 174.2.

IR: 1 624 cm^{-1} ($\nu_{C=O}$).

Anal. Calcd for $C_{24}H_{26}N_4O_6Zn.CH_3OH$: C, 53.24%; H, 5.36%; N, 9.93%. Found: C, 53.43%; H, 5.44%; N, 9.49%.

*[Zn(2-Cl-$C_6H_4COO)_2$(**L1**)$_2$] (**4**)*

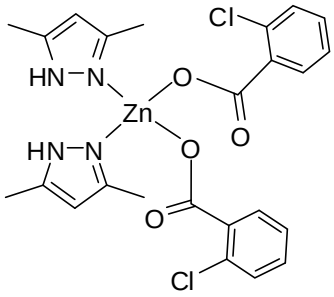

Complex **4** was synthesized using [$Zn(OAc)_2$] (0.18 g, 1.00 mmol), 2-Cl-C_6H_4COOH (0.31 g, 2.00 mmol) and **L1** (0.19 g, 2.00 mmol). Compound **4** was isolated as a white solid in a similar manner as **1**.

Yield: 0.36 g (64%).

^{1}H NMR ($CDCl_3$): δ 2.15 (s, 12H, C<u>H</u>$_3$-Pz); 5.85 (s, 2H, C<u>H</u>-Pz); 7.34 (d, 2H, 3-Bz); 7.43 (t, 4H, 4,5-Bz); 7.70 (d, 2H, 6-Bz).

^{13}C{^{1}H} NMR ($CDCl_3$): δ 11.8; 104.0; 126.9; 130.1; 131.0; 143.8; 149.2.

IR: 1 635 cm^{-1} ($\nu_{C=O}$).

Anal. Calcd for $C_{24}H_{24}Cl_2N_4O_4Zn$: C, 50.68%; H, 4.25%; N, 9.85%. Found: C, 50.99%; H, 4.311%; N, 9.45%.

*[Zn($C_6H_5COO)_2$(**L2**)$_2$] (**5**)*

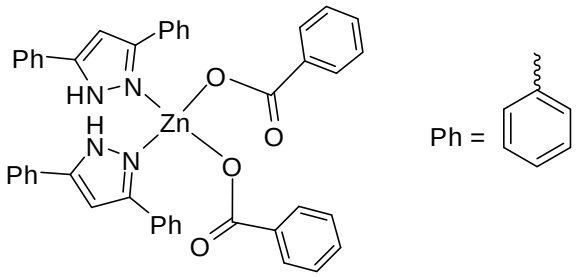

Reaction of $[Zn(OAc)_2]$ (0.18 g, 1.00 mmol), C_6H_5COOH (0.24 g, 2.00 mmol) and **L2** (0.44 g, 2.00 mmol) gave **5** that was isolated as a white solid by filtration and evaporation of filtrate.

Yield: 0.54 g (72%).

^{1}H NMR (DMSO): δ 7.18 (s, 2H, CH-Pz); 7.32 (t, $^5J_{HH}$ = 14.8 Hz, 6H, 4-Ph-Pz, 4-Bz); 7.46 (m, 10H, 3,5-Ph-Pz, 3,5-Bz); 7.83 (d, $^3J_{HH}$ = 7.6 Hz, 8H, 2,6-Ph-Pz); 7.95 (d, $^3J_{HH}$ = 7.6 Hz, 4H, 2,6-Bz).

$^{13}C\{^1H\}$ NMR (DMSO): δ 99.7; 125.1; 127.8; 128.0; 128.9; 129.5; 131.3; 134.1; 171.0.

Anal. Calcd for $C_{44}H_{34}N_4O_4Zn.0.5CH_3OH$: C, 69.94%; H, 4.75%; N, 7.33%. Found: C, 69.62%; H, 5.26%; N, 7.22%.

*$[Zn(3,5\text{-}NO_2\text{-}C_6H_3COO)_2(\mathbf{L2})_2]$ (**6**)*

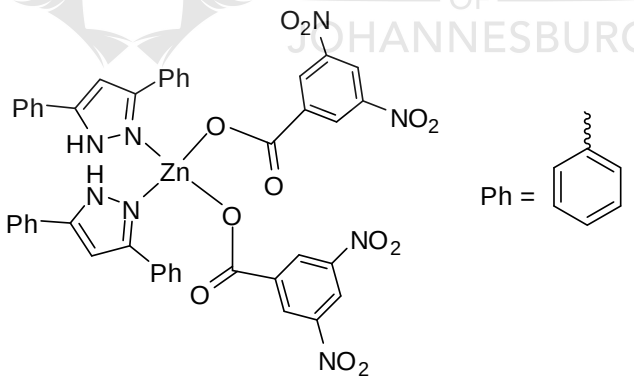

Reaction of $[Zn(OAc)_2]$ (0.18 g, 1.00 mmol), 3,5-NO_2-C_6H_3COOH (0.43 g, 2.00 mmol) and **L2** (0.44 g, 2.00 mmol) gave **6** as a white solid, obtained by evaporation of the solvent in vacuo. Crystals suitable for X-ray were obtained from a solution of **6** in DMSO upon slow evaporation of the solvent.

Yield: 0.61 g (66%).

^{1}H NMR (CDCl$_3$): δ 6.59 (s, 2H, C<u>H</u>-Pz); 7.10 (m, 8H, 3,5-Ph-Pz); 7.55 (m, 8H, 2,6-Ph-Pz); 7.72 (m, 4H, 4-Ph-Pz); 9.12 (s, 2H, 5-Bz); 9.24 (s, 4H, 2,6-Bz).

^{13}C{^{1}H} NMR (CDCl$_3$): δ 99.6; 120.5; 125.1; 128.9; 138.8; 148.0; 166.6.

Anal. Calcd for $C_{44}H_{30}N_8O_{12}Zn$: C, 56.94%; H, 3.26%; N, 12.07%. Found: C, 57.26%; H, 3.285%; N, 11.93%.

*[Zn(4-OH-C$_6$H$_4$COO)$_2$(**L2**)$_2$] (**7**)*

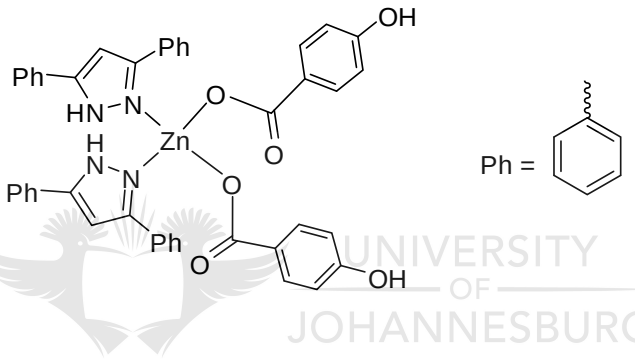

Complex **7** was synthesized using [Zn(OAc)$_2$] (0.18 g, 1.00 mmol), 4-OH-C$_6$H$_4$COOH (0.28 g, 2.00 mmol) and **L2** (0.44 g, 2.00 mmol). Compound **7** was isolated as a white solid by filtration of the reaction mixture after evaporation of the solvent from the filtrate.

Yield: 0.54 g (69%).

^{1}H NMR (DMSO): δ 6.75 (d, $^{3}J_{HH}$ = 8.4 Hz, 4H, 3,5-Bz); 7.18 (s, 2H, C<u>H</u>-Pz); 7.32 (t, $^{5}J_{HH}$ = 14.4 Hz, 4H, 4-Ph-Pz); 7.44 (t, $^{5}J_{HH}$ = 15.2 Hz, 8H, 3,5-Ph-Pz); 7.78 (d, $^{3}J_{HH}$ = 8.0 Hz, 4H, 2,6-Bz); 7.83 (d, $^{3}J_{HH}$ = 7.6 Hz, 8H, 2,6-Ph-Pz).

^{13}C{^{1}H} NMR (DMSO): δ 99.7; 114.6; 125.1; 127.9; 128.9; 131.6; 160.4.

Anal. Calcd for $C_{44}H_{34}N_4O_6Zn.CH_3OH$: C, 66.54%; H, 4.72%; N, 6.90%. Found: C, 66.09%; H, 4.65%; N, 7.00%.

*[Zn(2-Cl-$C_6H_4COO)_2$(**L2**)$_2$] (**8**)*

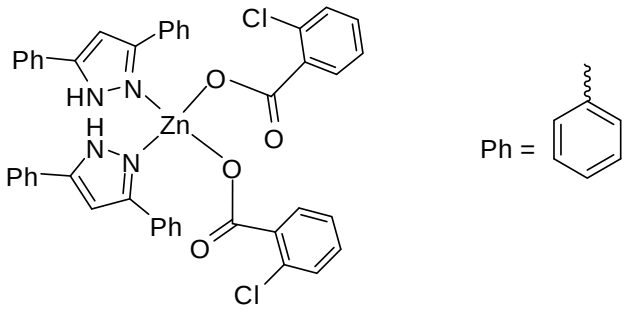

Reacting [$Zn(OAc)_2$] (0.18 g, 1.00 mmol), 2-Cl-C_6H_4COOH (0.31 g, 2.00 mmol) and **L2** (0.44 g, 2.00 mmol) using method B gave **8**. Compound **8** was isolated in a similar manner as **1** and was obtained as a white solid.

Yield: 0.50 g (61%).

^{1}H NMR (DMSO): δ 7.18 (s, 2H, C<u>H</u>-Pz); 7.32 (m, 4H, 4,5-Bz); 7.37 (m, 4H, 4-Ph-Pz); 7.42 (m, 8H, 3,5-Ph-Pz); 7.64 (d, $^3J_{HH}$ = 2.0 Hz, 2H, 3-Bz); 7.66 (d, $^3J_{HH}$ = 1.6 Hz, 2H, 6-Bz); 7.82 (d, $^3J_{HH}$ = 7.2 Hz, 8H, 2,6-Ph-Pz).

Anal. Calcd for $C_{44}H_{34}Cl_2N_4O_4Zn.(1/3\ mol)C_7H_8$: C, 65.64%; H, 4.12%; N, 6.61%. Found: C, 65.64%; H, 4.75%; N, 7.14%.

In order to examine the effect of the solvent on the product of the reaction, complexes **9** and **10** were synthesized by an overnight refluxing in methanol, according to method A.

*[Zn(3,5-NO_2-$C_6H_3COO)_2$**L4**] (**9**)*

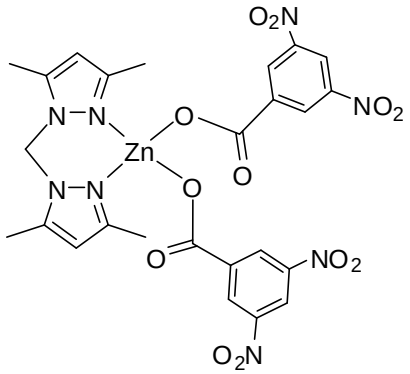

Reaction of [$Zn(OAc)_2$] (0.94 g, 5.13 mmol) and 3,5-NO_2-C_6H_3COOH (2.22 g, 10.0 mmol) with **L4** (1.03 g, 5.05 mmol) in methanol (50 mL) resulted in pale yellow single crystals, obtained after slow evaporation of the solvent. Crystals, suitable for X-ray analysis, were harvested and dried in vacuo.

Yield: 2.76 g (78%).

^{1}H NMR ($CDCl_3$): δ 2.37 (s, 6H, 5-C<u>H</u>$_3$-Pz); 2.46 (s, 6H, 3-C<u>H</u>$_3$-Pz); 6.07 (s, 2H, Pz-C<u>H</u>$_2$-Pz); 6.53 (s, 2H, Pz-<u>H</u>); 9.10 (s, 2H, 4-Bz); 9.25 (2s, 4H, 2,6-Bz).

^{13}C{^{1}H} NMR ($CDCl_3$): δ 10.9; 13.4; 58.7; 105.8; 120.6; 129.1; 138.9; 140.4; 147.6; 148.2; 166.7.

ESI-MS m/z (%): 690 [M^+, 2].

IR: 1 645 cm^{-1} ($\nu_{C=O}$); 1540 cm^{-1} ($\nu_{C=N}$).

Anal. Calcd for $C_{25}H_{22}N_8O_{12}Zn$: C, 43.40%; H, 3.20%; N, 16.20%. Found: C, 43.17%; H, 3.23%; N, 15.88%.

*[Zn(4-OH-$C_6H_4COO)_2$**L6**] (**10**)*

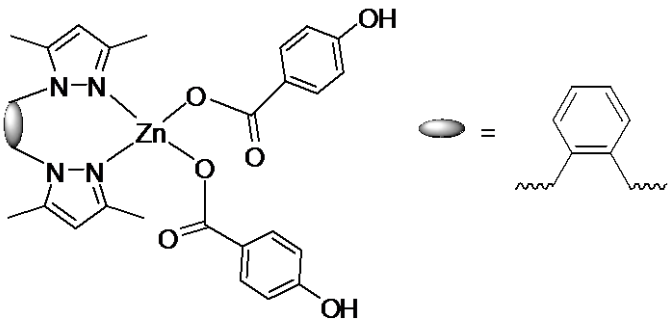

Complex **10** was prepared using [$Zn(OAc)_2$] (0.32 g, 1.73 mmol), 4-OH-C_6H_4COOH (0.48 g, 3.44 mmol) and **L6** (0.50 g, 1.70 mmol). After evaporation of the solvent in vacuo, a white solid was obtained, which was redissolved in toluene. The solution was concentrated and filtered. A white solid was obtained after drying the filtrate in vacuo.

Yield: 0.70 g (64%).

^{1}H NMR (DMSO): δ 2.10 (d, $^6J_{HH}$ = 6.8 Hz, 12H, C<u>H</u>$_3$-Pz); 5.33 (s, 4H, -C<u>H</u>$_2$-Pz); 5.89 (s, 2H, Pz-<u>H</u>); 6.52 (dd, $^3J_{HH}$ = 9.2 Hz, 2H, α-C<u>H</u>-Ph-Pz); 6.74 (d, $^3J_{HH}$ = 8.4 Hz, 4H, 3,5-Bz); 7.15 (dd, $^5J_{HH}$ = 9.2 Hz, 2H, β-C<u>H</u>-Ph-Pz); 7.76 (d, $^3J_{HH}$ = 8.4 Hz, 4H, 2,6-Bz).

$^{13}C\{^1H\}$ NMR (DMSO): δ 10.7; 13.5; 49.1; 105.2; 114.7; 124.1; 126.7; 127.5; 131.7; 135.5; 139.4; 146.4; 160.5; 171.2.

ESI-MS m/z (%): 498 [M- 4-OH-$C_6H_4COO]^+$, 3.

IR: 1 604 cm^{-1} ($\nu_{C=O}$).

Anal. Calcd for $C_{32}H_{32}N_4O_6Zn.(1/4\ mol)C_7H_8$: C, 61.69%; H, 5.22%; N, 8.53%. Found: C, 61.39%; H, 5.55%; N, 8.38%.

Complexes **11-13** were prepared using procedures for method B.

*$[Zn_2(C_6H_5COO)_4$**L6**$]_n$ (**11**)*

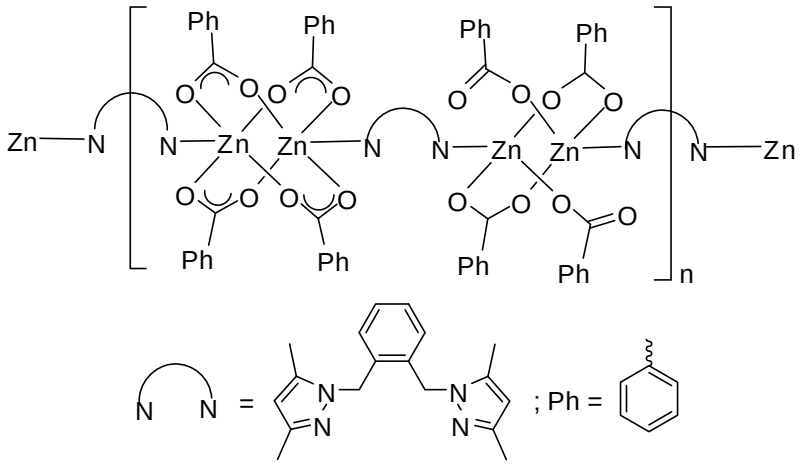

Complex **11** was synthesized using [$Zn(OAc)_2$] (0.18 g, 1.00 mmol), C_6H_5COOH (0.24 g, 2.00 mmol) and **L6** (0.29 g, 1.00 mmol). Pure crystals of **11**, suitable for X-ray analysis, were harvested from slow evaporation of the solvent.

Yield: 0.53 g (58%).

^{1}H NMR (DMSO): δ 2.10 (d, $^6J_{HH}$ = 3.6 Hz, 12H, C<u>H</u>$_3$-Pz); 5.33 (s, 4H, -C<u>H</u>$_2$-Pz); 5.88 (s, 2H, Pz-<u>H</u>); 6.54 (d, $^3J_{HH}$ = 8.4 Hz, 2H, α-C<u>H</u>-Ph-Pz); 7.15 (d, $^5J_{HH}$ = 8.8 Hz, 2H, β-C<u>H</u>-Ph-Pz); 7.41 (t, $^5J_{HH}$ = 15.2 Hz, 4H, 3,5-Bz); 7.48 (t, $^5J_{HH}$ = 14.0 Hz, 2H, 4-Bz); 7.93 (d, $^3J_{HH}$ = 8.0 Hz, 4H, 2,6-Bz).

$^{13}C\{^1H\}$ NMR ($CDCl_3$): δ 10.6; 13.4; 49.0; 105.1; 126.7; 127.4; 128.0; 129.5; 131.1; 134.4; 135.5; 139.3; 146.3; 171.4.

IR: 1 646 cm^{-1} ($\nu_{C=O}$).

Anal. Calcd for $C_{32}H_{32}N_4O_4Zn.(1/5\ mol)C_7H_8$: C, 64.85%; H, 5.48%; N, 8.96%. Found: C, 64.55%; H, 5.624%; N, 9.37%.

*[Zn(3,5-NO_2-$C_6H_3COO)_2$**L6**] (**12**)*

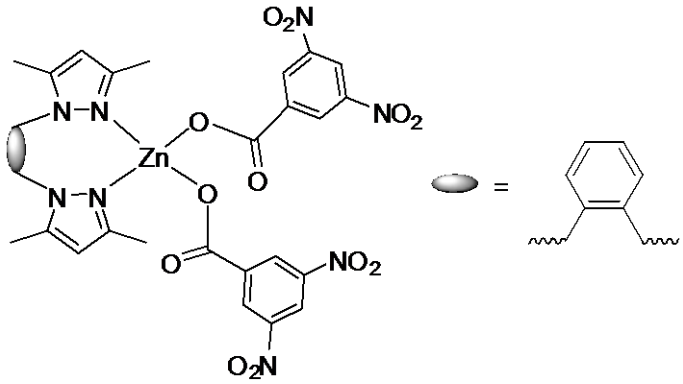

Complex **12** was prepared using [$Zn(OAc)_2$] (0.95 g, 5.16 mmol), 3,5-NO_2-C_6H_3COOH (2.26 g, 0.01 mol) and **L6** (1.50 g, 5.11 mmol). A white solid was obtained after evaporating the solvent in vacuo.

Yield: 2.47 g (61%).

^{1}H NMR (DMSO): δ 2.10 (d, $^6J_{HH}$ = 6.8 Hz, 12H, C<u>H</u>$_3$-Pz); 5.32 (s, 4H, C<u>H</u>$_2$-Pz); 5.88 (s, 2H, Pz-<u>H</u>); 6.53 (d, $^3J_{HH}$ = 3.2 Hz, 2H, α-C<u>H</u>-Ph-Pz); 7.16 (t, $^5J_{HH}$ = 5.6 Hz, 2H, β-C<u>H</u>-Ph-Pz); 8.90 (s, 4H, 2,6-Bz); 8.96 (s, 2H, 4-Bz).

^{13}C{^{1}H} NMR (DMSO): δ 10.6; 13.4; 49.0; 105.1; 120.4; 125.3; 126.7; 127.4; 128.2; 129.0 (d); 135.5; 139.3; 146.3; 148.1; 166.4.

Anal. Calcd for $C_{32}H_{28}N_8O_{12}Zn$: C, 43.40%; H, 3.20%; N, 16.20%. Found: C, 43.17%; H, 3.23%; N, 15.88%.

*[Zn(2-Cl-$C_6H_4COO)_2$**L6**] (**13**)*

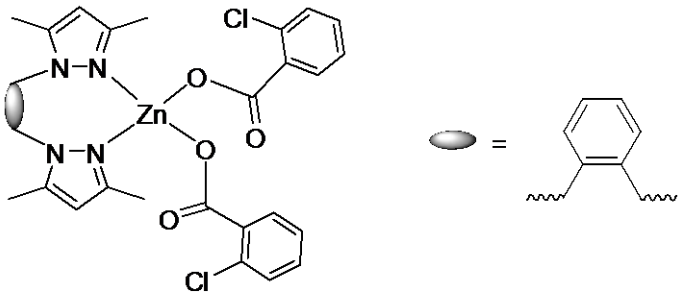

Complex **13** was prepared using [$Zn(OAc)_2$] (0.18 g, 1.00 mmol), 2-Cl-C_6H_4COOH (0.31 g, 2.00 mmol) and **L6** (0.29 g, 1.00 mmol) to afford a white solid after evaporation of the solvent in vacuo.

Yield: 0.45 g (67%).

^{1}H NMR (DMSO): δ 2.10 (2s, 12H, C<u>H</u>$_3$-Pz); 5.33 (s, 4H, -C<u>H</u>$_2$-Pz); 5.89 (s, 2H, Pz-<u>H</u>); 6.52 (m, 2H, α-C<u>H</u>-Ph-Pz); 7.16 (m, 2H, β-C<u>H</u>-Ph-Pz); 7.33 (m, 2H, 3-Bz); 7.40 (m, 2H, 4-Bz); 7.42 (d, $^5J_{HH}$ = 8.8 Hz, 2H, 5-Bz); 7.66 (d, $^3J_{HH}$ = 8.8 Hz, 2H, 6-Bz).

$^{13}C\{^1H\}$ NMR ($CDCl_3$): δ 10.7; 13.5; 49.1; 105.2; 126.7 (d); 127.5; 130.0; 130.5; 130.9; 135.5; 136.4; 139.4; 146.4; 171.1.

ESI-MS m/z (%): 671 $[M]^+$, 7; 694 $[M + Na]^+$, 2.

IR: 1 620 cm^{-1} ($\nu_{C=O}$).

Anal. Calcd for $C_{32}H_{30}Cl_2N_4O_4Zn$: C, 57.29%; H, 4.51%; N, 8.35%. Found: C, 57.23%; H, 4.58%; N, 8.08%.

2.5.2 Synthesis of copper(II) complexes

Complexes **14-23** were synthesized using method B.

*[Cu(C_6H_5COO)$_2$(**L1**)$_2$] (**14**)*

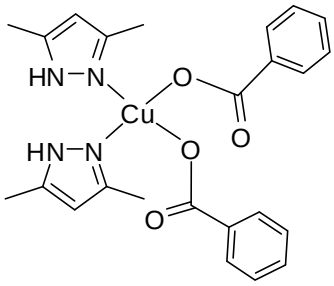

Complex **14** was obtained by reacting [Cu(OAc)$_2$] (0.20 g, 1.00 mmol), C_6H_5COOH (0.24 g, 2.00 mmol) and **L1** (0.19 g, 2.00 mmol). Blue single crystals were harvested from the reaction mixture upon slow evaporation of the solvent.

Yield: 0.41 g (82%).

IR: 1 627 cm^{-1} ($\nu_{C=O}$).

μ_{eff}: 1.67 BM.

ESI-MS m/z (%): 376 [M – C_6H_5COO]$^+$, 25.

Anal. Calcd for $C_{24}H_{26}CuN_4O_4$.(1 mol)H_2O: C, 55.86%; H, 5.47%; N, 10.86%. Found: C, 55.95%; H, 5.20%; N, 10.71%.

*[Cu(3,5-NO_2-C_6H_3COO)$_2$(**L1**)$_2$] (**15**)*

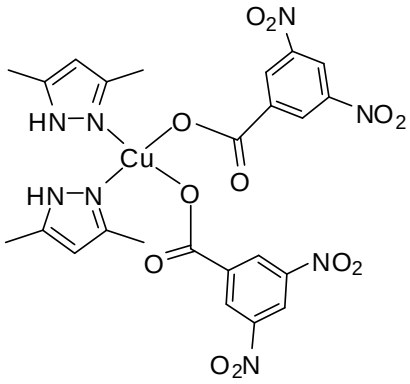

Complex **15** was synthesized using $[Cu(OAc)_2]$ (0.20 g, 1.00 mmol), 3,5-NO_2-C_6H_3COOH (0.43 g, 2.00 mmol) and **L1** (0.19 g, 2.00 mmol). Evaporation of the solvent in vacuo gave **15** as a green solid.

Yield: 0.45 g (66%).

IR: 1 620 cm^{-1} ($\nu_{C=O}$).

Anal. Calcd for $C_{24}H_{22}N_8O_{12}Cu.(1/3\ mol)C_7H_8$: C, 44.63%; H, 3.51%; N, 15.81%. Found: C, 44.85%; H, 3.627%; N, 15.74%.

*$[Cu(4\text{-}OH\text{-}C_6H_4COO)_2(\mathbf{L1})_2]$ (**16**)*

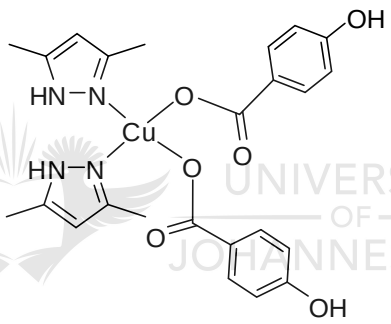

The reaction of $[Cu(OAc)_2]$ (0.20 g, 1.00 mmol), 4-OH-C_6H_4COOH (0.28 g, 2.00 mmol) and **L1** (0.19 g, 2.00 mmol) gave **16**, which was obtained as a green solid upon evaporation of the solvent in vacuo.

Yield: 0.33 g (62%).

IR: 1 674 cm^{-1} ($\nu_{C=O}$).

Anal. Calcd for $C_{24}H_{26}CuN_4O_6.(4\ mol)CH_3OH$: C, 51.09%; H, 6.43%; N, 8.51%. Found: C, 50.74%; H, 5.49%; N, 8.50%.

*[Cu(2-Cl-$C_6H_4COO)_2$(**L1**)$_2$] (**17**)*

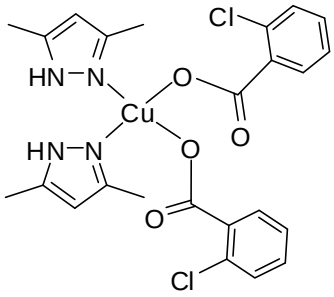

Complex **17** was prepared by reacting [$Cu(OAc)_2$] (0.20 g, 1.00 mmol) and 2-Cl-C_6H_4COOH (0.31 g, 2.00 mmol) with **L1** (0.19 g, 2.00 mmol). Complex **17** was obtained as a green solid by evaporation of the solvent in vacuo.

Yield: 0.31 g (55%).

IR: 1 574 cm^{-1} ($\nu_{C=O}$).

μ_{eff}: 1.87 BM.

Anal. Calcd for $C_{24}H_{24}CuCl_2N_4O_4$: C, 50.85%; H, 4.27%; N, 9.88%. Found: C, 50.79%; H, 4.12%; N, 9.78%.

*[$Cu(C_6H_5COO)_2(C_6H_5COOH)]_2$ (**18**)*

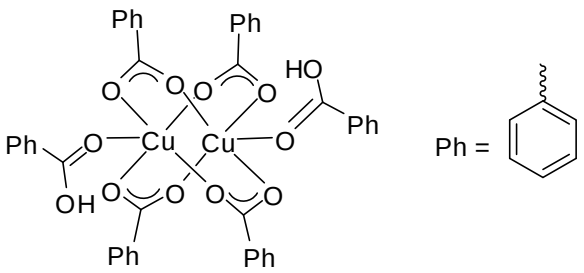

The reaction of [$Cu(OAc)_2$] (0.20 g, 1.00 mmol), C_6H_5COOH (0.24 g, 2.00 mmol) and **L2** (0.44 g, 2.00 mmol) resulted in a green solution of **18**. Upon evaporation of the solvent in

vacuo, a mixture of green and white solids was obtained. The solids were redissolved in methanol and slow evaporation of the solvent led to the crystallization of green solids. Compound **18** was isolated by filtration and was dried in vacuo.

Yield: 0.60 g (35%).

IR: 1 615 cm^{-1} ($\nu_{C=O}$).

Anal. Calcd for $C_{42}H_{32}Cu_2O_{12}$.(1 mol)CH_3OH: C, 58.11%; H, 4.20%. Found: C, 58.13%; H, 3.687%.

*[Cu(2-Cl-$C_6H_4COO)_2$(**L3**)$_2$] (**19**)*

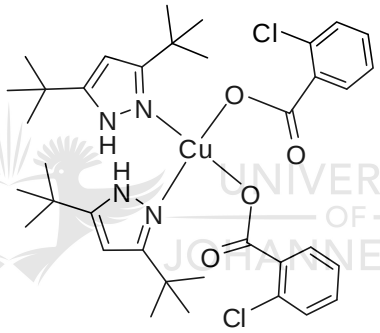

Complex **19** was synthesized using [$Cu(OAc)_2$] (0.20 g, 1.0 mmol), 2-Cl-C_6H_4COOH (0.31 g, 2.0 mmol) and **L3** (0.36 g, 2.0 mmol). Single blue crystals were obtained upon slow evaporation of the solvent.

Yield: 0.51 g (69%).

IR: 1 637 cm^{-1} ($\nu_{C=O}$).

Anal. Calcd for $C_{36}H_{48}CuCl_2N_4O_4$.(4 mol)CH_3OH: C, 55.64%; H, 7.47%; N, 6.49%. Found: C, 55.72%; H, 6.11%; N, 5.99%.

*[Cu(C_6H_5COO)$_2$**L4**] (**20**)*

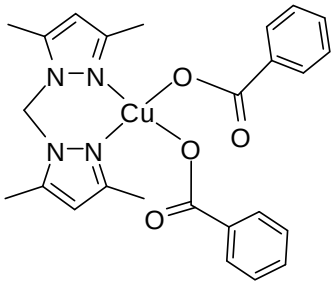

Complex **20** was obtained by reacting [Cu(OAc)$_2$] (0.20 g, 1.00 mmol) with C_6H_5COOH (0.24 g, 1.00 mmol) and **L4** (0.20 g, 1.00 mmol). After removal of the solvent in vacuo, **20** was isolated as a blue solid.

Yield: 0.29 g (56%).

IR: 1 628 cm^{-1} ($\nu_{C=O}$).

ESI-MS m/z (%): 267 [M – 2 C_6H_5COO]$^+$, 95.

Anal. Calcd for $C_{25}H_{26}N_4O_4Cu$.(2 mol)CH_3OH: C, 56.48%; H, 5.97%; N, 9.76%. Found: C, 56.36%; H, 5.429%; N, 9.32%.

*[Cu(2-Cl-C_6H_4COO)$_2$**L4**] (**21**)*

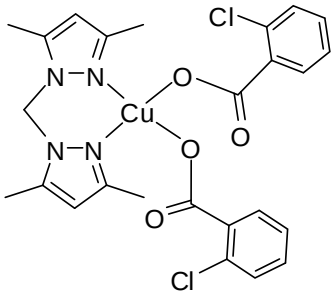

Complex **21** was synthesized using [$Cu(OAc)_2$] (0.20 g, 1.00 mmol), 2-Cl-C_6H_4COOH (0.31 g, 2.00 mmol) and **L4** (0.20 g, 1.00 mmol). A blue solid was obtained after removal of the solvent in vacuo.

Yield: 0.32 g (55%).

IR: 1 627 cm^{-1} ($\nu_{C=O}$).

Anal. Calcd for $C_{25}H_{24}Cl_2N_4O_4Cu$: C, 50.12%; H, 5.20%; N, 8.50%. Found: C, 50.64%; H, 4.901%; N, 8.08%.

$[Cu(C_6H_5COO)_2DMSO]_2$ ***(22)***

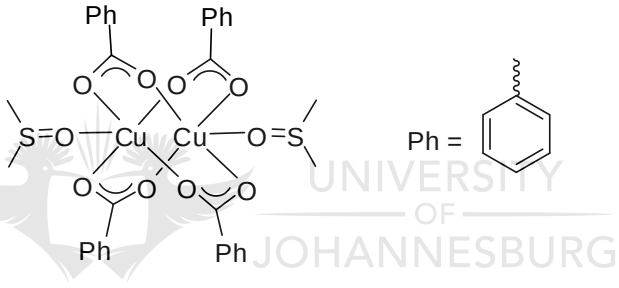

Reaction of [$Cu(OAc)_2$] (0.20 g, 1.00 mmol), C_6H_5COOH (0.24 g, 2.00 mmol) and **L5** (0.45 g, 1.00 mmol) resulted in the formation of some white solid during the reaction. After 2 h, the mixture was filtered and the green filtrate was evaporated in vacuo. A mixture of green and white solids was obtained. Redissolving the solids in DMSO followed by slow evaporation of the solvent gave green crystals of **22**.

Yield: 0.22 g (57%).

IR: 1 615 cm^{-1} ($\nu_{C=O}$).

Anal. Calcd for $C_{16}H_{16}CuO_5S$: C, 50.06%; H, 4.20%; S, 8.35%. Found: C, 49.72%; H, 4.324%; S, 7.957%.

*[Cu(C_6H_5COO)$_2$**L6**]$_2$ (**23**)*

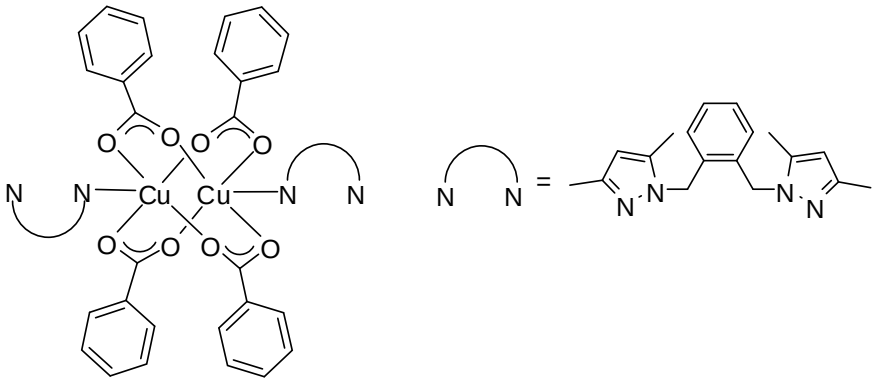

Complex **23** was prepared using [Cu(OAc)$_2$] (0.20 g, 1.00 mmol), C_6H_5COOH (0.24 g, 2.00 mmol) and **L6** (0.29 g, 1.00 mmol) in toluene and methanol mixture. During the reaction, a green solid precipitated from the reaction mixture. Compound **23** was then isolated by filtration and dried in vacuo. The solid was redissolved in DMSO, from which single green crystals grew upon slow evaporation of the solvent.

Yield: 0.34 g (57%).

IR: 1 627 cm^{-1} ($\nu_{C=O}$).

Anal. Calcd for $C_{46}H_{42}Cu_2N_4O_8$.(1 mol)CH_3OH: C, 60.18%; H, 4.94%; N, 5.97%. Found: C, 59.20%; H, 4.709%; N, 6.08%.

*[Cu(2-Cl-$C_6H_4COO)_2$**L6**]$_{2n}$* ***(24)***

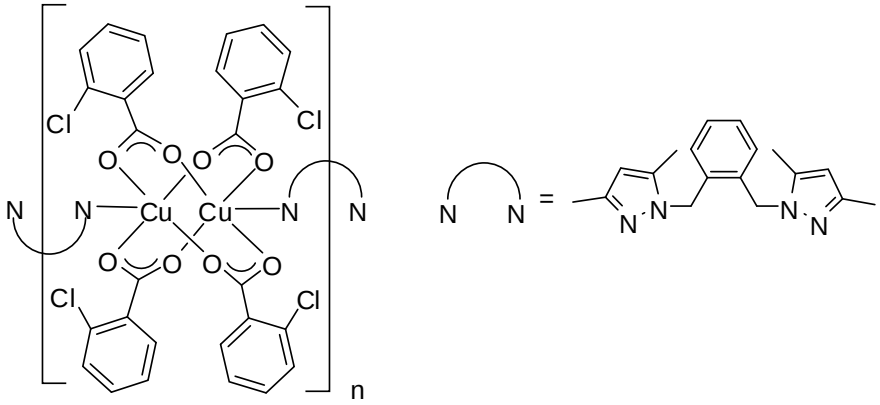

Complex **24** was synthesized using [$Cu(OAc)_2$] (0.20 g, 1.00 mmol), 2-Cl-C_6H_4COOH (0.31 g, 2.00 mmol) and **L6** (0.29 g, 1.00 mmol) in methanol (15 mL) and toluene (5 mL), which afforded green crystals after slow evaporation of the solvent.

Yield: 0.44 g (66%).

IR: 1 631 cm^{-1} ($\nu_{C=O}$)

μ_{eff}: 2.308 BM.

ESI-MS m/z (%): 692 $[M + Na]^+$, 20; 512 $[M – 2\text{-Cl-}C_6H_4COO]^+$, 100.

Anal. Calcd for $C_{32}H_{30}Cl_2CuN_4O_4.(1/2\ mol)C_7H_8$: C, 59.62%; H, 4.79%; N, 7.83%. Found: C, 59.72%; H, 4.65%; N, 8.07%.

Compounds **25** and **26** were synthesized following the procedures for method A as a means of studying the effect of the solvent on the structure of the product.

*[Cu(4-OH-C_6H_4COO)$_2$**L6**]$_2$ (**25**)*

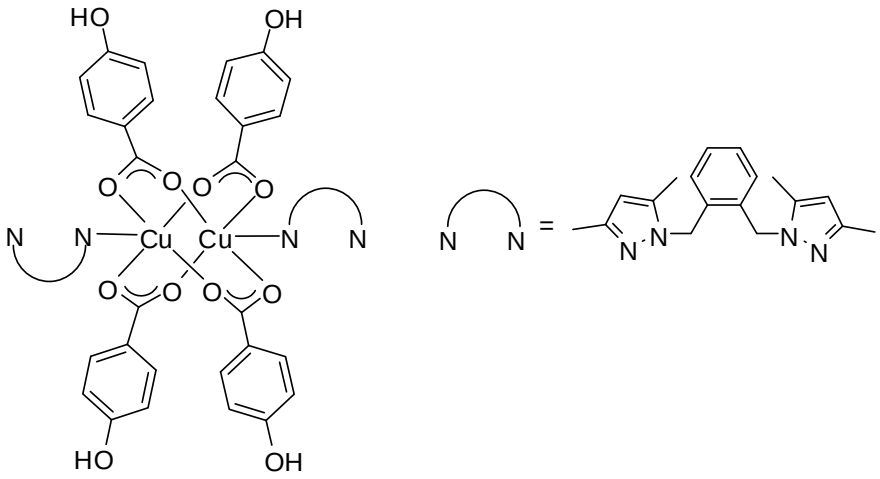

Method A was used to react [Cu(OAc)$_2$] (0.20 g, 1.00 mmol), 4-OH-C_6H_4COOH (0.28 g, 2.00 mmol) and **L6** (0.29 g, 1.00 mmol) in methanol (50 mL). Complex **25** was obtained as green solid upon evaporation of methanol in vacuo. Green crystals, suitable for X-ray analysis, were obtained after slow evaporation of a CH_2Cl_2 solution of **25**.

Yield: 0.43 g (68%).

ESI-MS m/z (%): 494 [M – 4-OH-C_6H_4COO]$^+$, 100.

IR: 1 625 cm^{-1} ($\nu_{C=O}$).

μ_{eff}: 2.826 BM.

Anal. Calcd for $C_{32}H_{32}CuN_4O_6$.(3/4 mol)CH_2Cl_2: C, 56.53%; H, 4.85%; N, 8.05%. Found: C, 56.98%; H, 5.36%; N, 7.56%.

*[Cu(3,5-NO_2-$C_6H_3COO)_2$**L6**]$_n$ (**26**)*

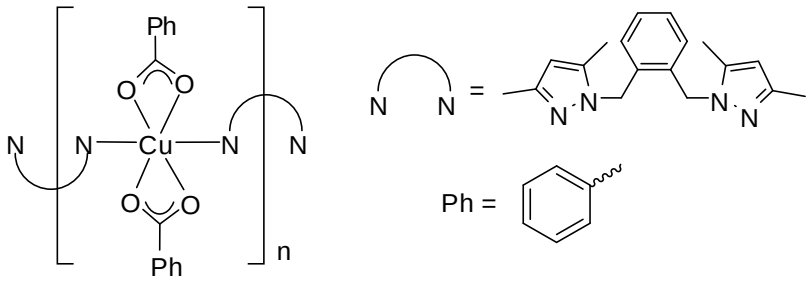

Complex **26** was obtained by reacting [$Cu(OAc)_2$] (0.20 g, 1.00 mmol), 3,5-NO_2-C_6H_3COOH (0.43 g, 2.00 mmol) and **L6** (0.29 g, 1.00 mmol) in methanol (50 mL). A purple precipitate was observed in the reaction mixture and the precipitate was isolated by filtration. The crude compound was dissolved in DMSO and single crystals were obtained upon slow evaporation of the solvent.

Yield: 0.47 g (78%).

μ_{eff}: 1.75 BM.

ESI-MS m/z (%): 568 [M - 3,5-NO_2-C_6H_3COO]$^+$, 18.

IR: 1 624 cm^{-1} ($\nu_{C=O}$).

Anal. Calcd for $C_{32}H_{28}CuN_8O_{12}$.(1 mol)CH_3OH: C, 48.80%; H, 3.97%; N, 13.80%. Found: C, 48.64%; H, 3.37%; N, 14.02%.

2.6 Results and discussion

2.6.1 Preparation and characterization of L3

Compound **L3** was prepared by heating the two liquid reagents, 2,2`,6,6`-tetramethyl-3,5-heptanedione and hydrazine monohydrate at 70 ^oC. The resultant product solidified after 2 h. The conventional method used to synthesize **L3** involves refluxing of the two reagents in ethanol for four days, after which the product was isolated by filtration and evaporation of the

filtrate.[86] The current method represents not only a simple process to prepare **L3**, but it is also a green process.

2.6.2 Preparation and characterization of metal complexes

A number of copper and zinc complexes with three types of pyrazolyl compounds (Figure 2.1) and four different benzoic acids (Figure 2.2) were synthesized using two methods, A and B, and metal(II) acetates in methanol and/or toluene. The mole ratios of reactants were dependent on the type of pyrazole used. Metal(II) acetates, benzoic acids and pyrazoles were reacted in mole ratios of 1:2:2 for ligands **L1**, **L2** and **L3** and 1:2:1 for **L4**, **L5** and **L6**.

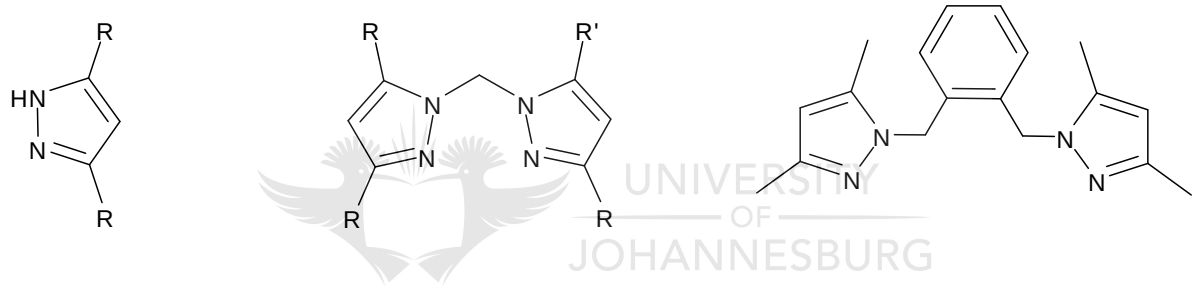

R = CH_3 (**L1**)
R = C_6H_5 (**L2**),
R = $C(CH_3)_3$ (**L3**)

R = CH_3 (**L4**),
R = C_6H_5 (**L5**)

L6

Figure 2.1. Structures of the pyrazolyl ligands used.

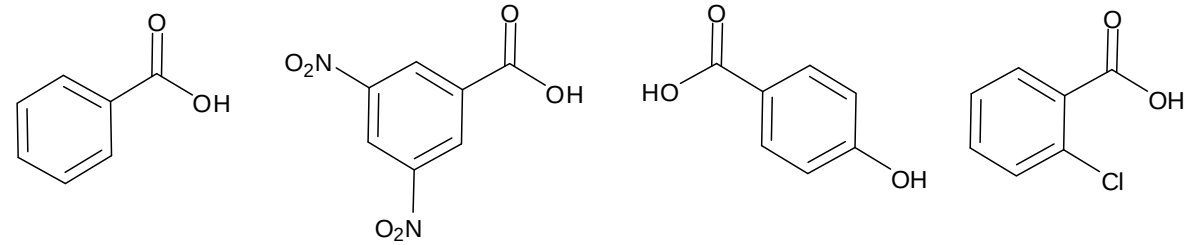

C_6H_5COOH | 3,5-NO_2-C_6H_3COOH | 4-OH-C_6H_4COOH | 2-Cl-C_6H_4COOH

Figure 2.2. Structures of the benzoic acids used.

[86] Coispean, G.; Elguero, J. *Bull. Soc. Chim. Fr.* **1970**, 2717.

2.6.2.1 Method A

Method A involves overnight refluxing of the reactants in one pot in which the metal(II) acetate and the benzoic acid were first stirred under reflux for 5 h. In the process the benzoic acid gets deprotonated forming a metal(II) benzoate and acetic acid. When the pyrazole-based compound is added to the reaction mixture, it binds to the metal. Scheme 2.1 gives an outline of the reagents involved and the expected complexes.

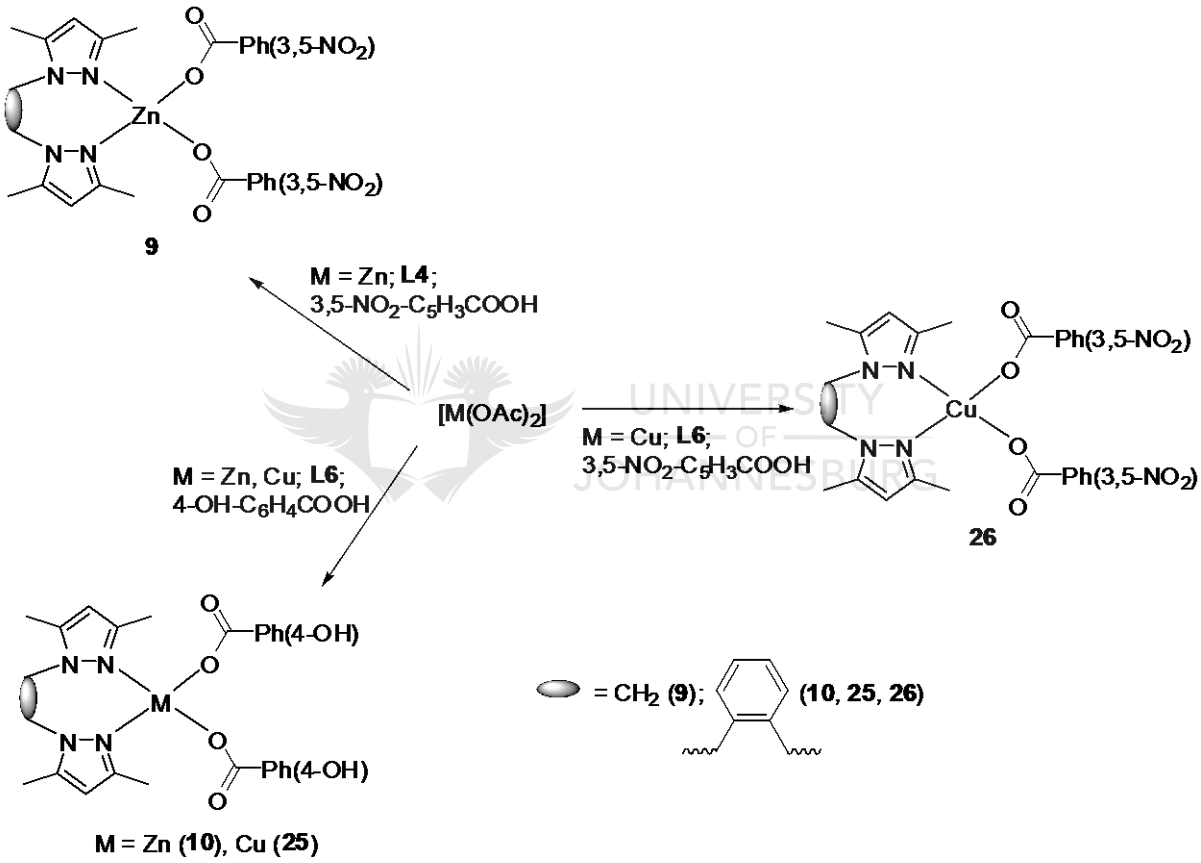

Scheme 2.1. Complexation reaction following method A.

Zinc products were either pale yellow or white in colour; while the colour of the copper products varied from blue to green to purple. Most products obtained were soluble in methanol and/or toluene, while others were only soluble in DMSO and/or CH_2Cl_2. Analytical techniques such as NMR, IR, mass spectrometry and elemental analysis, were used to

characterize these compounds. NMR spectrometry was used only for the zinc(II) products as the copper complexes were paramagnetic.

2.6.2.1.1 Characterization of Zn complexes synthesized by method A

Complex **9** is used as a typical zinc(II) product to analyze the ^{1}H NMR spectrum of the zinc complexes (Figure 2.3) as evidence of formation of the expected product. The spectrum shows significant shifts in the peaks for the protons of **L4** as well as the benzoate protons. For this compound, the peaks at 2.37 and 2.46 ppm corresponding to the methyl protons of **L4** shifted from 2.15 and 2.38 ppm for free **L4**, respectively. Also, the protons of the bridging CH_2 were found at 6.07 ppm, compared to 5.76 ppm for uncoordinated **L4**. The protons on the pyrazole rings also showed shifts to 6.53 from 6.03 ppm of the free **L4**.

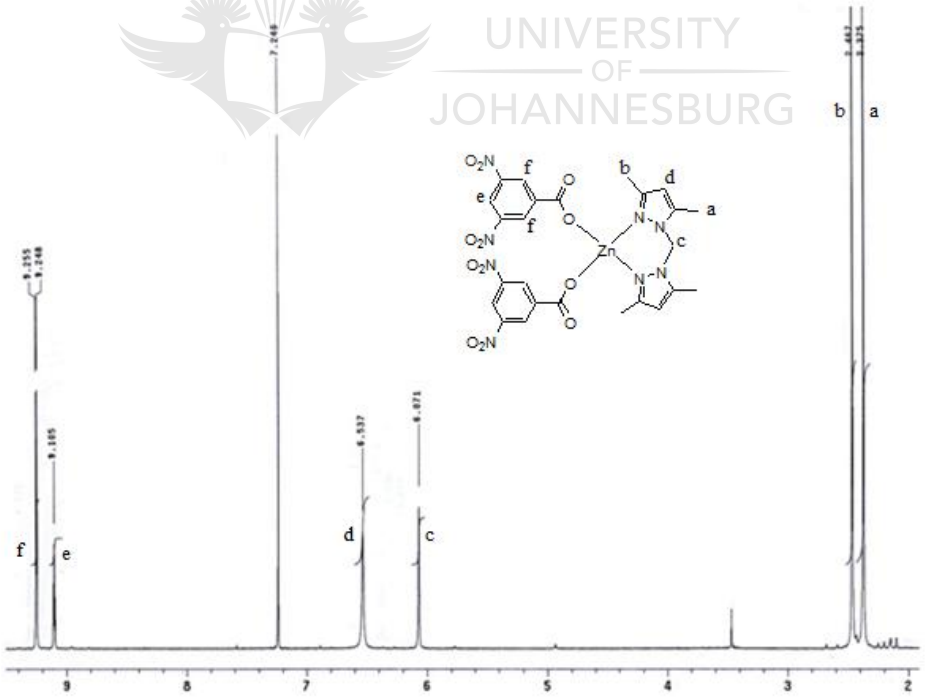

Figure 2.3. ^{1}H NMR spectrum of **1** obtained in $CDCl_3$.

Furthermore, the peaks at 9.10 and 9.25 ppm, which correspond to the protons of 3,5-NO_2-C_6H_3COO shifted from 9.00 and 8.88 ppm for 3,5-NO_2-C_6H_3COOH, respectively. The peaks for the protons *ortho* to the benzene ring in the carboxylate group moved from 8.88 ppm for 3,5-NO_2-C_6H_3COOH to 9.25 ppm for the complex. Similarly, the *para* protons in the carboxylate ligand shifted from 9.00 ppm to 9.11 ppm in the complex. These shifts in the protons of the ligands give evidence of their complexation with the zinc.

Mass spectrometry was also run for most of the compounds and from the spectrum of complex **9**, a peak at m/z = 690 was observed. This value corresponds to the molecular ion of complex **9**. Moreover, the IR of **9** shows a band at 1 645 cm^{-1} that corresponds to the C=O bond of 3,5-NO_2-C_6H_3COO, compared to 1 699 cm^{-1} for 3,5-NO_2-C_6H_3COOH. Hence, the shift in the band can be attributed to the effect of the metal on the C=O bond. The last characterization technique used was elemental analysis, which provided proof of formation of pure **9** since the found and calculated values are comparable.

2.6.2.1.2 Characterization of Cu complexes synthesized by method A

The products obtained from the reaction of copper(II) acetate using method A were analyzed by different techniques. Complex **25** is used as an example of how the characterization process was carried out. IR spectrum of **25** gave a band at 1 625 cm^{-1}, indicating the effect of the metal on the C=O stretching of the benzoate group, which in the free benzoic acid appears at 1698 cm^{-1}. The absence of OH stretching band, typically observed around 3 000 cm^{-1}, indicates the deprotonation of the acid and hence possible bonding of the oxygen to the copper. Thus, from the IR spectrum of the product, evidence of the coordination of the benzoate groups and **L6** to the metal was obtained.

Furthermore, the mass spectrum of the product showed a peak at m/z = 494 that corresponds to the mass of the molecular ion after the loss of one benzoate group. Lastly, the element analysis of the product showed good agreement between the found and calculated values confirms the composition of **25** as formulated.

In trying to synthesize the copper analogue of **9**, a glue-like blue compound was obtained, but attempts to clean the product to a powder or crystal were unsuccessful.

2.6.2.2 Method B

The second method used for complexation is a 1 h, room temperature reaction. This method has been previously been used by Baruah's group in order to coordinate benzoic acids and pyrazoles to zinc(II) and copper(II). Similar to method A, method B consists of a two step one pot reaction. Firstly, the metal(II) acetate and the appropriate benzoic acid were stirred in methanol for 30 min. During this process, a displacement reaction is expected to take place, involving the simultaneous deprotonation of the benzoic acid and the coordination of the benzoate ion to the metal centre and breaking of the metal-acetate bond. Thus, a freed acetate ion gets protonated to acetic acid. Then, a toluene solution of ligand **L** is added to the stirring mixture, allowing the solution to stir for another 30 min. According to Baruah, the solvent system is crucial in getting the right type of product. Depending on the solvent used, either the mononuclear or the binuclear complex is formed. The former compound is obtained when the reaction is carried out in a mixed solvent of methanol and toluene; the binuclear complex is formed when the same reaction is carried out in dimethylformamide. On the other hand, the binuclear compound can also be formed from the mononuclear one on dissolution in dimethylformamide. It was suggested that during the conversion, the solvent molecule gets coordinated to the metal centre, leading to the formation of a five coordinated species. This

compound then helps the mononuclear complex to lose one molecule of carboxylic acid, resulting in the binuclear complex.

2.6.2.2.1 L1 complexes of metal(II) benzoate

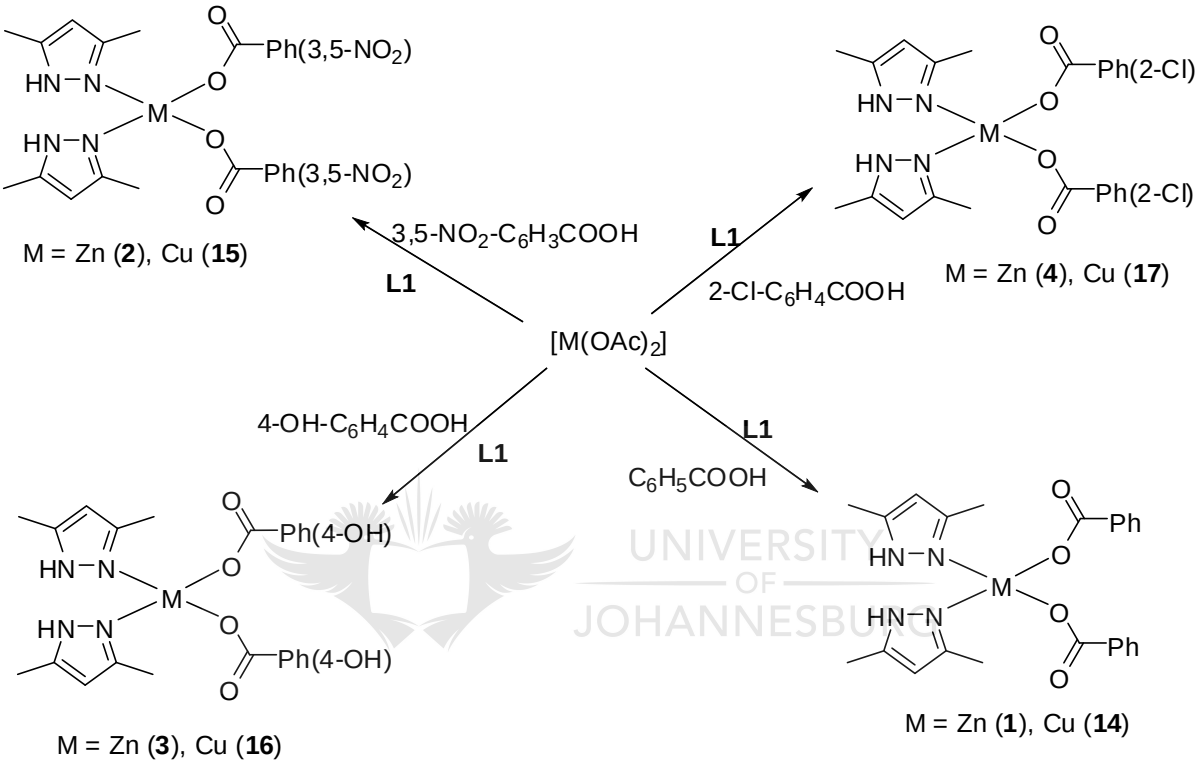

Scheme 2.2. Synthesis of **L1** metal(II) benzoate complexes.

The first ligand type used was **L1** and its reactions with metal(II) acetates and benzoic acids were expected to give mononuclear complexes as depicted in Scheme 2.2. A typical example of the complexes formed is **1**. From the ^{1}H NMR spectrum of **1**, there is clear indication of the formation of the expected product as the peaks corresponding to **L1** as well as the benzoate protons are present and shifted. Thus, the protons of the two methyl groups of **L1** appear as a broad singlet at 2.24 ppm instead of two singlets, due to the effect of the zinc on the ligand. A similar observation was made for the benzoate group, where the *ortho* protons

of C_6H_5COO, appear as a doublet at 8.18 ppm in **1**, while these normally come at 8.11 ppm in the acid. In addition to the NMR spectrum, the elemental analysis of the product shows good agreement between the found and calculated values.

2.6.2.2.2 Complexes of L4 metal(II) benzoate

Several zinc(II) and copper(II) complexes of the different benzoates were made to react with **L4** using method B (Scheme 2.3). But this ligand system was not as successful as the **L1** system. Most of the products were obtained as glue-like compound, which could not be cleaned. A similar observation was obtained previously when the synthesis of the copper analogue of complex **9** was attempted. A possible explanation for the failure in getting the expected complexes can be due to the methylene linker on **L4**. The presence of this linker brings a major change in the orientation of the pyrazolyl ligand around the metal centre. Also, the glue texture of the products obtained might be due to solvents and/or water trapped in the compound, possibly because of the hygroscopic nature of the compound formed.

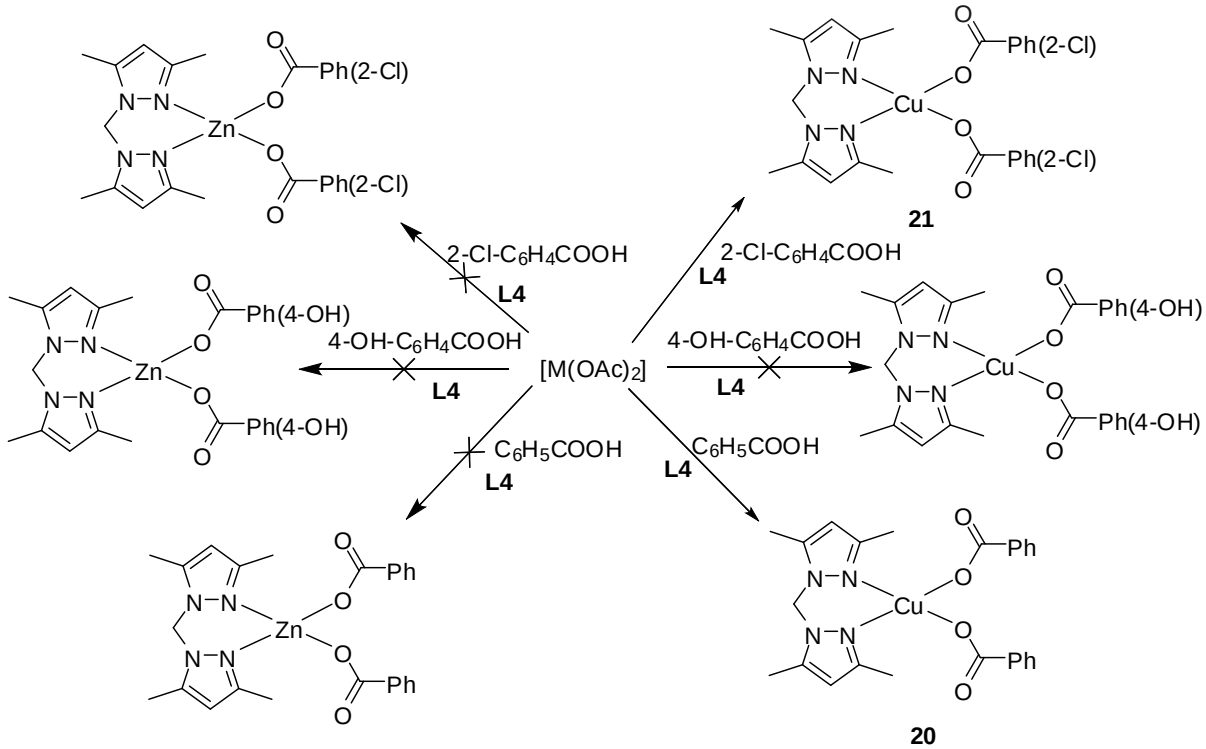

Scheme 2.3. Synthesis of **L4** metal(II) benzoate complexes.

Complex **21** is one of the two complexes that were successfully synthesized from **L4**. The IR spectrum of **21** shows a band at 1 627 cm^{-1} for the C=O stretching of the benzoate ion. In addition to the IR, the elemental analysis of the product provides confirmation of the coordination of the ligands to the copper(II) centre in that the found and calculated values for the expected complex are very close to each other.

2.6.2.2.3 Complexes of L6 metal(II) benzoate

Method B was used to synthesize four complexes of **L6**; the expected complexes are illustrated in Scheme 2.4.

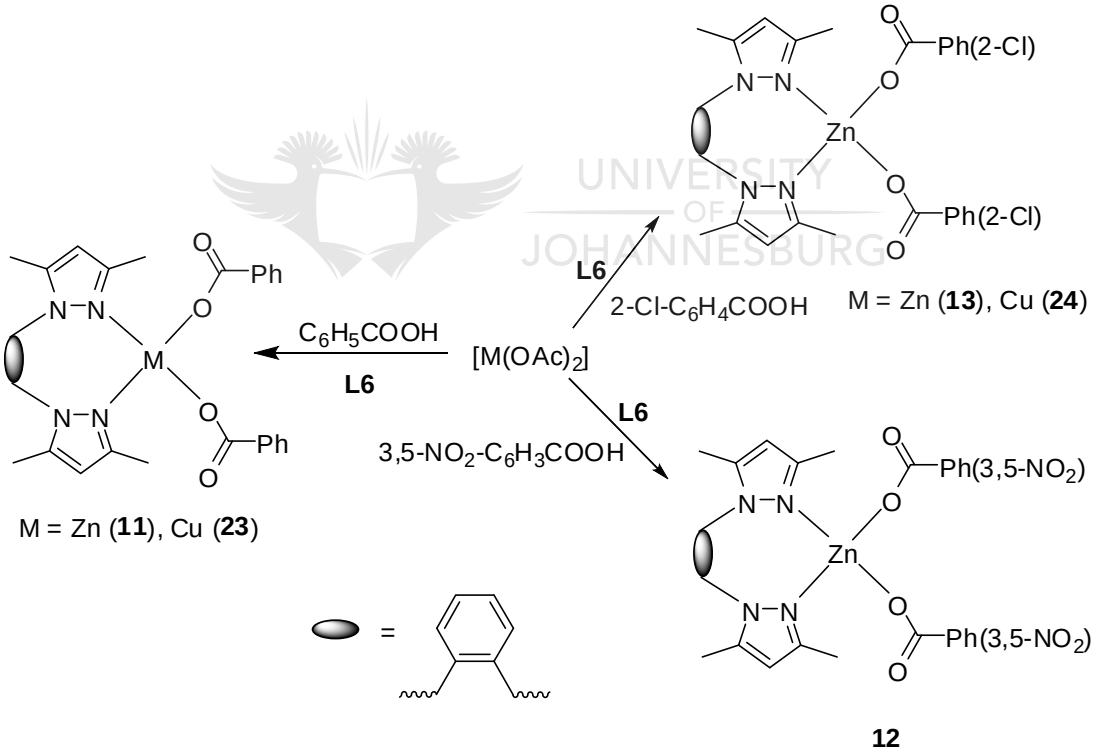

Scheme 2.4. Synthesis of **L6** metal(II) benzoate complexes.

One typical complex of this system is complex **12**. The ^{1}H NMR spectrum of the product shows that the ligands, **L6** as well as 3,5-NO_2-C_6H_3COO, are under the influence of zinc

metal. Thus, the methyl groups on **L6** are no longer two singlets, as in the unreacted compound, but appear as a doublet in the ^{1}H NMR spectrum of the product. A similar observation was made regarding the protons of the benzoate that appear as a singlet peak. In addition to the NMR data, the elemental analysis of the product shows a good correlation between the found and calculated values.

Since method B seems to have worked for most of the complexes that were attempted to be made, it was hoped that by applying this method to ligands **L2**, **L3** and **L5**, it might be possible to get the expected complexation products. These compounds are slightly modified versions of **L1** and **L4**.

2.6.2.2.4 Complexes of L2 metal(II) benzoate

Reaction of **L2** with metal(II) acetate and different benzoic acids is expected to give the products in Scheme 2.5. The zinc complexes were formed more readily than their copper analogues. Hence, only one copper product was obtained from this reaction, the structure of which did not turn out to be the expected one.

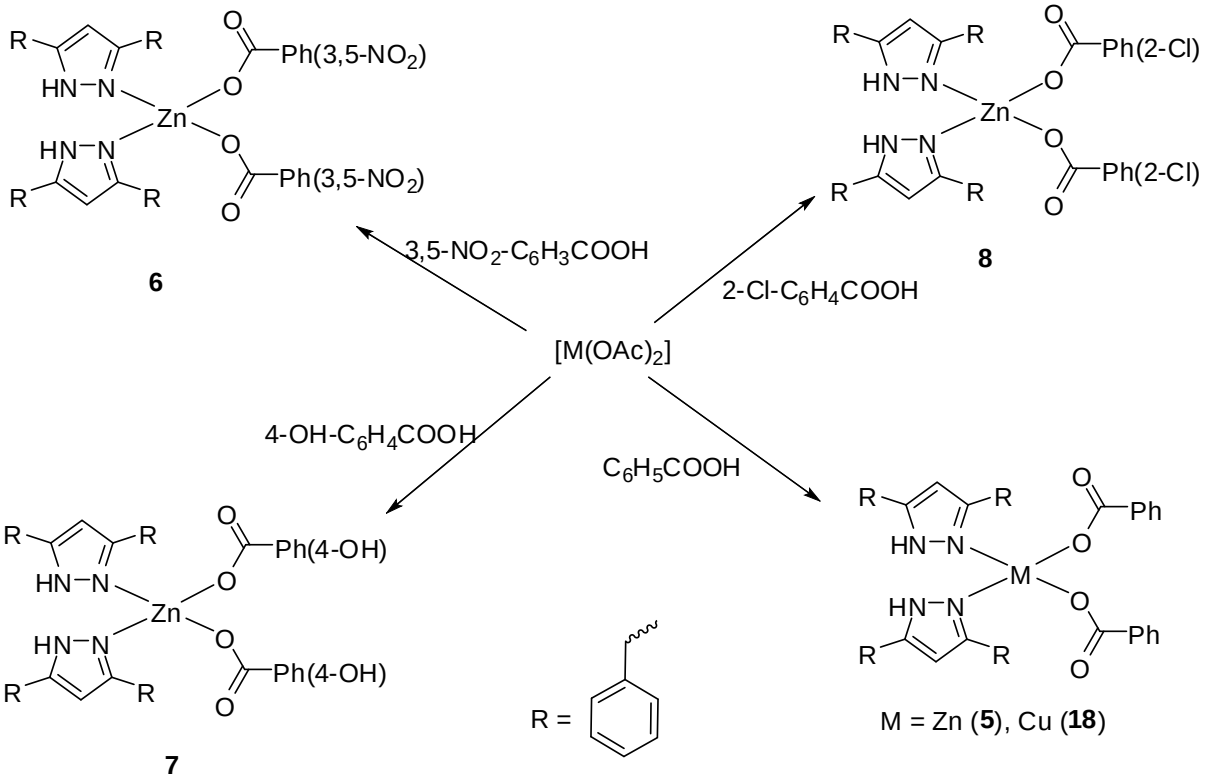

Scheme 2.5. Synthesis of **L2** metal(II) benzoate complexes.

In an attempt to synthesize **18**, the reaction was carried out, after which the solvent was allowed to evaporate slowly. During this process, white precipitates started forming on top of the solution, while at the same time some green crystals were growing at the bottom of the flask. The green crystals were harvested for X-ray analysis. The IR spectrum and the elemental analysis of the green solid showed that the benzoate groups were coordinated to the copper, but not the pyrazole ligand. Hence, the expected product was not formed, but from literature, there was a high possibility that the copper(II) benzoate adopted a paddle wheel geometry.[66] When extended to other benzoic acids, the complexation reaction failed.

Encouraged by the interesting behaviour of copper towards **L2**, the influence of the nature of the pyrazolyl compound on complexation was further examined. For this target, zinc(II) complexes of **L2** were prepared under the same conditions. From the characterization of the

products, the expected complexes were formed. A typical ^{1}H NMR spectrum, of complex **6**, shows the shifts in the peaks for the protons of 3,5-NO_2-C_6H_3COO and **L2** (Figure 2.4). Moreover, the elemental analysis of the product shows that the found and calculated values agree. Hence, contrary to copper, the coordination of **L2** to zinc is feasible.

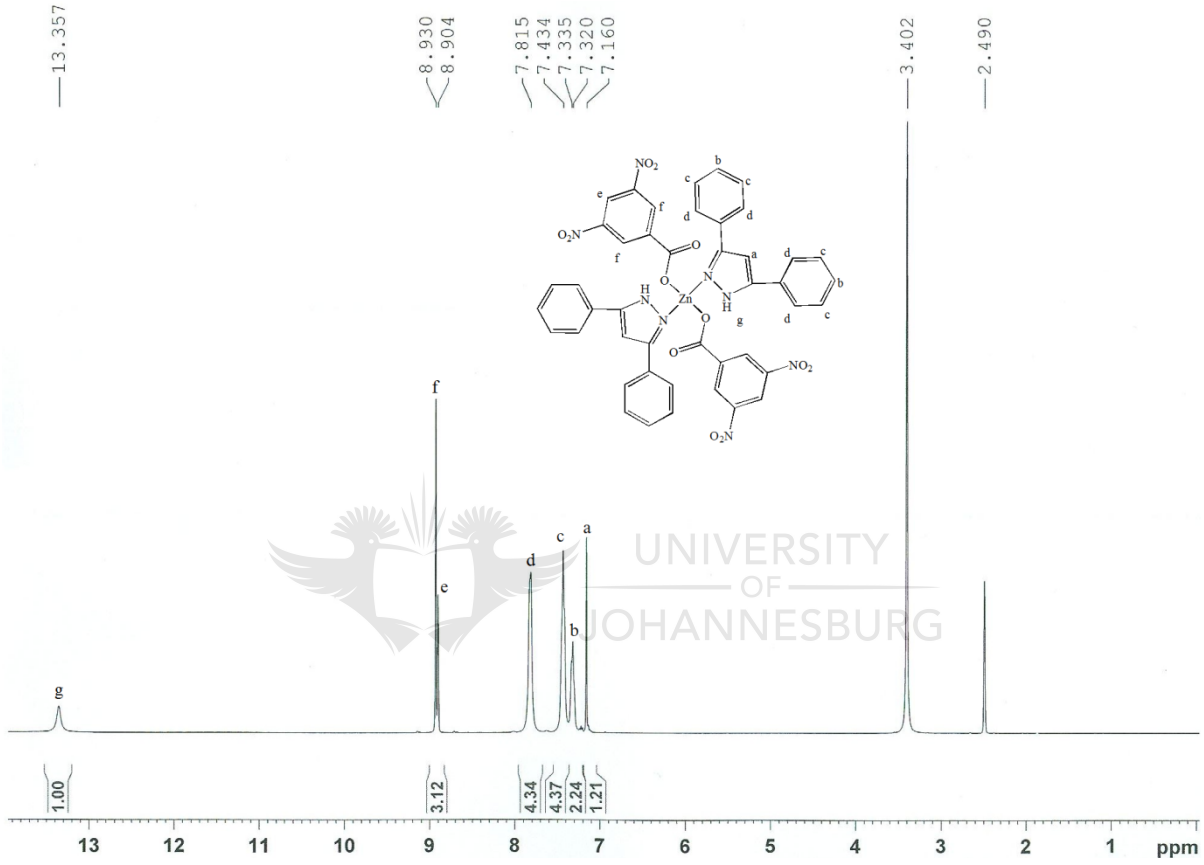

Figure 2.4. ^{1}H NMR spectrum of **6** in $CDCl_3$.

2.6.2.2.5 Complexes of L3 metal(II) benzoate and L5 metal(II) benzoate

Compounds **L3** and **L5**, the tertiary-butyl analogue of **L1** and the phenyl analogues of **L4**, respectively, were also used in an attempt to get the expected products in Scheme 2.6.

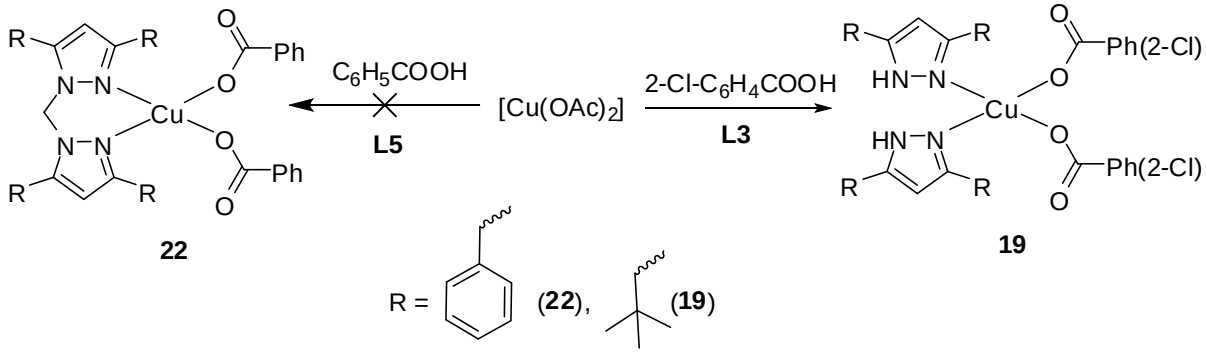

Scheme 2.6. Synthesis of **L3** and of **L5** copper(II) benzoate complexes.

In order to make complex **22**, reaction of $[Cu(OAc)_2]$, C_6H_5COOH and **L5** was carried out. At the end of the reaction time, the solvent was removed in vacuo to give a green solid, which was then dissolved in DMSO. Slow evaporation of the DMSO gave rise to similar observations made for complex **18**: white precipitates were formed along with green crystals. The IR and elemental analysis of the green crystals show that, like complex **18**, complex **21** was found to be a copper(II) benzoate complex, without any pyrazole ligand bonded to the copper.

Complex **19** was the last one synthesized using 2-Cl-C_6H_4COOH and **L3**. The data obtained from IR spectrum and elemental analysis show that the expected product was formed, which is a tetrahedral copper(II) complex, coordinated to two 2-Cl-C_6H_4COO groups through the oxygen atoms and two **L3** ligands. Hence, unlike complexes **18** and **22**, **19** could be synthesized to get the expected product. A possible explanation might be that the paddle wheel structure is already formed during the first step of the reaction. Since the pyrazole ligand is only added last, it has to get close enough to the metal centre for any interaction. In the case of **L2** and **L5**, the presence of the phenyl rings on the pyrazole ring makes the ligand more bulky than **L3**, which has tertiary-butyl groups as substituents on the pyrazole rings.

The smaller **L3** is therefore able to interact with the copper and hence to form a bond with the metal, while **L2** and **L5** were not successful in doing that.

2.6.3 Molecular structure determination

12 crystal structures have been obtained for the complexes synthesized, out of which three are zinc complexes. The crystal structures were attached to the tip of a MiTeGen MicroMount©. Each crystal was mounted in a stream of cold nitrogen at 100(1) K and centered in the X-ray beam by using a video camera. The crystal evaluation and data collection were performed on a Bruker Quazar SMART APEXII diffractometer with Cu for **26** and Mo all other complexes. The crystallographic parameters for these complexes are given in Tables 2.1, 2.2 and 2.3.

2.6.3.1 Zinc crystal structures

The crystal structure obtained for complex **6** (Figure 2.5) shows that it is monometallic tetrahedral zinc(II) coordinated to two **L2** ligands through the nitrogen atoms and to two benzoate groups through two oxygen atoms.

Table 2.1. Crystal data and structure refinement for complexes **6**, **9**, **11** and **14**.

	6	**9**	**11**	**14**
Empirical formula	$C_{44}H_{30}N_8O_{12}Zn$	$C_{25}H_{22}N_8O_{12}Zn$	$C_{47}H_{46}N_4O_9Zn_2$	$C_{24}H_{26}CuN_4O_4$
Formula weight	928.13	691.88	941.66	498.03
Temperature	100(2) K	100(1) K	100(2) K	100(2) K
Wavelength	0.71073 Å	0.71073 Å	0.71073 Å	0.71073 Å
Crystal system	Monoclinic	Orthorhombic	Triclinic	Monoclinic
Space group	P21/c	Pbca	P-1	$P2_1/n$
a	13.9192(8) Å	19.3372(6) Å	11.7904(9) Å	15.968(12) Å
b	13.7516(7) Å	14.7646(5) Å	13.5706(10) Å	10.809(9) Å
c	21.5005(12) Å	19.7508(7) Å	15.0723(19) Å	16.095(13) Å
α	90°	90°	104.927(2)°	90°
β	103.4660(10)°	90°	97.351(2)°	108.44(5)°
γ	90°	90°	107.660(2)°	90°
Volume	4002.3(4) $Å^3$	5639.0(3) $Å^3$	2164.1(4) $Å^3$	2635(4) $Å^3$
Z	4	8	2	4
Density (calculated)	1.540 Mg/m^3	1.630 Mg/m^3	1.445 Mg/m^3	1.255 Mg/m^3
Absorption coefficient	0.693 mm^{-1}	0.952 mm^{-1}	1.170 mm^{-1}	0.862 mm^{-1}
F(000)	1904	2832	976	1036
Crystal size	0.21 x 0.11 x 0.04 mm^3	0.25 x 0.20 x 0.10 mm^3	0.26 x 0.16 x 0.09 mm^3	0.51 x 0.19 x 0.13 mm^3
Theta range for data collection	1.50 to 28.34°	2.02 to 25.73°	1.66 to 28.37°	2.45 to 27.09°
Index ranges	-18<=h<=18, -17<=k<=18, -28<=l<=28	-23<=h<=23, -17<=k<=18, -24<=l<=24	-15<=h<=15, -18<=k<=18, -20<=l<=20	-20<=h<=20, -13<=k<=13, -20<=l<=20
Reflections collected	77200	91479	61915	34499
Independent reflections	9969 [R(int) = 0.0689]	5332 [R(int) = 0.0655]	10788 [R(int) = 0.0358]	5755 [R(int) = 0.0334]
Completeness to theta = 25.00°	99.7 %	99.2 %	99.7 %	99.0 %
Absorption correction	Semi-empirical from equivalents	Multi-scan with SADABS	Semi-empirical equivalents	Numerical with SADABS
Max. and min. transmission	0.9728 and 0.8682	0.9108 and 0.7968	0.9020 and 0.7507	0.8954 and 0.6670
Refinement method	Full-matrix least-squares on F^2	Full-matrix least-squares on F^2	Full-matrix least-squares on F^2	Full-matrix least-squares on F^2
Data / restraints / parameters	9969 / 7 / 586	5332 / 0 / 419	10788 / 0 / 565	5755 / 0 / 302
Goodness-of-fit on F^2	1.030	0.972	1.022	0.981
Final R indices [I>2sigma(I)]	R1 = 0.0402, wR2 = 0.0838	R1 = 0.0414, wR2 = 0.1010	R1 = 0.0348, wR2 = 0.0835	R1 = 0.0303, wR2 = 0.0827
R indices (all data)	R1 = 0.0656, wR2 = 0.0947	R1 = 0.0547, wR2 = 0.1104	R1 = 0.0456, wR2 = 0.0901	R1 = 0.0349, wR2 = 0.0855
Largest diff. peak and hole	0.529 and -0.582 e.$Å^{-3}$	0.994 and -0.487 e.$Å^{-3}$	1.858 and -1.410 e.$Å^{-3}$	0.386 and -0.383 e.$Å^{-3}$

Table 2.2. Crystal data and structure refinement for complexes **17**-**19** and **22**

	17	**18**	**19**	**22**
Empirical formula	$C_{24}H_{24}Cl_2CuN_4O_4$	$C_{42}H_{32}Cu_2O_{12}$	$C_{50}H_{53}Cl_4Cu_2N_4O_8$	$C_{32}H_{32}Cu_2O_{10}S_2$
Formula weight	566.91	855.76	1106.84	767.78
Temperature	100(2) K	100(2) K	100(2) K	100(2) K
Wavelength	0.71073 Å	0.71073 Å	0.71073 Å	0.71073 Å
Crystal system	Monoclinic	Monoclinic	Triclinic	Monoclinic
Space group	C2/c	P21/c	P-1	C2/c
a	23.468(4) Å	10.7446(14) Å	11.525(3) Å	18.9578(9) Å
b	10.1880(16) Å	11.5305(15) Å	14.613(3) Å	15.3435(7) Å
c	11.6142(18) Å	18.3776(19) Å	15.812(4) Å	23.6189(11) Å
α	90°	90°	91.084(5)°	90°
β	119.046(3)°	125.013(6)°	98.107(5)°	103.8530(10)°
γ	90°	90°	102.833(5)°	90°
Volume	2427.6(7) $Å^3$	1864.8(4) $Å^3$	2567.0(10) $Å^3$	6670.4(5) $Å^3$
Z	4	2	2	8
Density (calculated)	1.551 Mg/m^3	1.524 Mg/m^3	1.432 Mg/m^3	1.529 Mg/m^3
Absorption coefficient	1.159 mm^{-1}	1.207 mm^{-1}	1.092 mm^{-1}	1.456 mm^{-1}
F(000)	1164	876	1142	3152
Crystal size	0.10 x 0.08 x 0.07 mm^3	0.15 x 0.10 x 0.05 mm^3	0.13 x 0.13 x 0.05 mm^3	0.17 x 0.14 x 0.03 mm^3
Theta range for data collection	1.99 to 28.39°	2.22 to 28.37°	1.30 to 25.35°	1.73 to 28.34°
Index ranges	-31<=h<=30, -11<=k<=13, -15<=l<=15	-14<=h<=14, -15<=k<=15, -24<=l<=24	-13<=h<=13, -17<=k<=17, -19<=l<=19	-25<=h<=25, -20<=k<=20, -31<=l<=31
Reflections collected	12439	33983	43088	91850
Independent reflections	3050 [R(int) = 0.0504]	4651 [R(int) = 0.0502]	9389 [R(int) = 0.0634]	8314 [R(int) = 0.0640]
Completeness to theta = 25.00°	99.9 %	99.5 %	100.0 %	99.8 %
Absorption correction	Semi-empirical from equivalents	Semi-empirical from equivalents	Semi-empirical from equivalents	Semi-empirical from equivalents
Max. and min. transmission	0.9233 and 0.8929	0.9421 and 0.8397	0.9474 and 0.8710	0.9576 and 0.7899
Refinement method	Full-matrix least-squares on F^2	Full-matrix least-squares on F^2	Full-matrix least-squares on F^2	Full-matrix least-squares on F^2
Data / restraints / parameters	3050 / 0 / 161	4651 / 0 / 254	9389 / 39 / 631	8314 / 0 / 419
Goodness-of-fit on F^2	1.034	0.980	1.007	1.010
Final R indices [I>2sigma(I)]	R1 = 0.0367, wR2 = 0.0867	R1 = 0.0292, wR2 = 0.0687	R1 = 0.0481, wR2 = 0.1318	R1 = 0.0267, wR2 = 0.0601
R indices (all data)	R1 = 0.0532, wR2 = 0.0951	R1 = 0.0417, wR2 = 0.0752	R1 = 0.0742, wR2 = 0.1487	R1 = 0.0401, wR2 = 0.0664
Largest diff. peak and hole	0.783 and -0.570 e.$Å^{-3}$	0.530 and -0.411 e.$Å^{-3}$	2.192 and -1.190 e.$Å^{-3}$	0.446 and -0.347 e.$Å^{-3}$

Table 2.3. Crystal data and structure refinement for complexes **23-26**.

	23	**24**	**25**	**26**
Empirical formula	C_{64} H_{64} Cu_2 N_8 O_8	$C_{23}H_{19}$ $Cl_2CuN_2O_4$	$C_{64}H_{64}Cu_2N_8O_{12}\cdot 8(H_2O)$	$[C_{32}H_{28}CuN_8O_{12}]_n$
Formula weight	1200.31	1043.68	1408.44	780.16
Temperature	100(2) K	100(1) K	100(1) K	100(1) K
Wavelength	0.71073 Å	1.54178 Å	0.71073 Å	0.71073 Å
Crystal system	Triclinic	Tetragonal	Monoclinic	Monoclinic
Space group	$P\bar{1}$	$P4_2/n$	$P2_1/n$	$P2_1/c$
a	10.468(5) Å	16.2772(2) Å	9.7157(3) Å	14.1819(5) Å
b	10.853(6) Å	16.2772(2) Å	21.1150(6) Å	19.8388(7) Å
c	13.430(4) Å	17.3126(2) Å	17.2695(5) Å	11.9610(5) Å
α	79.52(5)°	90°	90°	90°
β	73.95(4)°	90°	101.485(2)°	96.814(2)°
γ	88.13(4)°	90°	90°	90°
Volume	1441.6(12) $Å^3$	4586.93(10) $Å^3$	3471.85(18) $Å^3$	3341.5(2) $Å^3$
Z	1	4	2	4
Density (calculated)	1.383 Mg/m^3	1.511 Mg/m^3	1.347 Mg/m^3	1.551 Mg/m^3
Absorption coefficient	0.801 mm^{-1}	3.766 mm^{-1}	0.689 mm^{-1}	0.732 mm^{-1}
F(000)	626	2128	1476	1604
Crystal size	0.18 x 0.10 x 0.08 mm^3	0.31 x 0.27 x 0.13 mm^3	0.11 x 0.10 x 0.08 mm^3	0.21 x 0.10 x 0.08 mm^3
Theta range for data collection	2.71 to 30.53°.	2.55 to 71.70°	2.88 to 30.57°	1.45 to 30.58°
Index ranges	-14<=h<=14, -15<=k<=15, -19<=l<=19	-19<=h<=20, -19<=k<=18, -20<=l<=21	-13<=h<=13, -30<=k<=29, -24<=l<=24	-20<=h<=20, -28<=k<=28, -17<=l<=17
Reflections collected	24268	73596	57027	124724
Independent reflections	8738 [R(int) = 0.0209]	4438 [R(int) = 0.0374]	10549 [R(int) = 0.0511]	10132 [R(int) = 0.0709]
Completeness to theta = 25.00°	99.0 %	99.6 %	98.5 %	98.9 %
Absorption correction	Numerical with SADABS	Analytical with SADBS	Analytical with SADABS	Multi-scan with SADABS
Max. and min. transmission	0.9387 and 0.8692	0.6402 and 0.3881	0.9470 and 0.9281	0.9438 and 0.8615
Refinement method	Full-matrix least-squares on F^2	Full-matrix least-squares on F^2	Full-matrix least-squares on F^2	Full-matrix least-squares on F^2
Data / restraints / parameters	8738 / 0 / 374	4438 / 66 / 330	10549 / 14 / 450	10132 / 0 / 485
Goodness-of-fit on F^2	0.971	1.049	1.006	1.043
Final R indices [I>2sigma(I)]	R1 = 0.0300, wR2 = 0.0740	R1 = 0.0635, wR2 = 0.1680	R1 = 0.0449, wR2 = 0.1162	R1 = 0.0289, wR2 = 0.0834
R indices (all data)	R1 = 0.0358, wR2 = 0.0773	R1 = 0.0646, wR2 = 0.1697	R1 = 0.0654, wR2 = 0.1280	R1 = 0.0373, wR2 = 0.0875
Largest diff. peak and hole	0.507 and -0.310 $e.Å^{-3}$	1.666 and -0.742 $e.Å^{-3}$	0.671 and -0.568 $e.Å^{-3}$	0.486 and -0.502 $e.Å^{-3}$

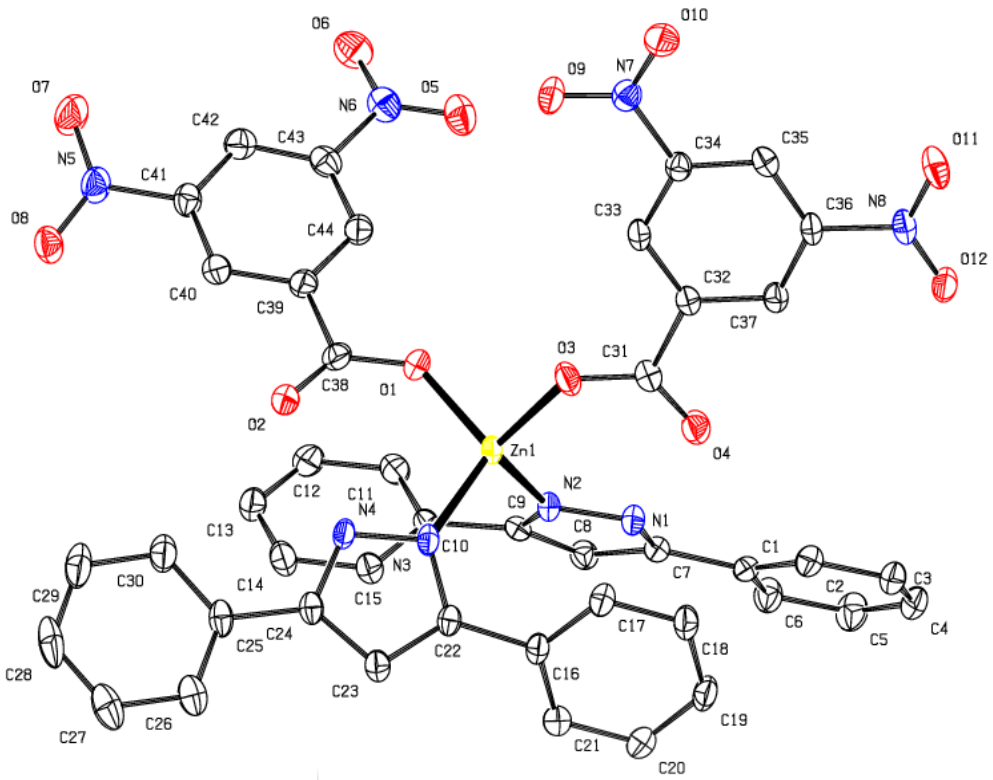

Figure 2.5. A molecular drawing of **6** and all H atoms are omitted for clarity.

Compound **6** was found to have average Zn-O and Zn-N bond lengths are 1.94 and 2.00 Å respectively. The angles around the zinc centre varies from 100.7° for O(1)-Zn(1)-O(3) to 116.78° for O(3)-Zn(1)-N(3). These angles show the distorted tetrahedral geometry adopted by the complex (Table 2.4). The structure of **6** can be compared to a similar complex of formula [Zn(**L1**)$_2$(**Bz**)$_2$] (where Bz = benzoate group) synthesized by Baruah.[75] The average Zn-O bond length in [Zn(**L1**)$_2$(**Bz**)$_2$] is 1.93 Å, which is very close to the average Zn-O bond length of **6** (1.94 Å). The angles around the zinc centre are between 102.45° and 114.59° in [Zn(**L1**)$_2$(**Bz**)$_2$], and for **6**, the angles vary from 110.7° to 116.78°.

Table 2.4. Selected bond lengths (Å) and bond angles (°) for complex **6**.

Bond length (Å)		Bond angles (°)	
O(1)-Zn(1)	1.9327(15)	O(2)-C(38)-O(1)	127.3(2)
O(3)-Zn(1)	1.9509(15)	C(38)-O(1)-Zn(1)	132.52(15)
N(3)-Zn(1)	1.9968(17)	C(31)-O(3)-Zn(1)	127.84(15)
N(1)-N(2)	1.351(2)	O(1)-Zn(1)-O(3)	100.71(7)
N(2)-Zn(1)	2.0016(18)	O(1)-Zn(1)-N(3)	111.63(6)
C(38)-O(2)	1.235(3)	O(3)-Zn(1)-N(3)	116.78(7)
C(38)-O(1)	1.275(2)	O(1)-Zn(1)-N(2)	107.04(7)
C(31)-O(3)	1.277(2)	O(3)-Zn(1)-N(2)	113.15(6)
N(3)-N(4)	1.354(2)	N(3)-Zn(1)-N(2)	107.11(7)

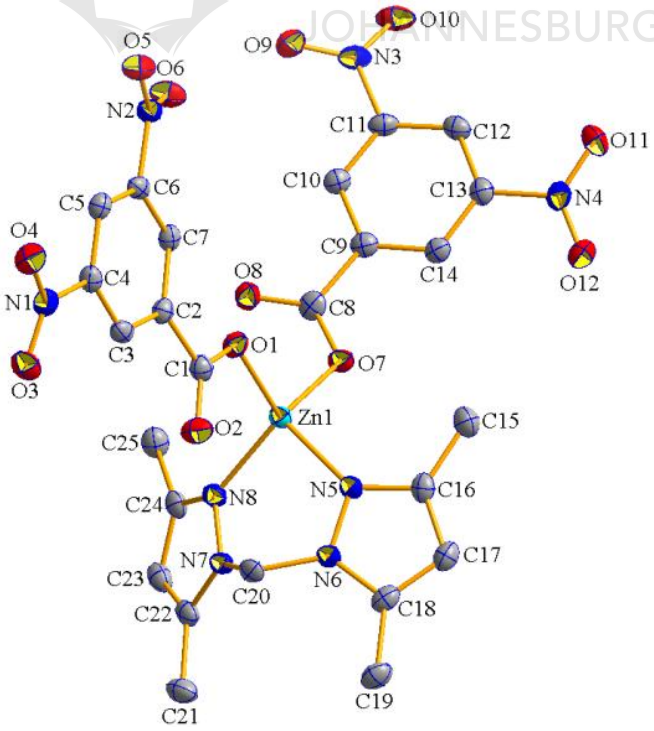

Figure 2.6. A molecular drawing of **9** and all H atoms are omitted for clarity.

Likewise, compound **9** has a tetrahedral geometry with the zinc binding to two oxygen atoms from the two 3,5-NO_2-C_6H_3COO groups and to the two nitrogen atoms from **L4** (Figure 2.6). The two Zn-O bonds are of almost the same length as well as the two Zn-N bond distances that are very close to each other. The bond angles around the zinc centre are important as they are different, showing that the complex has a distorted tetrahedral geometry. N(8)-Zn(1)-N(5) has the smallest angle while O(1)-Zn(1)-N(5) shows the largest angle. This can be explained by the bulky substituents on the phenyl ring of the benzoate. One important torsion angle is C(22)-N(7)-C(20)-N(6) that is 119.8^o. This angle gives a clear indication of how ligand **L4** bends itself to the most stable position in the complex (Table 2.5).

Table 2.5. Selected bond lengths (Å) and bond angles (^{o}) for complex **9**.

Bond length (Å)		**Bond angles (^{o})**	
Zn(1)-O(1)	1.939(2)	O(1)-Zn(1)-O(7)	103.39(9)
Zn(1)-O(7)	1.945(2)	O(1)-Zn(1)-N(5)	118.81(9)
Zn(1)-N(5)	2.032(3)	O(7)-Zn(1)-N(5)	103.27(9)
Zn(1)-N(8)	2.040(2)	O(1)-Zn(1)-N(8)	116.66(9)
C(1)-C(2)	1.512(4)	N(6)-C(20)-N(7)	111.3(2)
O(1)-C(1)	1.274(4)	O(7)-Zn(1)-N(8)	120.16(10)
O(2)-C(1)	1.224(4)	N(5)-Zn(1)-N(8)	94.56(10)
C(1)-C(2)	1.512(4)	C(1)-O(1)-Zn(1)	116.01(19)
O(7)-C(8)	1.268(4)	C(8)-O(7)-Zn(1)	116.82(19)
O(8)-C(8)	1.233(4)	N(7)-N(8)-Zn(1)	116.77(18)
N(5)-N(6)	1.374(3)	N(6)-N(5)-Zn(1)	119.31(18)
N(7)-N(8)	1.377(3)		

When compared to compound **6** and to [Zn(**L1**)$_2$(**Bz**)$_2$], the average Zn-O bond length of **9** is 1.942 Å, which is very close to similar bonds in both compounds. The angles around the zinc centre are between 94.56^o and 116.66^o for **9**, which is slightly larger than both **6** and [Zn(**L1**)$_2$(**Bz**)$_2$]. The larger difference in angles for complex **9** is due to the bulky substituents on the phenyl rings. The steric hindrance thus enlarges the separation between the benzoates and closes that within **L4**. Also, the CH_2 linker in **L4** helps in keeping the two nitrogen atoms, which are bonded to zinc, closer together.

Compound **9** can be compared to the structure of **6** and it can be observed that changing the substituent groups on the pyrazole ring and the introduction of a CH_2 linker affect the bonds around the metal centre. Thus, even if the average Zn-O bond length does not change by much, the angles around the zinc do undergo changes, such that the N(3)-Zn(1)-N(2) bond angle is 107.11^o for **6** compared to 94.56^o in **9**. This value for **6** is close to the N-Zn-N bond angle for reported complex [Zn(**L1**)$_2$(**Bz**)$_2$] (107.72^o), indicating that the phenyl groups on the pyrazole ring do not have any effect on the orientation of the pyrazole ligand around the metal.

From the previous two crystal structures, a similar structure was expected for complex **11**, with two pyrazoles and two benzoates coordinated to the zinc centre. But, the crystal structure of **11** (Figure 2.7) is a polymeric chain with bidentate 5-coordinated square pyramidal, Zn(1) and 4-coordinated tetrahedral zinc, Zn(2), linked together by **L6**. The square pyramidal zinc centre is part of a paddle wheel bidentate fragment of the chain. So, there are four benzoate groups bridging between two zinc centres. Then, the axial position at the zinc centre is occupied by a nitrogen atom from **L6**, while the other nitrogen forms a bond with a 4-coordinated zinc centre. This tetrahedral zinc is also bonded to three benzoate

(a)

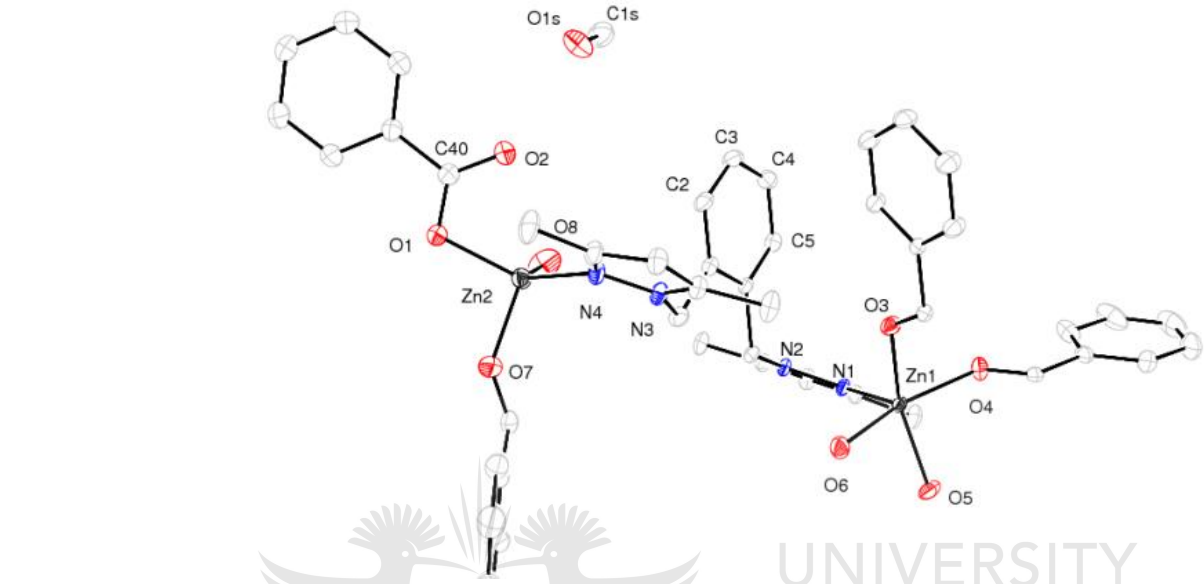

(b)

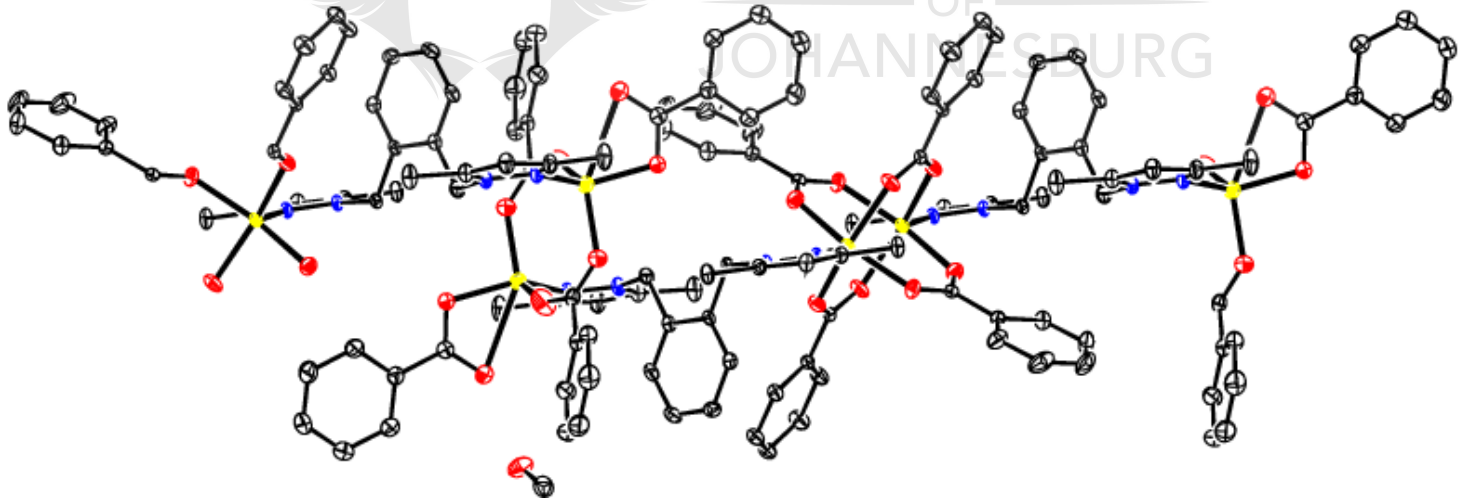

Figure 2.7. A molecular drawing of **(a) 11** with all H atoms omitted for clarity and **(b)** polymeric chain of the complex.

groups, two of which act as bridging ligands, thus linking this zinc to a similar tetrahedral zinc. This second zinc is in turn bonded to a nitrogen atom of **L6** with the other nitrogen bonded to another paddle wheel square pyramidal zinc(II), hence forming the chain. Interestingly, the benzoate behaves in two types of coordination modes, namely one as bidentate bridge to clip dinuclear units, while the other as a monodentate ligand.

When compared with literature values, the Zn(1)-O and Zn(2)-O bond lengths in **11** fall within the normal values,[65] ranging from 2.028 to 2.063 Å and from 1.915 to 1.988 Å, respectively. The slightly longer bond lengths around Zn(1) might be explained in terms of the geometry around the metal. At the square pyramidal zinc(II) centre, there are four Zn-O bonds compared to only three for the tetrahedral centre. The extra bond implies an extra phenyl ring that brings more bulkiness to the coordination sphere around Zn(1) compared to Zn(2). Therefore, as a means of counteracting the steric hindrance around Zn(1), the Zn-O bonds lengthen to give rise to a more stable complex. The bond angles around Zn(1) give an indication that the geometry around the metal is distorted square pyramidal. Similarly, the angle around Zn(2) shows that it adopts a distorted tetrahedral geometry (Table 2.6), with Zn-O bonds comparable with those in **9** and **6**.

Table 2.6. Selected bond lengths (Å) and bond angles (°) for complex **11**.

Bond length (Å)		Bond angles (°)	
N(1)-Zn(1)	2.0439(16)	O(3)-Zn(1)-O(5)	157.06(6)
N(4)-Zn(2)	1.9979(17)	O(3)-Zn(1)-N(1)	103.68(6)
O(7)-Zn(2)	1.9888(15)	O(5)-Zn(1)-N(1)	99.24(6)
O(8)-Zn(2)	1.9155(17)	ON(1)-Zn(1)-O(4)	99.82(6)
Zn(1)-Zn(1)#1	3.0423(5)	O(3)-Zn(1)-O(6)	86.07(6)
C(40)-O(2)	1.245(3)	O(8)-Zn(2)-O(1)	101.28(8)
O(1)-Zn(2)	1.9561(15)	O(8)-Zn(2)-O(7)	117.52(8)
O(3)-Zn(1)	2.0328(14)	O(1)-Zn(2)-O(7)	96.97(6)
O(4)-Zn(1)	2.0521(14)	O(8)-Zn(2)-N(4)	114.23(8)
O(5)-Zn(1)	2.0366(14)	O(1)-Zn(2)-N(4)	128.65(7)
O(6)-Zn(1)	2.0630(15)	O(7)-Zn(2)-N(4)	97.92(7)
N(1)-Zn(1)-O(6)	102.99(6)	O(4)-Zn(1)-O(6)	157.18(6)

The crystal structure of **11** does not match the spectroscopic characterization results that were obtained, like the ^{1}H NMR spectrum (Figure 2.8). According to the integration of the peaks, the expected product was a mononuclear zinc(II) coordinated to one **L6** and two benzoate groups, but the crystal structure revealed otherwise. The difference might either result from the mononuclear product being the kinetically stable one while the thermodynamically more stable one is the polymeric product or from the effect of solvent on the arrangement of the complex. Research has been done concerning this topic and results show that solvents can have direct effect on the structure of a compound.[87]

[87] Lucky, R. A.; Sui, R.; Lo, J. M. H.; Charpentier, P. A. *Cryst. Growth Des.* **2010**, *10*, 1599.

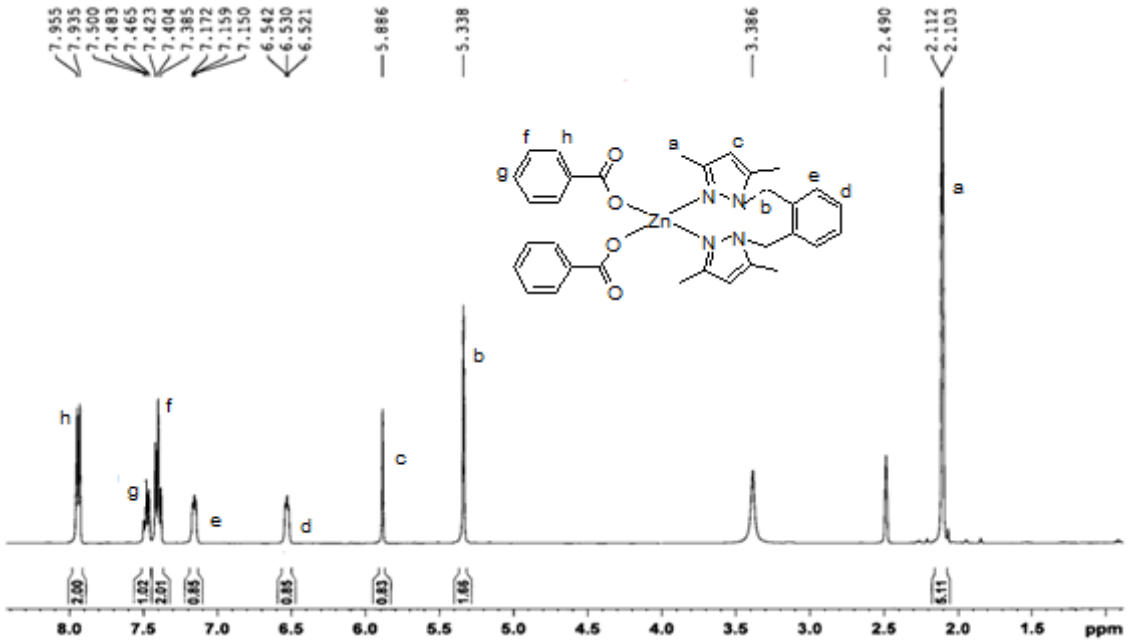

Figure 2.8. ^{1}H NMR spectrum of complex **11** in DMSO.

2.6.3.2 Copper crystal structures

From the structures of compounds **14** and **17**, both were found to be monometallic compounds with two pyrazolyl and two benzoates coordinated to the copper(II) centre, **14** being tetrahedral (Figure 2.9) while **17** has an octahedral geometry (Figure 2.10) due to the different binding modes of the carboxylates.

The structure of complex **14** shows a monometallic copper(II) centre, with two pyrazoles and two benzoate groups bonded to the metal; the copper is coordinated to one oxygen atom per benzoate group bonded to it and has a tetrahedral centre. Baruah reported the structure of **14** as *cis* and *trans*-coordination, as discussed in previous section 1.4.2 in Fig. 1.14,[78] but **14** crystallized out in only one form and without any solvent molecules, making it different from Baruah's complex.

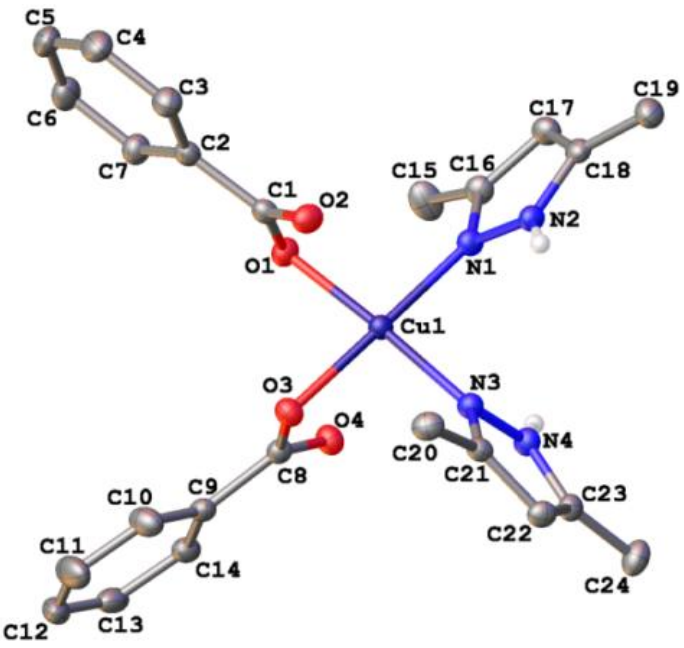

Figure 2.9. A molecular drawing of **14** and all H atoms are omitted for clarity.

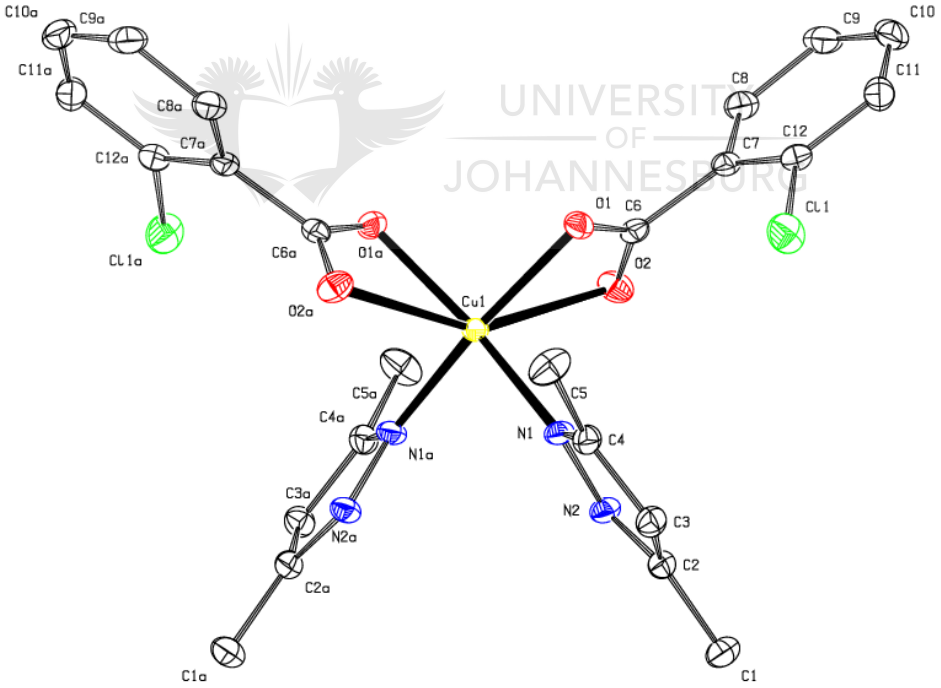

Figure 2.10. A molecular drawing of **17** and all H atoms are omitted for clarity.

Complex **17** also is monometallic, with two pyrazoles and two benzoate groups bonded to the copper, which is coordinated to four oxygen atoms from the two benzoate group resulting in

the octahedral centre. Compound **17** might have this structure because the *ortho* chloride on the benzoate, which even if electron withdrawing, renders the carboxylate group more acidic compared to the unsubstituted benzoate molecule. The increase in acidity can be attributed to the steric hindrance that forces the carboxyl group to twist out of the plane of the benzoate ring. In so doing, the carboxylate group is more acidic than the unsubstituted one, thus both donor atoms of the carboxylate bind to the metal centre for complex **17**. Despite the difference in geometries, the average Cu-O bond lengths for **14** and **17** are very close, 1.9955 and 1.9855 Å respectively (Table 2.7).

Table 2.7. Selected bond lengths (Å) and bond angles (^{o}) for complexes **14** and **17**.

14		**17**	
Cu(1)-O(1)	1.9966(18)	N(1)-Cu(1)	1.9815(18)
Cu(1)-N(3)	1.979(2)	O(1)-Cu(1)	1.9855(15)
Cu(1)-N(1)	1.986(2)	C(6)-O(2)	1.248(3)
Cu(1)-O(3)	1.9944(19)	C(6)-O(1)	1.273(3)
O(1)-C(1)	1.267(2)	C(6)-O(1)-Cu(1)	102.96(14)
O(2)-C(1)	1.2517(19)	N(1)-Cu(1)-N(1)#1	92.39(11)
O(4)-C(8)-O(3)	121.89(14)	N(1)-Cu(1)-O(1)	91.22(7)
O(2)-C(1)-O(1)	122.04(15)	N(1)#1-Cu(1)-O(1)	161.93(7)
N(3)-Cu(1)-N(1)	90.93(8)	N(1)#1-Cu(1)-O(1)#1	91.22(7)
N(3)-Cu(1)-O(3)	90.47(8)	O(1)-Cu(1)-O(1)#1	90.81(9)
N(1)-Cu(1)-O(3)	177.72(5)		
N(3)-Cu(1)-O(1)	176.61(5)		
N(1)-Cu(1)-O(1)	92.36(8)		
O(3)-Cu(1)-O(1)	86.27(7)		

Unlike complexes **14** and **17**, **18** has a paddle wheel structure with bridging benzoate groups between the two copper centres at the equatorial positions. The axial positions, which were expected to be occupied by the pyrazoles were instead occupied by benzoic acids that coordinate through one oxygen atom per benzoic acid (Figure 2.11).

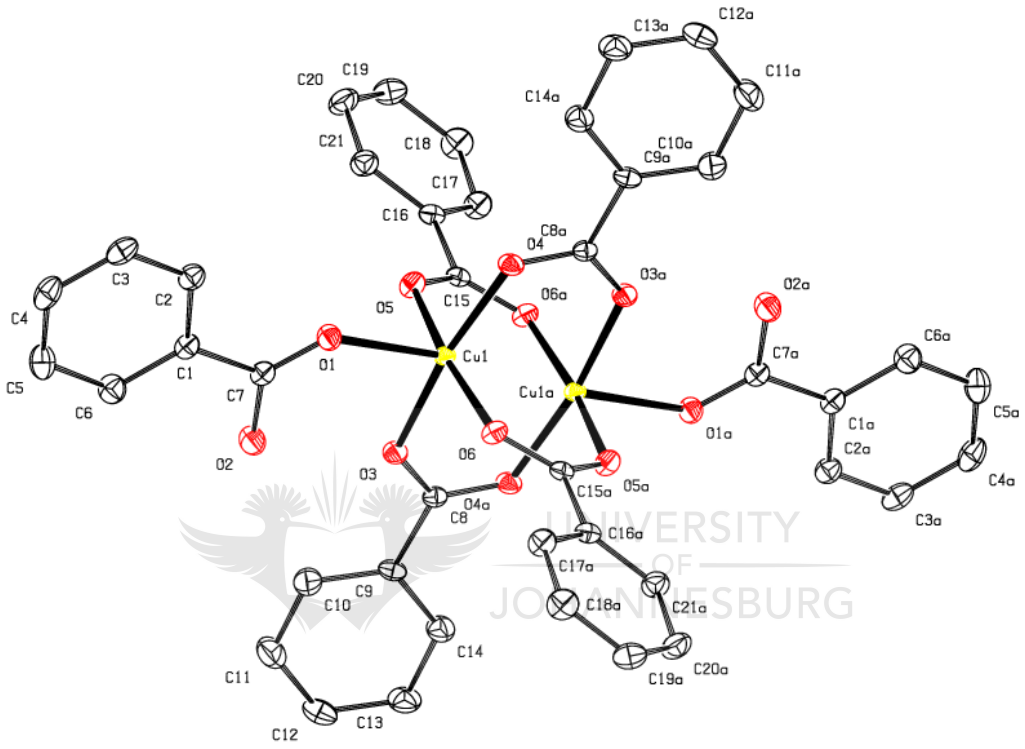

Figure 2.11. A molecular drawing of **18** and all H atoms are omitted for clarity

This structure has been reported previously by Kowata *et al.* who synthesized the complex by stirring copper(II) carbonate with benzoic acid in methanol at 100 ^{o}C.[88] In this complex, there is an intramolecular hydrogen bond (O(3)-O(2) = 2.63 Å) between a bridging benzoate and an axial benzoic acid. Owing to the H-bond, the Cu-O(3) bond distance is longer by 0.05 Å on average compared with the other Cu-O bridge distances. Compound **18** shows many

[88] Kawata, T.; Uekusa, H.; Ohba, S.; Furukawa, T.; Tokii, T.; Muto, Y.; Kato, M. Acta Cryst. **1992**, B48, 253.

similarities to this reported structure.[88] Firstly, the H-bond in the complex results in O(2)-O(3) bond length of 2.6163 Å . Secondly, the Cu-O(3) bond length is 0.0437 Å on average longer than the equatorial Cu-O bonds. The selected bond distances and angles are illustrated in Table 2.8.

Table 2.8. Selected bond lengths (Å) and bond angles (°) for complex **18**.

Bond length (Å)		**Bond angle (°)**	
Cu(1)-O(5)	1.9481(13)	O(5)-Cu(1)-O(3)	89.07(6)
Cu(1)-O(4)#1	1.9552(13)	O(6)-Cu(1)-O(3)	89.44(5)
Cu(1)-O(3)	1.9966(13)	O(5)-Cu(1)-O(6)	169.46(6)
Cu(1)-O(1)	2.1859(13)	O(5)-C(15)-O(6)#1	125.64(16)
C(7)-O(1)	1.223(2)	O(5)-Cu(1)-O(4)#1	89.08(6)
C(7)-O(2)	1.321(2)	O(4)#1-Cu(1)-O(3)	169.16(5)
		C(7)-O(1)-Cu(1)	129.73(12)
		O(1)-C(7)-O(2)	123.26(17)

When the ligand was changed from 3,5-diphenylpyrazoles (**L2**) to the tertiary-butyl analogue (**L3**), compound **19** was obtained, the crystal structure of which shows that **19** is also a bimetallic complex with a paddle wheel geometry. The two octahedral copper centres are linked by a bond and the four benzoates are bridging ligands between the two metals. The axial positions are occupied by the pyrazole ligands. The structure shows disorder in the tertiarybutyl groups and the chloro substituent on the benzoate (Figure 2.12).

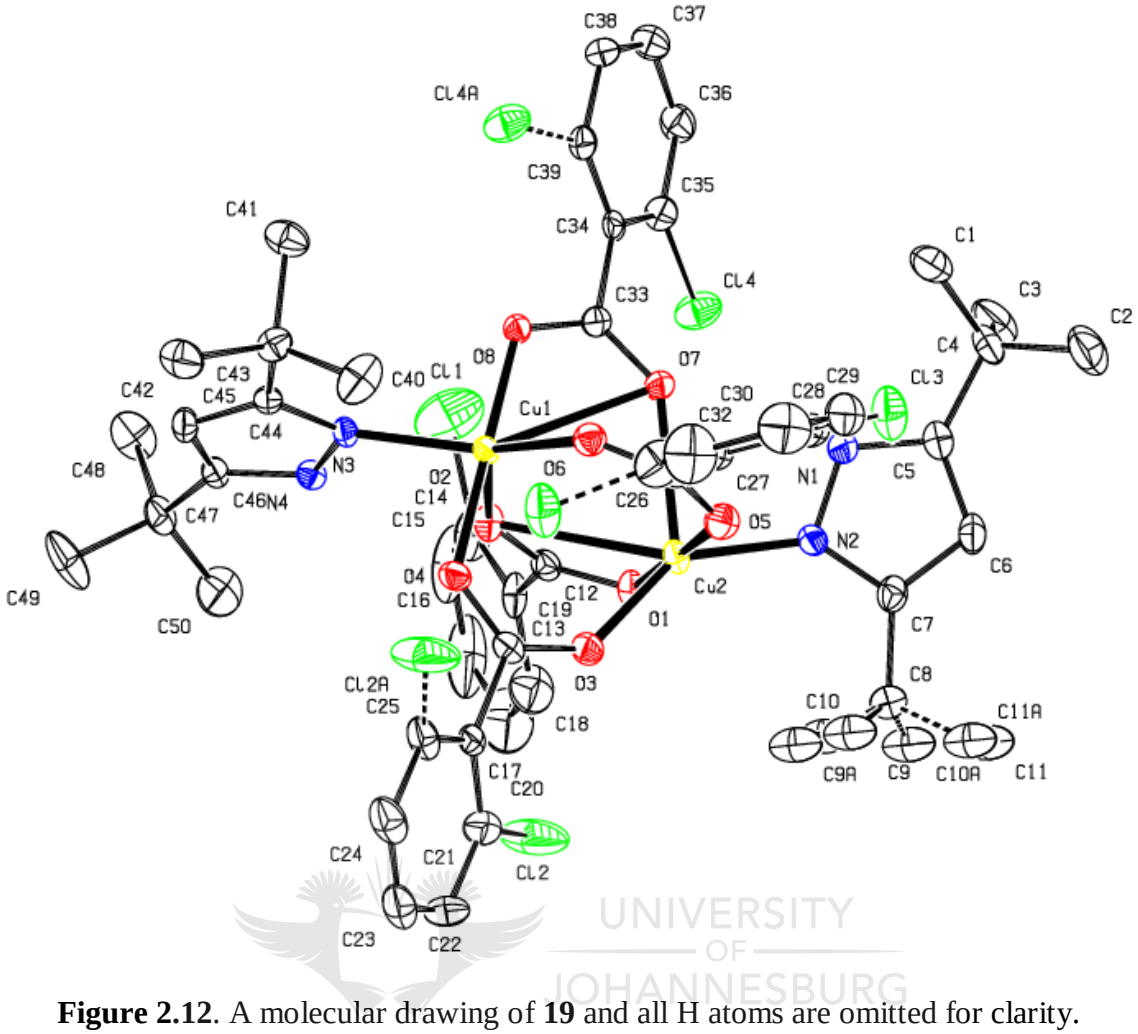

Figure 2.12. A molecular drawing of **19** and all H atoms are omitted for clarity.

When compared to **17**, it is clear that the substituent on the pyrazole is the cause for the difference in the geometries of the copper centres. The tertiary-butyl groups are sterically more demanding than the methyl groups, hence the coordination of two **L3** and two benzoates to a monometallic Cu centre would have given rise to a very unstable complex. Therefore, this paddle wheel geometry is the preferred one as it allows reduced steric interaction between the chloride and the tertiary-butyl groups. This is supported by the average Cu-O and Cu-N bond lengths for **19**, which are 1.9932 and 2.0215 Å respectively, compared to the average Cu-O and Cu-N bond lengths for **17**, which are 1.9855 and 1.9815 Å, respectively. Thus, the longer bond length around Cu in **19** is the consequence of steric

bulkiness of the pyrazole ligands. The selected bond distances and angles of **19** are illustrated in Table 2.9.

Table 2.9. Selected bond lengths (Å) and bond angles (^{o}) for **19**.

Bond lengths (Å)		**Bond angles (^{o})**	
Cu(1)-O(8)	1.903(2)	O(8)-Cu(1)-O(4)	175.91(12)
Cu(1)-O(4)	1.919(2)	O(8)-Cu(1)-O(6)	92.69(11)
Cu(1)-O(6)	1.988(3)	O(4)-Cu(1)-O(6)	90.01(11)
Cu(2)-O(1)	1.902(3)	O(8)-Cu(1)-N(3)	91.30(11)
Cu(1)-N(3)	2.019(3)	O(4)-Cu(1)-N(3)	88.08(11)
Cu(2)-O(1)	1.902(3)	O(6)-Cu(1)-N(3)	147.08(12)
Cu(2)-O(5)	1.922(3)	O(5)-C(26)-O(6)	127.4(4)
Cu(2)-O(3)	1.973(3)	O(7)-C(33)-O(8)	125.5(3)
Cu(2)-O(7)	2.437(2)		
Cu(2)-N(2)	2.024(3)		

An attempt was made to coordinate pyrazolyl compound **L5**, to copper benzoate, but similar to **18**, complex **22** was obtained as a paddle wheel structure, the equatorial positions occupied by bridging benzoates and DMSO molecules at the axial positions (Figure 2.13). The structure of **22** has also been reported in literature and the Cu-O bond lengths reported varied between 1.963 and 2.135 Å, which is comparable to those in **22** (1.942-2.155 Å). The axial Cu-O bond in the reported structure is 2.135 Å, a value close to that of the same bond in **22**.[89] Selected bond lengths and angles are given in Table 2.10.

[89] Judas, N. *Acta Cryst*. **2005**, E61, m2217.

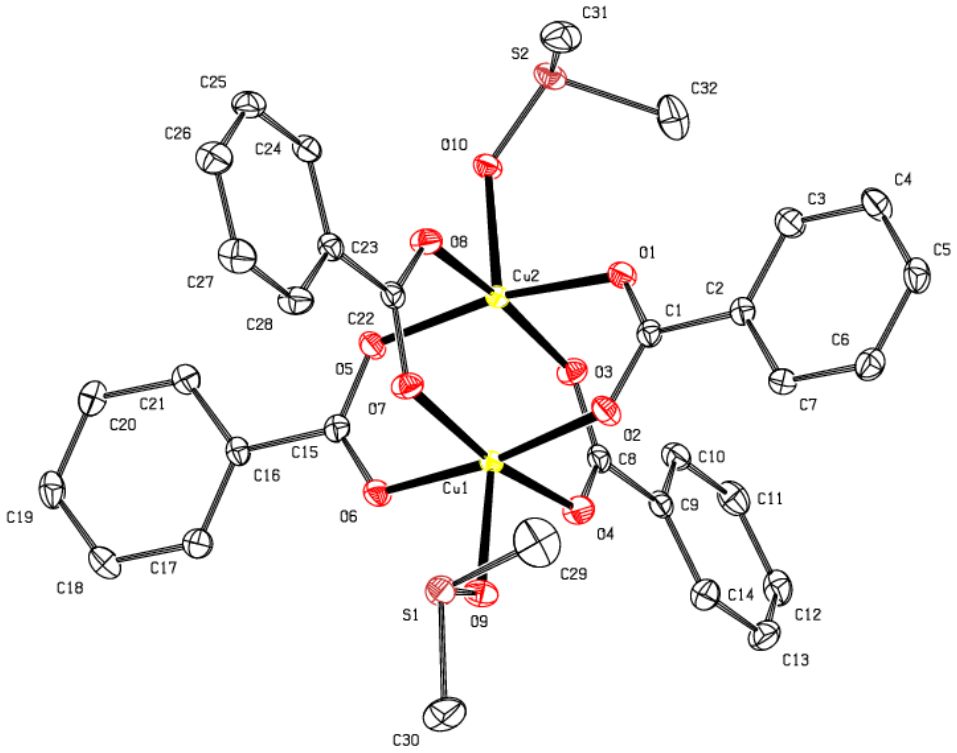

Figure 2.13. A molecular drawing of **22** and all H atoms are omitted for clarity.

Table 2.10. Selected bond lengths (Å) and bond angles (°) for **22**.

Bond lengths (Å)		**Bond angles (°)**	
O(4)-Cu(1)	1.9695(13)	O(7)-C(22)-O(8)	125.48(17)
O(7)-Cu(1)	1.9828(12)	O(1)-C(1)-O(2)	125.86(16)
O(2)-Cu(1)	1.9562(12)	O(6)-Cu(1)-O(2)	170.88(5)
O(3)-Cu(2)	1.9549(12)	O(6)-Cu(1)-O(4)	90.98(5)
O(5)-Cu(2)	1.9718(12)	O(6)-Cu(1)-O(7)	89.35(5)
O(6)-Cu(1)	1.9425(12)	O(2)-Cu(1)-O(7)	89.01(5)
O(9)-Cu(1)	2.1553(12)	O(6)-Cu(1)-O(9)	93.49(5)
O(1)-Cu(2)	2.0069(12)	O(8)-Cu(2)-O(3)	170.00(5)
O(8)-Cu(2)	1.9497(13)		
O(10)-Cu(2)	2.1615(12)		

Crystal structures of complexes **23**, **24** and **25** (Figure 2.14) showed that all three copper complexes have bimetallic paddle wheel geometries with an octahedral metal centre, similar to **18** and **22**, except that the axial positions are occupied by the pyrazolyl ligands. Unlike **25** and **23**, which are bimetallic complexes, compound **24**, with an electron withdrawing chloride on the benzoate ring, is polymeric, the units are interlinked through the N atoms of the pyrazolyl ligand. The coordination around the copper centres is the same for all three complexes: the two copper metals are bonded to each other and are also linked together by four benzoate groups. Complex **24** differs only in terms of the other nitrogen of **L6** which binds to another similar paddle wheel copper, hence forming the chain. Nevertheless, the Cu-Cu bond length is almost similar in all three cases, as well as the Cu-O and Cu-N bond lengths and bond angles. The bond angles are also very closely related for complexes **23**, **24** and **25**. These values fall within the standard values for the paddle wheel structure of copper(II) carboxylate discussed in section in 1.4.2 Fig. 1.13, the Cu-O bond lengths (1.964-2.115 Å) are very close to those for complexes **23**, **24** and **25** (Table 2.11).[77]

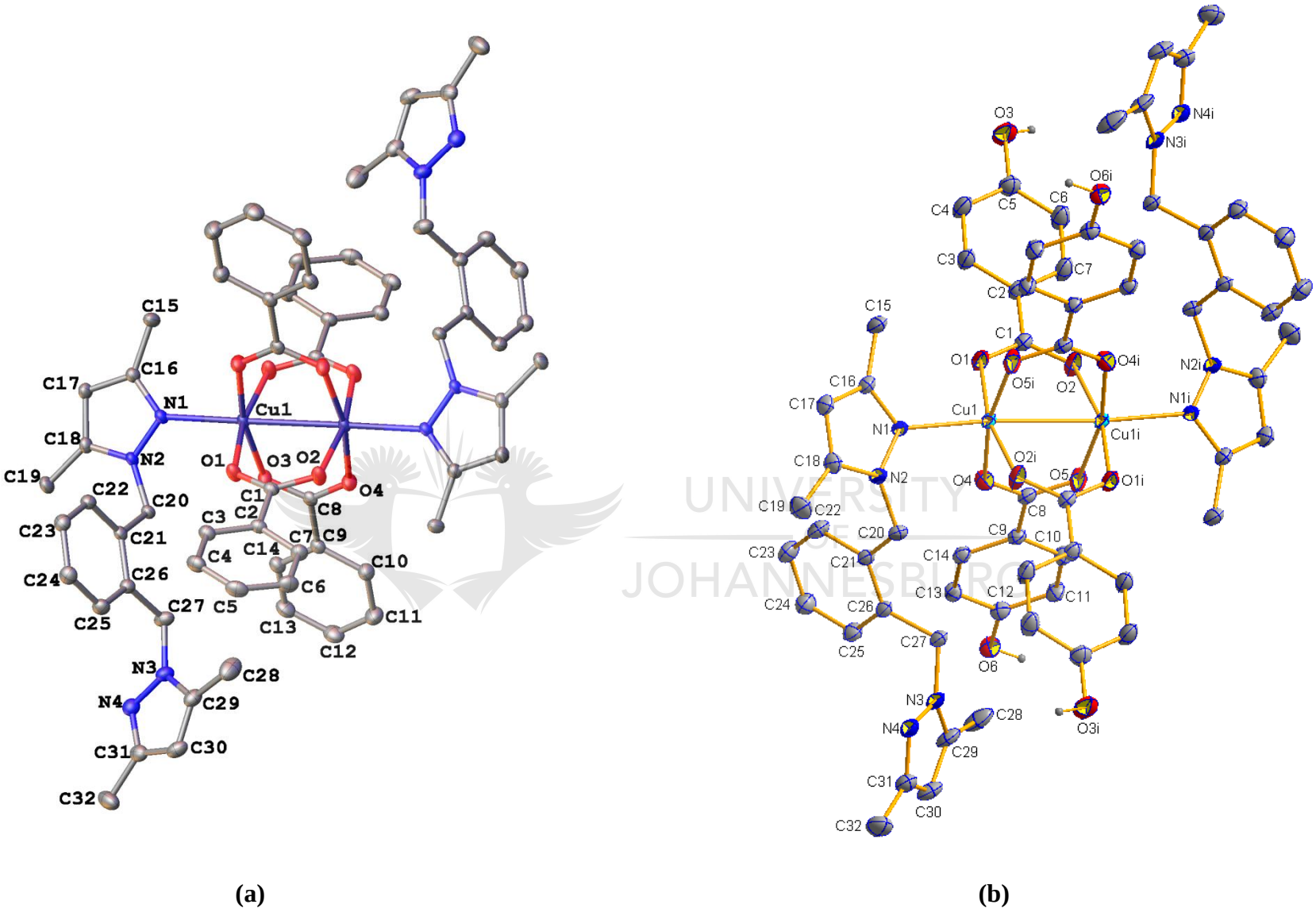

(a) **(b)**

Figure 2.14.(I) Molecular drawings of **(a) 23** and **(b) 25** and all H atoms are omitted for clarity.

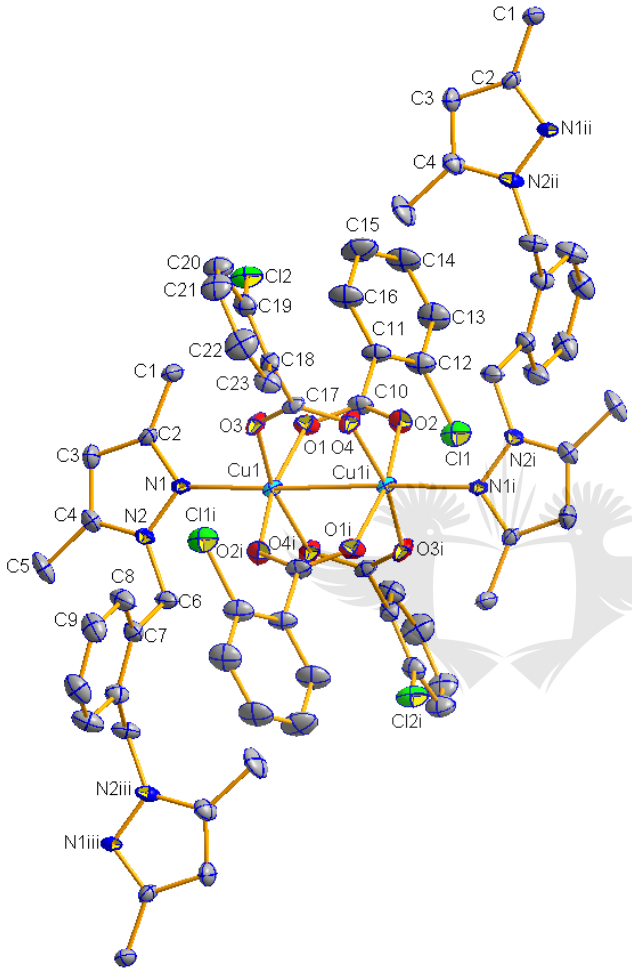

(c)

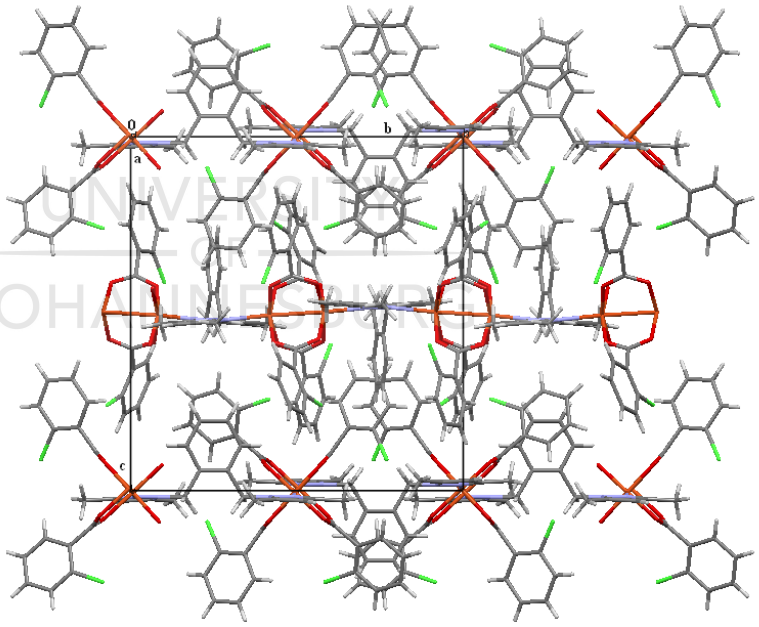

(d)

Figure 2.14.(II) (c) Molecular drawings of **23** and **(d)** A packing diagram of **23** viewed along the a axis. Chains are formed due to the bridging ligand (atoms N1, N2, and C1-C9). All H atoms and minor components of disordered atoms were omitted for clarity.

Table 2.11. Selected bond lengths (Å) and bond angles (^{o}) for Cu complexes **23-25**.

	23	**24**	**25**
Cu(1)-O(1)	1.9666(13)	1.9645(14)	1.965(3)
Cu(1)-O(3)	1.9839(14)		1.964(3)
Cu(1)-O(5)#1		1.9595(15)	
Cu(1)-N(1)	2.1925(16)	2.1928(15)	2.212(4)
Cu(1)-Cu(1)#1	2.6845(15)	2.6958(4)	2.6999(11)
O(3)-Cu(1)-O(1)	88.86(6)		89.02(15)
O(3)-Cu(1)-O(2)#1	89.62(6)		89.97(13)
O(1)-Cu(1)-O(2)#1	167.18(4)	165.98(6)	166.13(13)
O(3)-Cu(1)-O(4)#1	167.09(4)		166.16(13)
O(1)-Cu(1)-O(4)#1	90.02(6)	91.06(7)	88.03(13)
O(2)#1-Cu(1)-Cu(1)#1	83.35(5)	79.54(4)	82.82(10)
O(4)#1-Cu(1)-Cu(1)#1	84.78(5)	83.92(4)	83.78(9)
O(2)#1-Cu(1)-O(4)#1	88.63(6)	90.44(7)	89.65(15)

Alternatively, the crystal structure of copper complex **26** shows that it has a polymeric structure with an octahedral geometry around the metal centre; each copper coordinated to four oxygen donor atoms from two benzoates. The copper centres are linked by ligand **L6** via the nitrogen atoms, hence giving rise to a network (Figure 2.15). The average Cu-O bond length is 1.952 Å, which is smaller than that of the paddle-wheel structures **23**, **24** and **25**. The bond angles around the copper centre show a slight distortion in the octahedral geometry from the O(1)-Cu(1)-N(3) bond angle of 92.51^{o} (Table 2.12).

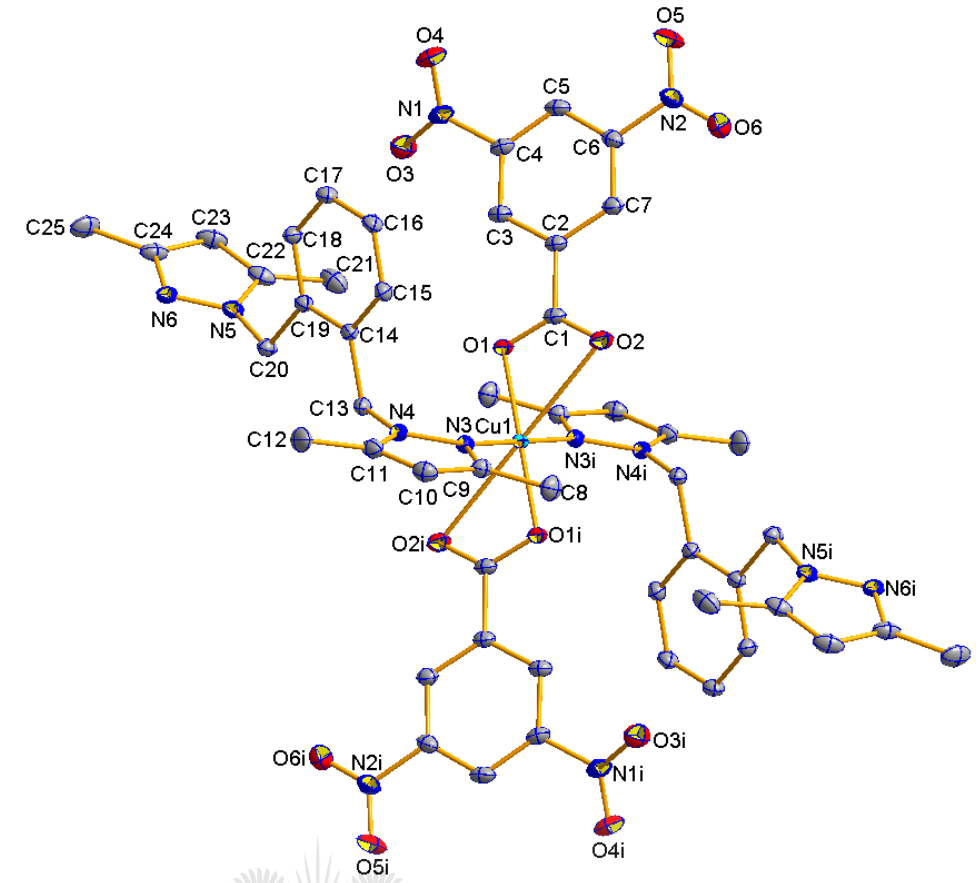

(a)

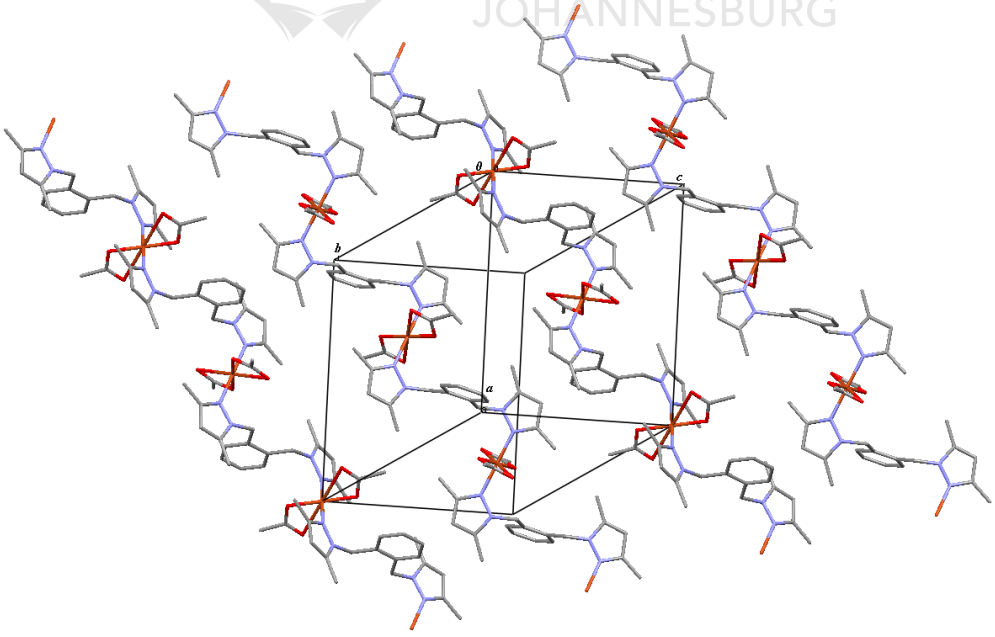

(b)

Figure 2.15.(a) A molecular drawing of **26** and all H atoms are omitted for clarity; **(b)** A packing diagram of **26** with all H atoms and the phenyl rings with the NO_2 groups were omitted for clarity. The complex forms continuous chains propagating in the [1 0 1] direction.

Table 2.12. Selected bond lengths (Å) and bond angles (°) for Cu complex **26**.

Bond lengths (Å)		Bond angles (°)	
Cu(1)-O(1)	1.938(3)	O(7)-Cu(2)-N(6)#2	90.82(3)
Cu(1)-N(3)	1.993(8)	O(7)-Cu(2)-N(6)	89.18(3)
Cu(2)-O(7)	1.966(9)	O(1)#1-Cu(1)-O(1)	180.0
Cu(2)-N(6)	1.995(3)	O(1)#1-Cu(1)-N(3)	87.49(3)
O(1)-C(1)	1.280(6)	O(1)-Cu(1)-N(3)	92.51(3)
O(2)-C(1)	1.233(0)	N(4)-C(13)-C(14)	113.95(8)
		O(2)-C(1)-O(1)	125.45(10)

2.7 Conclusion

Six pyrazolyl compounds (**L1**-**L6**) were prepared, except **L1**, and were used to coordinate to zinc(II) and copper(II) acetates. Compound **L3** was synthesized in a novel, green manner. Benzoic acids with different substituents on the ring have also been employed as primary ligand that binds to the metal via the oxygen donor atom. Two pathways have been employed to synthesize the complexes, methods A and B. It was observed that irrespective of which method is used, the same product is obtained. Yet, method B was used for the synthesis of most of the complexes since it was the fastest pathway and did not require any heating. The yields of the complexes, as well as the ligands were moderate to fairly good. The ligands and complexes were characterized by different techniques including NMR, IR, MS, CHN analysis. X-ray analysis was also done on some complexes and different structures were obtained: monometallic, bimetallic and polymeric. These different structures and geometries were obtained because the ligands have more than one coordination mode and also because of the steric bulkiness of some ligands. In most cases the metal was bonded to the benzoate and the pyrazolyl ligands but in complexes like **22**, the N donor ligand did not coordinate to the

copper. All the complexes synthesized showed stability in air, which make them interesting for what their application as potential initiators for the polymerization of lactide and ε-caprolactone.

CHAPTER 3

POLYMERIZATION OF D,L-LACTIDE AND ε-CAPROLACTONE

3.1 Introduction

Polycaprolactone (PCL) and polylactide (PLA) are important aliphatic polyesters that show interesting properties such as controlled degradability, biocompatibility with the potential to be made from monomers derived from renewable sources (in the case of PLA). The physical, thermal and mechanical properties of the polymers depend on their molecular weights and degrees of crystallinity. PCL and PLA also display the rare property of being miscible with many other polymers like poly(vinylchloride) and are mechanically soluble with others such as polyethylene and natural rubber. PCL biodegrades between several months and several years, depending on the molecular weight and degree of crystallinity of the polymer, as well as the conditions of degradation.[90] Many microbes in nature are able to completely biodegrade PCL.[91] These polyesters find useful application in different fields: scaffolds in tissue engineering,[92,93,94] in long-term drug delivery systems,[95,96,97] in microelectronics,[98] as adhesives,[89] and in packaging (trash bags and food containers).[99]

[90] Joshi, P.; Madras, G. *Polym. Degrad. Stab*. **2008**, *93*,1901.

[91] Gross, R. A.; Kalra, B. *Science* **2002**, *297*, 803.

[92] Lam, C. X. F.; Teoh, S. H.; Hutmacher, D. W. *Polym. Int*. **2007**, *56*, 718.

[93] Pena, J.; Corrales, T.; Izquierdo-Barba, I.; Doadrio, A. L.; Vallet-Regi, M. *Polym. Degrad. Stab*. **2006**, *91*, 1424.

[94] Jenkins, M. J.; Harrison, K. L.; Silva, M. M. C. G.; Whitaker, M. J.; Shakesheff, K. M.; Howdle, S. M. *Eur. Polym. J*. **2006**, *42*, 3145.

[95] Sinha, V. R.; Bansal, K.; Kaushik, R.; Kumria, R.; Trehan, A. *Int. J. Pharm*. **2004**, *278*, 1.

[96] Chandra, R.; Rustgi, R. *Prog. Polym. Sci*. **1998**, *23*, 1273.

[97] Chen, D. R.; Bei, J. Z.; Wang, S. G. *Polym. Degrad. Stab*. **2000**, *67*, 455.

[98] Hedrick, J. L.; Magbitang, T. E.; Connor, F.; Glauser, T.; Volksen, W.; Hawker, C. J.; Lee, V. Y.; Miller, R. D. *Chem. Eur. J*. **2002**, *8*, 3308.

[99] Ikada, Y.; Tsuji, H. *Macromol. Rapid Commun*. **2000**, *21*, 117.

PCL and PLA can be produced by two main methods: (i) polycondensation of hydroxycarboxylic acid and lactic acid respectively and (ii) by the ring opening polymerization (ROP) of ε-caprolactone (ε -CL) and lactide respectively, the latter being the most convenient method of synthesizing the polymers. A wide range of catalytic systems have been studied such as enzymatic, organic and metal initiators touching on virtually every section of the periodic table. The most common complexes used for this purpose are $[Sn(Oct)_2]$ and $[Al(O^iPr)_3]$, but they show some disadvantages such as low percentage conversions, poor stereocontrol and instability of complex in air. Thereupon, developing well-defined initiators that possess high activity and stereocontrol for the ROP of cyclic esters has attracted significant attention in many research groups. In an attempt to counteract the drawbacks of the existing systems, a range of the zinc(II) and copper(II) complexes synthesized were used as potential initiators for the ROP of the cyclic esters ε-CL and D,L-lactide.

3.2 Materials

All polymerization reactions were carried out in reactor tubes and under a dry nitrogen atmosphere using Schlenk techniques. ε-CL was obtained from Sigma Aldrich and sodium hydroxide pellets from Merck and were used as received. D,L-lactide was obtained from Purac biochem and used as received. Dichloromethane, toluene and methanol were dried and kept on molecular sieves before use.

3.3 Instrumentation

Nuclear magnetic resonance (^1H and $^{13}C\{^1H\}$) spectra were recorded in chloroform-d ($CDCl_3$) on a Varian Gemini 2 000 instrument (300 MHz for ^1H NMR) and a Bruker Ultrashield 400 instrument (400 MHz for ^1H NMR and 100 MHz for $^{13}C\{^1H\}$ NMR) at room

temperature. ^{1}H and $^{13}C\{^{1}H\}$ chemical shifts were referenced to the residual signals of the protons or carbons of the NMR solvents and are quoted in ppm: $CDCl_3$ at 7.24 and 77.0 ppm for ^{1}H and $^{13}C\{^{1}H\}$ spectra respectively. Molecular weight and molecular weight polydispersity of polymers were determined by size exclusion chromatography (SEC) and by Matrix-Assisted Laser Desorption Ionization Time-of-Flight mass spectrometry (MALDI-TOF MS). SEC analysis was done at the University of Mauritius using a WGE Dr.Bures Q1000 Gel Permeation Chromatogram and at Kyoto University, Japan, using a JASCO GULLIVER system (PU-980, CO-965, RI-930, and UV-1570) equipped with polystyrene gel columns (Shodex columns K803, K804, K805), using THF as an eluent at a flow rate of 1.0 mL/min, calibrated by polystyrene standards at 40 ^{o}C. MALDI-TOF MS measurements were done at Kyoto University and University of Tokyo, Japan, using a Schimadzu Biotech Axima CFRplus. Thermal analysis of the polymers was carried out using a Mettler-Toledo DSC 822^{e} and Perkin Elmer STA 6000 Simultaneous Thermal Analyzer.

3.4 Synthesis of PCL

ε-CL (1.14 g, 0.01 mol) and the required amount of initiator, depending on the ratio of [monomer]:[initiator] ([M]/[I]) used, were weighed in a reactor tube and stirred at 110 ^{o}C. The polymerization of ε-CL was carried out in bulk with [M]/[I] ratios of 50:1, 1 500:1 and 3 333:1. After the required reaction time, the reaction mixture was quenched by rapid cooling to room temperature and the crude product was analyzed by ^{1}H NMR in $CDCl_3$. The polymers were cleaned by first dissolving the crude product in CH_2Cl_2, followed by the addition of cold methanol. A white precipitate is formed, which was isolated by filtration and dried in vacuo.

3.5 Synthesis of PLA

D,L-Lactide (1.44 g, 0.01 mol) and the required amount of initiator to keep the [M]/[I] ratio at 100:1 were dissolved in toluene (2.5 mL) in a reactor tube and stirred at 110 ^{o}C. After specified time intervals, each reaction was quenched via rapid cooling with liquid nitrogen. The solvent was removed in vacuo and the percentage conversion was determined from the ^{1}H NMR spectrum. The polymer was cleaned by first dissolving the crude product in dichloromethane (15 mL) and adding a hydrochloric acid solution in methanol (0.5 M, 15 mL) to the mixture. The solution was shaken vigorously and allowed to stand to allow the layers to separate. The aqueous layer was then washed with dichloromethane (3 x 10 mL). The combined organic layer was then washed with distilled water (15 mL), followed by sodium hydroxide solution (1.0 M, 15 mL). The basic aqueous layer was washed with CH_2Cl_2 (3 x 10 mL). The organic phase was dried over anhydrous magnesium sulphate, filtered and concentrated in vacuo, yielding a white fluffy solid.

In some cases, the D,L-lactide polymerization was repeated using methanol (0.05 mL) as an additive to the reaction.

From the ^{1}H NMR spectrum of the crude product, the integration of the methine proton of the monomer ($I_{CHmonomer}$) and that of polymer ($I_{CHpolymer}$) allowed the calculation of the percentage conversion to be made using Equation 1.

$$\% \text{ Conversion} = \frac{I_{CH\ polymer}}{I_{CH\ monomer} + I_{CH\ polymer}} \times 100 \qquad (1)$$

$I_{CH\ polymer}$: intensity of the methine of the polymer

$I_{CH\ monomer}$: intensity of the methine of the monomer

Thus, most of the complexes synthesized in Chapter 2 were evaluated as initiators for the ROP of ε-CL and D,L-lactide. In order to have a better comparison of the activity of the different complexes, they were separated into different categories based on the secondary ligand in the structure. Hence, two main groups of complexes based on pyrazolyl ligands were looked at, one with a linker in the pyrazolyl ligand (**L4** and **L6**) and the other without any linker (**L1** and **L2**).

3.6 Kinetic study for ε-CL ROP

Complexes of the two categories of ligands, linker and no linker, were used as initiators for the polymerization of ε-CL and the kinetics of polymerization were studied.

3.6.1 Initiator system with linker

In order to study the effectiveness of this system towards initiating the polymerization of ε-CL, zinc(II) and copper(II) complexes of **L6**, **10**-**13** and **23**-**26**, were used. The first set of polymerization kinetics using these complexes was carried out using [M]/[I] ratio of 50:1 at 110 ^{o}C in a solvent-free medium. From the kinetic plot (Figure 3.1), it was observed that all the reactions were complete after 48 h, except for the reaction with complex **23**. The initiator performance of complexes decreased in the order: **12** > **13** > **11** > **26** > **10** > **24** > **25** > **23**. The best performing initiator for this polymerization is **12**, of formula [Zn(3,5-NO_2-$C_6H_3COO)_2$**L6**], while the slowest initiation was shown by compound **23**, [$Cu_2(C_6H_5COO)_4$(**L6**)$_2$] (Figure 3.1).

In general, the polymerization reactions were faster for zinc initiator systems than for copper systems, justifying the common use of zinc complexes as initiators for this type of polymerization.[10] Compound **26**, the copper analogue of **12**, shows lower activities than all

the zinc complexes in general. However, in comparison with the other polymeric copper complex **24**, **26** displays better activity and a possible explanation might be the difference in the structures. On one hand, **26** is a polymeric complex with a copper(II) centre bonded to four donor atoms from two benzoate groups and **L6** acts as a bridging ligand between two copper centres. On the other hand, **24** has a bimetallic metal centre with four bridging benzoates and **L6** at the axial positions, with a Cu-Cu bond, and **L6** acting as the bridging ligand between the two copper units. In order for the monomer molecule to get into contact with the metal, this Cu-Cu bond has to be broken first, which requires extra energy. Thus, the lower activity of the dinuclear copper initiators is an account of the Cu-Cu bond.

The difference in activities of bimetallic complexes **23** and **25** can be attributed to the different benzoates. The lower activity of **23** than **25** can be due to the presence of a *para* hydroxyl group on the benzoate ring for **25**, while **23** does not have any substituents on the benzoate. So, despite the fact that the average Cu-O bond in **23** (1.983 Å) is longer than in **25** (1.964 Å), the metal centre in **23** is not electrophilic enough for the monomer to interact with it. The difference between the ability of zinc complexes **11** and **12** to initiate polymerization of ε-CL might also be attributed to a combined effect of the substituents on the benzoate and the structure of the complexes. Compound **11**, a polymeric complex with 4-coordinate and 5-coordinate zinc centres, has a more crowded coordination sphere than monometallic **12**. It is therefore easier for the monomer to interact with the zinc(II) centre in **12** than in **11**, resulting in higher activity of **12**.

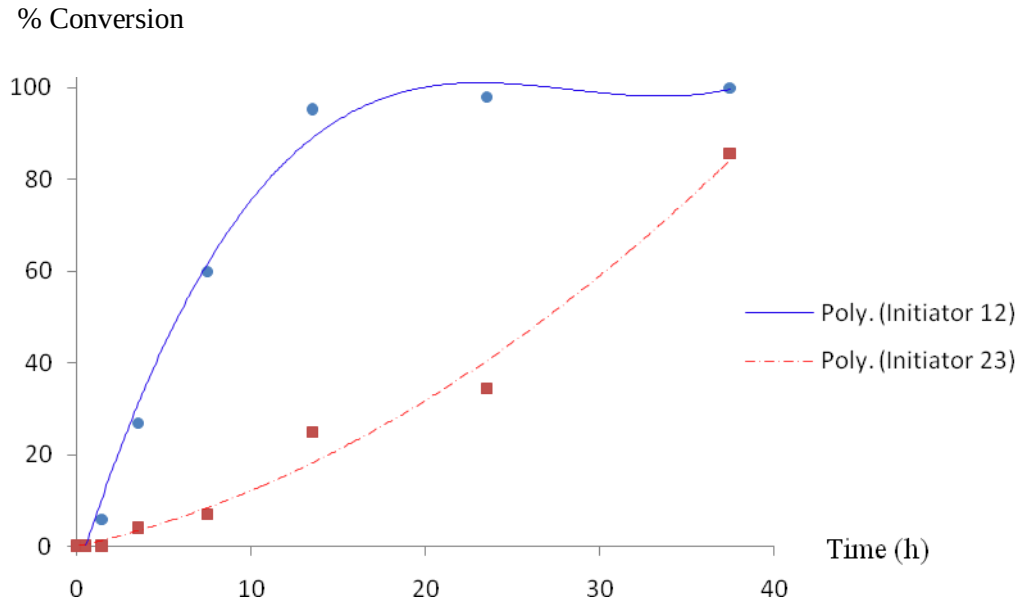

Figure 3.1. Kinetic plot for ε-CL ROP using compounds **12** and **23** at [M]/[I] = 50:1.

It was observed that increasing the [M]/[I] ratio, from 50:1 to 1 500:1, resulted in a radical slowing down of the rate of polymerization. This might be due to the larger number of growing chains, which is in fact caused by the higher concentration of active sites for lower [M]/[I] ratio. Yet, when the ratio was further increased to 3 333:1, the rate of polymerization did not undergo any major change, as was expected, which gives an indication that other factors come into play, like steric interactions among the growing polymer chains. The kinetics of polymerization for the different [M]/[I] ratios using initiator **26** are illustrated in Figure 3.2.

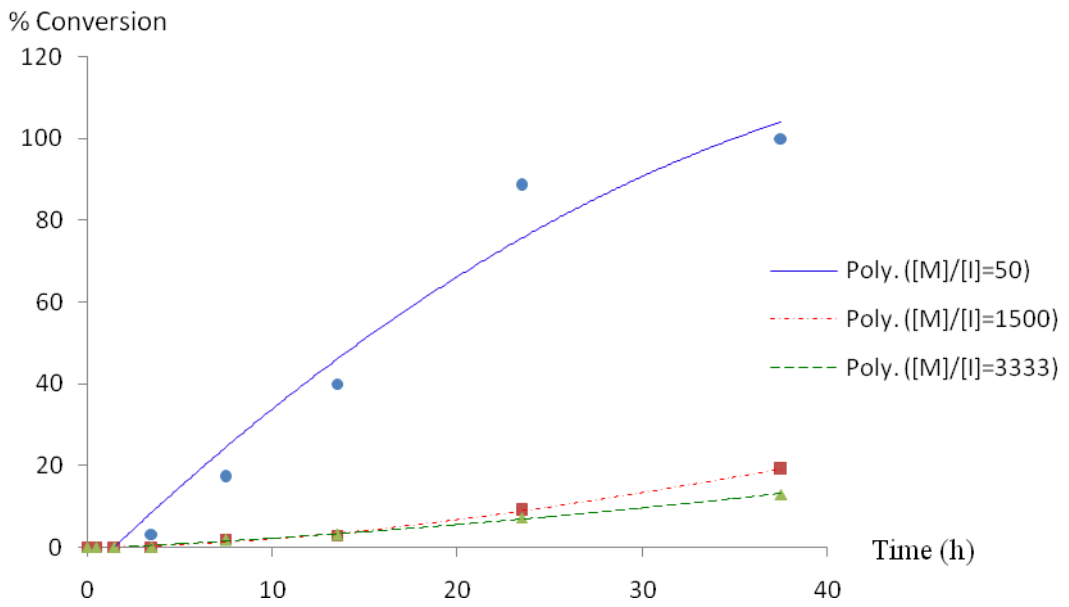

Figure 3.2. Kinetic plot for ε-CL ROP **26** at [M]/[I] = 50:1, 1 500:1 and 3 333:1.

From the **L6** ligand system, the complex that shows the best activity for the ROP of ε-CL is **12** and in order to improve on the activity of this particular complex, the linker on the pyrazole ligand was changed. Complex **9**, of ligand **L4** coordinated to zinc(II), was used to initiate the polymerization of ε-CL with [M]/[I] ratio of 50:1. When compared to complex **12**, **9** was found to initiate polymerization at a lower rate, showing that the ancillary ligand has an important effect on the ability of the complex to initiate polymerization. Compound **21**, the copper analogue of complex **24**, was also tested for its efficiency as initiator and it displayed higher activity than **24**. The most probable reason for **24** to initiate polymerization faster than **21** is the monometallic structure of **24** compare to polymeric **21**. This confirms the better activities of monometallic complexes over bimetallic ones. It can be concluded that depending on the metal and also the structure, the linker on the pyrazolyl ligand has different effects on the behaviour of the complex as initiator.

3.6.2 Initiator system with no linker

In order to carry out a more in-depth study of the effect of the ancillary ligand on polymerization, the secondary ligand was changed to pyrazoles with no linker. Thus, **L1** complexes of zinc(II) and copper(II), **1-4** and **14-17**, were assessed in the polymerization of ε-CL in bulk at 110 ^{o}C using [M]/[I] = 50:1.

From the kinetic study, the activities of the complexes can be arranged in decreasing order of **15** > **3** > **4** > **2** > **1** > **16** > **17** > **14**. It is interesting to find the best performing complex to be a copper complex of formula [Cu(3,5-NO_2-$C_6H_3COO)_2$(**L1**)$_2$] (compound **15**), the activity of which is followed by four zinc(II) complexes. The monometallic structures of the copper complexes might be the reason for the activity of **15**. On the other hand, the lowest rate of polymerization was shown by **14**, which differs from the best performing initiator only in the benzoate bonded to the copper. The primary ligands in the complexes show decreasing activities from hydroxyl- to chloro- to nitro- and lastly benzoates; the trend is different from the linker system. Representative results of polymerization initiated by compounds **14** and **15** are given in Figure 3.3.

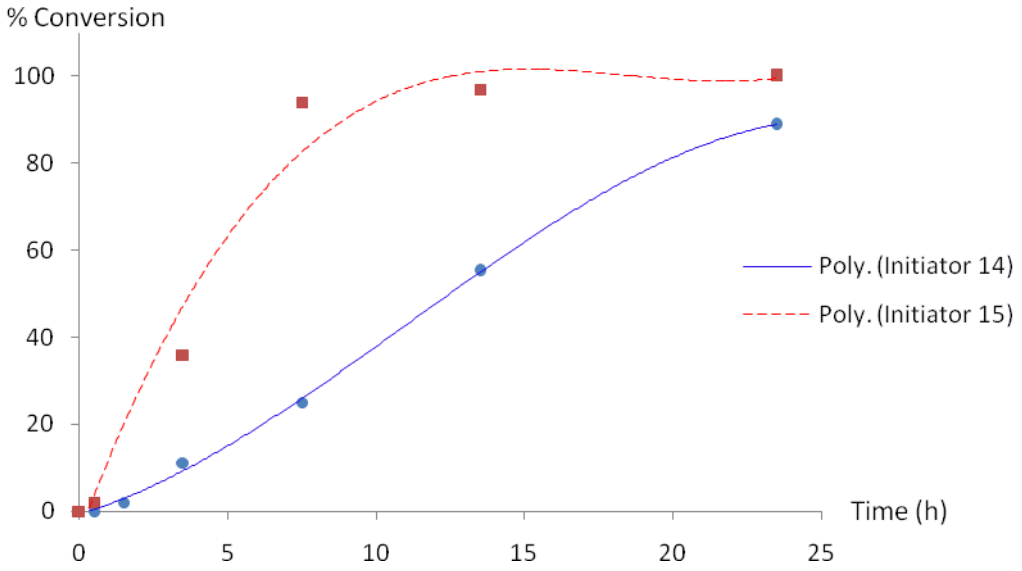

Figure 3.3. ROP of ε-CL using **14** and **15** as initiators at [M]/[I] = 50:1.

The polymerization reaction of ε-CL using complex **1** was repeated using higher [M]/[I] ratios of 1 500:1 and 3 333:1 (Figure 3.4). Similar to the previous initiator system (with a linker on the ancillary ligand), lower rates of monomer conversion are observed for **L1** complexes when the [M]/[I] ratio is increased. In this case though, the ratio 3 333:1 exhibits faster polymerization than the ratio 1 500:1. A possible explanation for the better performance of the higher [M]/[I] ratio of 3 333:1 is that the number of polymer chains growing from the metal centre is fewer, and hence there are less steric interactions among these chains. While in the case of [M]/[I] ratio of 1 500:1, there are twice as many metal-oxygen bonds available for insertion of monomer, resulting in more chains as compared to longer chains for the higher [M]/[I] ratio. From this study, the best [M]/[I] ratio for ε-CL ROP is 50:1.

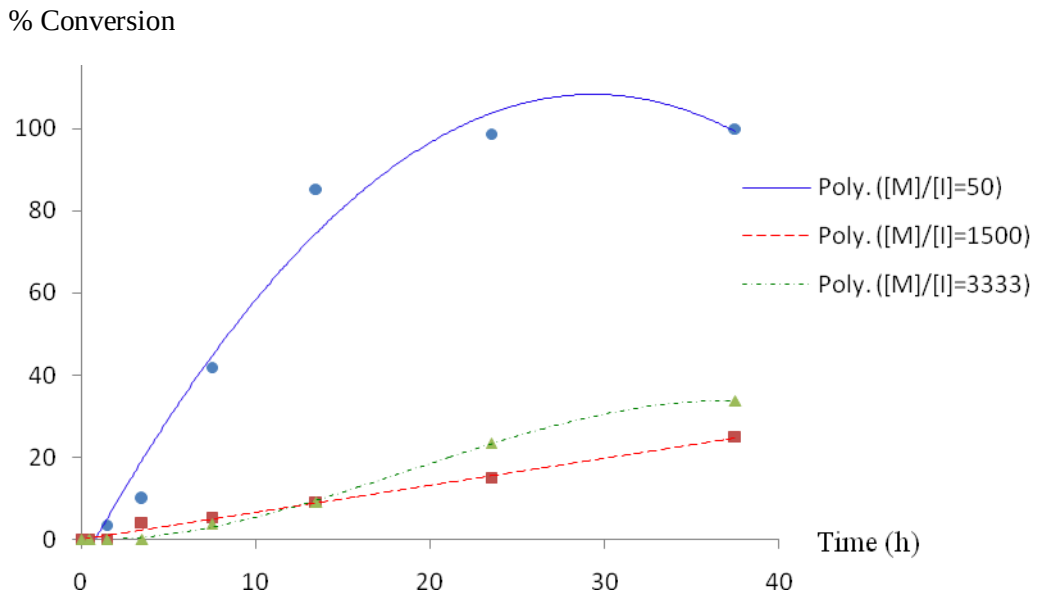

Figure 3.4. ROP of ε-CL using **1** at [M]/[I] = 50:1, 1 500:1 and 3 333:1.

From the results obtained, it is obvious that the ancillary ligand has a major influence on the polymerization reaction. This could be seen when changes were brought to the ancillary ligand, which reflected on the polymerization rates. Since the presence of a linker in the pyrazole appears to affect the efficiency of the initiator, changing the substituent groups on the pyrazole is also expected to influence the behaviour of the complexes. In addition, the best initiators for the different systems was found to be complexes of 3,5-NO_2-C_6H_3COO. So, compound **6**, an **L2** complex of formula [Zn(3,5-NO_2-$C_6H_3COO)_2$(**L2**)$_2$], was assessed for the polymerization of ε-CL and its activity was compared to complexes **2**, **9** and **12** (Figure 3.5).

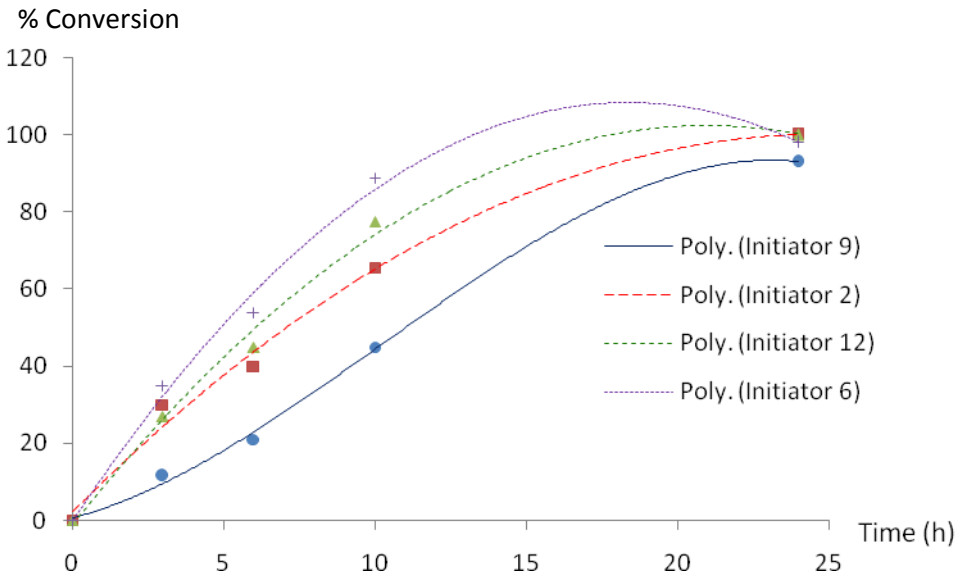

Figure 3.5. Kinetic plot for ROP using **L1**, **L2**, **L4** and **L6** complexes of [Zn(3,5-NO_2-$C_6H_3COO)_2$] at [M]/[I] = 50:1.

The performance of the zinc(II) complexes decreased from **6** > **12** > **2** > **9**. An alternative interpretation of the result is to compare the pyrazolyl ligands and the order of activity decreases as follows: **L2** > **L6** > **L1** > **L4**. Hence, **L2** complex of zinc(II) benzoate initiates the ROP of ε-CL at a faster rate than the other pyrazolyl analogues. The phenyl groups on the pyrazole rings contribute to the steric bulkiness of the ancillary ligand, which appears to have a positive effect on the polymerization of the cyclic esters. But when the substituent on the pyrazole is a methyl group, the activity of the complex drops such that the presence of the appropriate linker is important to improve the effectiveness of the complex towards ROP of ε-CL.

Since all the complexes used were able to initiate the polymerization of ε-CL, their effectiveness as initiator was then tested for a monomer of smaller ring. Thus, polymerization

of D,L-lactide was carried out using these zinc(II) and copper(II) complexes as potential initiators.

3.7 Kinetic study for D,L-lactide ROP

Similar to ε-CL polymerization, the complexes used for D,L-lactide polymerization were classified into two categories of initiators: linker and no-linker systems.

3.7.1 Initiator system with linker

The first polymerization reaction performed is the ROP using complexes of **L6** at [M]/[I] = 100:1 and 110 ^{o}C in toluene. Similar to polymerization of ε-CL, all eight complexes used are able to initiate polymerization of D,L-lactide, with varying activities. The performance of the complexes was in decreasing order of: **25** > **23** > **11** > **13** > **10** > **26** > **12** > **24**. Contrary to the polymerization of ε-CL, the trend in the activities of the initiators is different for the ROP of D,L-lactide when complexes of **L6** are used. Thus, the first and second best performing initiators are copper(II) systems of 4-OH-C_6H_4COO and C_6H_5COO respectively. The activities of these two are followed by three zinc complexes. The initiator showing the lowest initiation rate is the one employing complex **24**, a copper complex of 2-Cl-C_6H_4COO, as initiator (Figure 3.6).

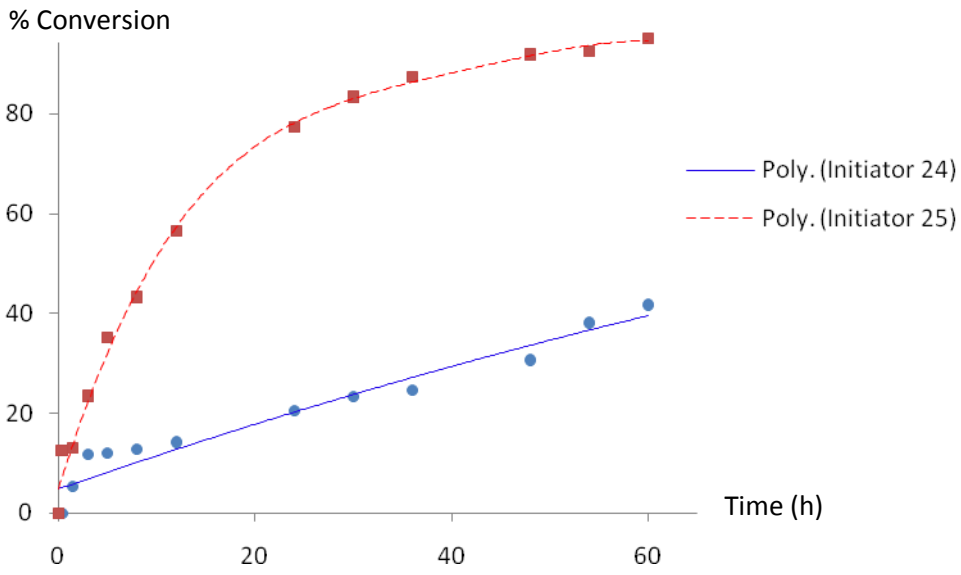

Figure 3.6. ROP of D,L-lactide using complexes of **L6** at [M]/[I] = 100:1 in toluene.

Since the polymerization of cyclic esters using [$Sn(Oct)_2$] requires the presence of butanol in order to perform at its best,[39] the effect of an alcohol on the polymerization of D,L-lactide was studied. In this respect, the polymerization of D,L-lactide was repeated for complex **26** in the presence of methanol, used as additive (Figure 3.7). Unexpectedly, it was observed that the polymerization slows down in the presence of methanol. The methanol might be acting as a quenching agent by terminating the end group of the growing chain, resulting in the slowing down of the reaction.

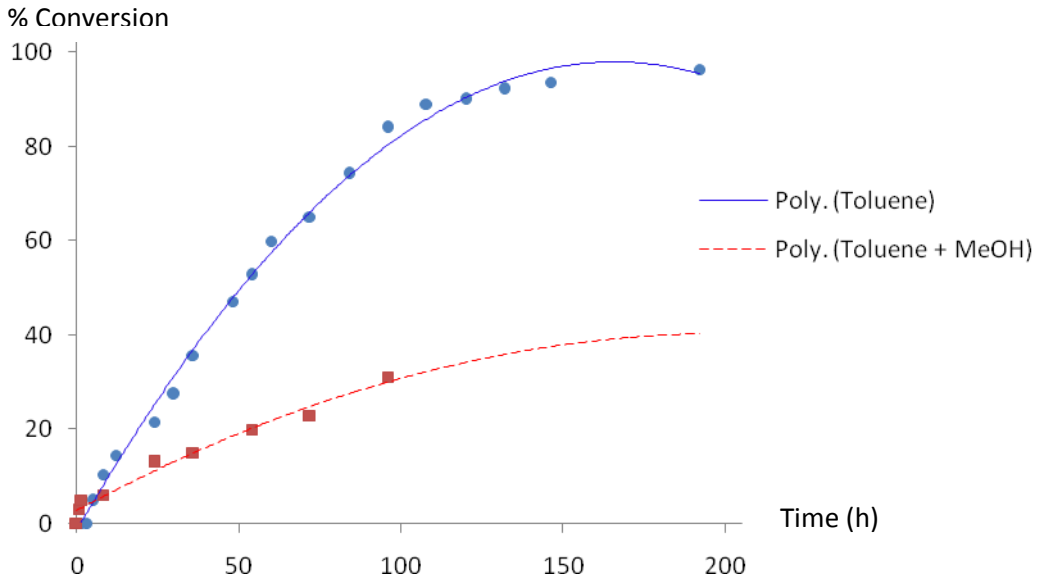

Figure 3.7. ROP of D,L-lactide using **26** at [M]/[I] = 100:1 in different solvents.

From the linker system, it can be concluded that in general, copper complexes were better initiators than zinc complexes for D,L-lactide ROP. When methanol was added to the reaction mixture, the polymerization rate was lowered. In order to compare the effect of the linker on the pyrazolyl ligand to the pyrazoles with no linker on the polymerization of lactide, complexes of **L1** and **L2** were employed.

3.7.2 Initiator system without any linker

ROP of D,L-lactide using complexes of **L1** was carried out in toluene and from the kinetic study, the activities of the complexes as initiators were found to be very similar. The best performance was showed by **14**, which has formula $[Cu(C_6H_5COO)_2(\mathbf{L1})_2]$, and the worst performing initiator was found to be **3** of formula $[Zn(4\text{-}OH\text{-}C_6H_4COO)_2(\mathbf{L1})_2]$ (Figure 3.8). The other complexes showed very close similarity in their activities towards the ROP of D,L-lactide.

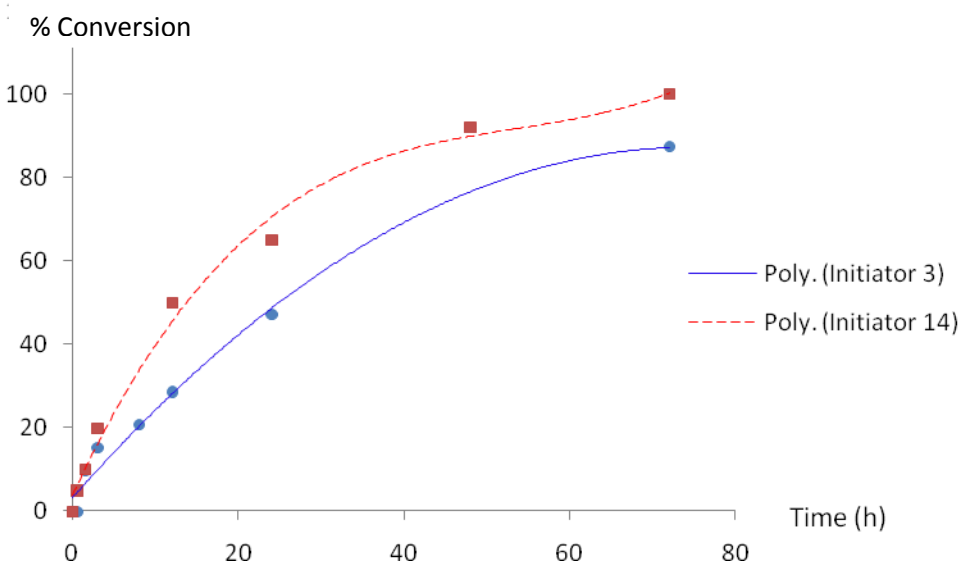

Figure 3.8. ROP of D,L-lactide in toluene using **L1** complexes **3** and **14**.

The polymerization reaction using **1** as initiator was repeated in the presence of methanol and it was observed that, unlike the linker system, the methanol did influence polymerization rate (Figure 3.9). The alcohol actually sped up the kinetics of the ROP, hence showing better performance than the same reaction carried out in toluene only.

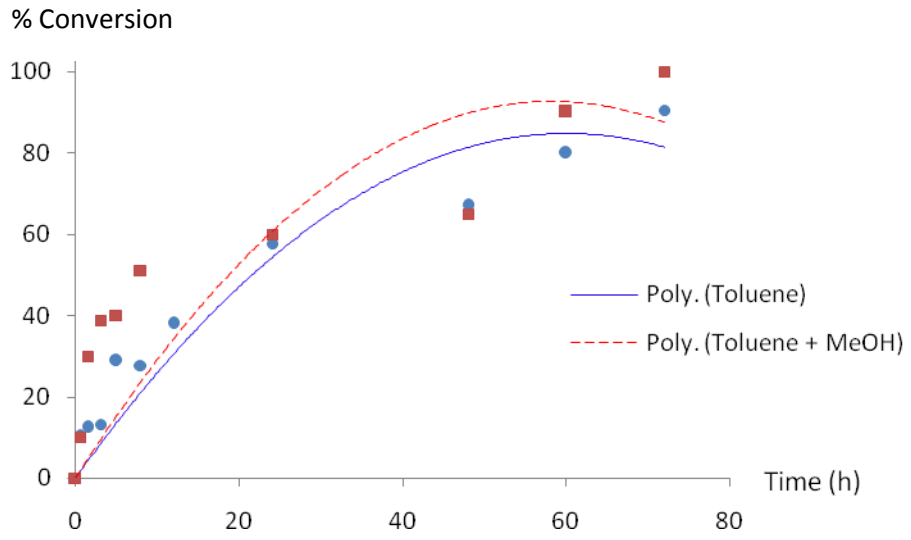

Figure 3.9. ROP of D,L-lactide using **1** in different solvents.

The participation of methanol in this particular system can be compared to the results obtained for the calculations run for [$Sn(OAc)_2$] in the presence of methanol. Thus, [$Sn(Oct)_2$] was found to result in faster polymerization of lactide when combined with a protic agent like an alcohol. Recent investigations[42] have allowed for the characterization of several intermediate tin complexes and strongly support a coordination-insertion mechanism rather than a cationic or activated-monomer mechanism.[100] Support for the coordination-insertion mechanism has recently been obtained theoretically (Scheme 3.1).[101]

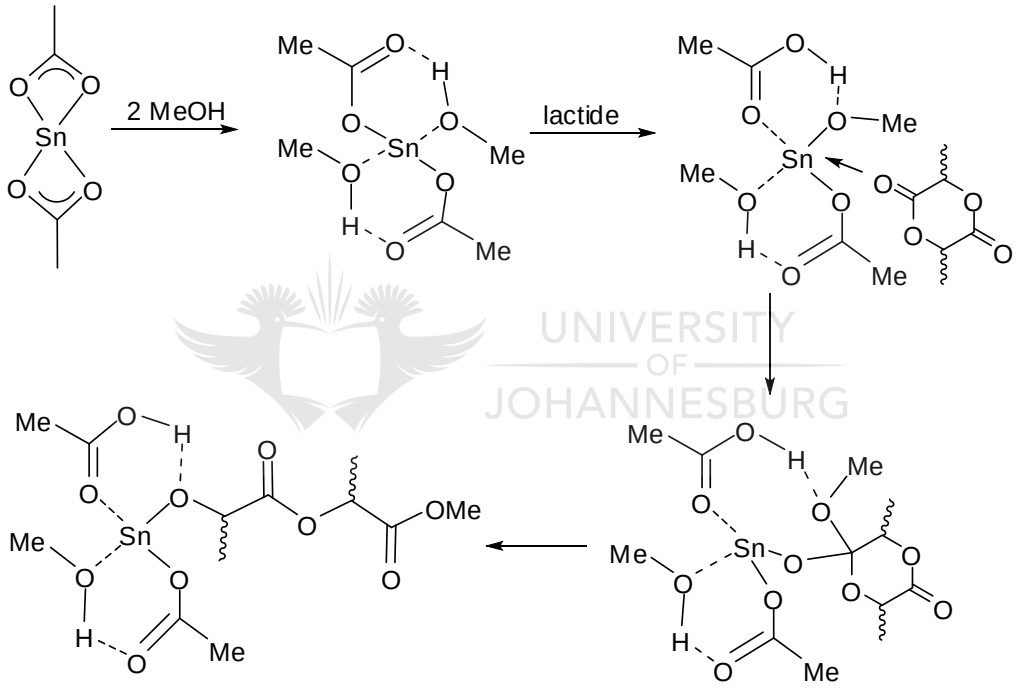

Scheme 3.1. Predicted mechanism for the [$Sn(Oct)_2$]-initiated ROP of lactide in the presence of methanol.

[100] Schwach, G.; Coudane, J.; Engel, R.; Vert, M. *J. Polym. Sci., Part A: Polym. Chem.* **1997**, *35*, 3431.

[101] Ryner, M.; Stridsberg, K.; Albertsson, A. C.; von Schenk, H.; Svensson, M. *Macromolecules* **2001**, *34*, 3877.

Two molecules of methanol were found to coordinate to [$Sn(OAc)_2$] as a model for [$Sn(Oct)_2$]. Both coordinations are favoured by about 59-63 kJ/mol and occur in an associative fashion, with retention of the two octanoate moieties (H-bonds are formed between the alcohol and octanoate ligands). A weak complexation of lactide was then predicted (coordination enthalpy of 16 kJ/mol). Notably, the latter coordination step induces a proton migration from methanol to the nearby octanoate ligand, so that the alcohol ligand is converted into an alkoxide. Subsequently, the insertion occurs in two steps: (i) nucleophilic attack of this alkoxide on the coordinated lactide followed by (ii) ring opening, resulting formally in the insertion of a lactide moiety into the O-H bond of a coordinated methanol. These calculations suggest that the octanoic acid remains coordinated to tin during propagation, but taking into consideration both the entropic term and the reaction temperature, the authors concluded that it might also be possible that the octanoic acid dissociates from the tin alkoxide complex during ROP. Hence, this theory supports the results obtained for the **L1** system.

Moreover, the kinetics of the zinc complexes of different ancillary pyrazolyl ligands were studied and it can be concluded that complex **2**, which is coordinated to **L1**, shows the best activity, followed by **12** with **L6**. The complex with **L2**, **6** comes after **12** with only a slight difference in the performance. Lastly, complex **9** exhibits the lowest rate of initiation for the polymerization of D,L-lactide in toluene. The **L4** linker appears to have a negative effect on the polymerization, similar to the ROP of ε-CL.

3.8 Characterization of PCL and PLA

If using the metal complexes synthesized as initiators is assumed to be living polymerization, reaction should proceed according to Equation 2 (not taking induction period into consideration).

$$-d[M]/dt = k_p [M][I] \qquad (2)$$

k_p: rate constant

From Equation 2, linear plot of $\ln[M]_o/[M]_t$ against time, t can also be obtained using Equation 3.

$$\ln([M]_o/[M]_t) = k_{app}\, t \qquad (3)$$

k_{app}: apparent rate constant of polymerization ($k_{app} = k_p [I]$)

t: time

In addition to the k_{app} values, the degree of polymerization, DP_n, can be calculated from the ^{1}H NMR spectrum of the polymerization mixture. The DP_n, the number of repeat units in an average polymer chain at time in a polymerization reaction, is the ratio of the number of monomer used to the number of moles of initiator. DP_n is obtained using Equation 4 for PCL and Equation 5 for PLA.

$$DP_n\,(PCL) = \frac{I(CH)}{I(CH)_{EG}} \times 114 \qquad (4)$$

$$DP_n\,(PLA) = \frac{[I(CH)]/2}{I(CH)_{EG}} \times 144 \qquad (5)$$

I(CH): intensity of CH of polymer

$I(CH)_{EG}$: intensity of CH end group of the initiator

Moreover, number average molecular weight of the polymers synthesized, M_n (^{1}H NMR), was calculated from the ^{1}H NMR spectra of the polymer mixtures for the polymerization reactions using Equation 6.

$$M_n\ (^1\text{H NMR}) = Mr_{monomer} \times \frac{I(CH)}{I(CH)_{EG}} + Mr_{Initiator} \qquad (6)$$

3.8.1 PCL characterization

The apparent rate constant of polymerization, k_{app}, was obtained from the slope of the graph of $\ln([M]_o/[M]_t)$ against time. Considering the linker system (initiators of **L4** and **L6**), complex **12** showed the highest k_{app} value while the lowest rate constant was obtained for initiator system **23**. The molecular weights of the PCL produced using the initiators of **L6** and **L4**, were determined by ^{1}H NMR spectroscopy and from the results obtained (Table 3.1) the highest M_n was obtained for complex **9** (6 651 Da), while the lowest one is for PCL formed using **21** (2 393 Da).

Size exclusion chromatography (SEC), calibrated to polystyrene standards, was also run on the polymers synthesized by **9**, **10**, **12**, **13** and **23** and HPLC grade THF was used as eluent. M_n values as well as the polydispersity index (PDI), which is the ratio of M_w/M_n, were obtained (Table 3.1). SEC molecular weights, calibrated on polystyrene standards, were multiplied by 0.56 as a correcting factor for PCL.[102]

[102] Baran, J.; Duda, A.; Kowalski, A.; Szymanski, R.; Penczek, S. *Macromol. Symp*. **1997**, *123*, 93.

Table 3.1. Bulk ε-CL ROP using complexes of **L4** and **L6**, [M]/[I] = 50:1 at 110 ^{o}C.

Complex	% Conversion	k_{app} (h^{-1})	M_n (^{1}H NMR)	M_n (SEC)[a]	PDI
9	100	0.109	6 651	2 146	1.57
10	100	0.103	5 550	2 121	1.84
11	73	0.115	3 530	3 976	2.15
12	94	0.227	4 100	4 574	1.58
13	100	0.186	6 046	3 077	1.77
21	98	0.070	2 393	-	-
23	98	0.041	4 065	858	2.16
24	93	0.079	3 900	-	-
25	92	0.063	3 160	-	-
26	100	0.087	5 250	-	-

[a] Using a correcting factor 0.56 for M_n.

The molecular weights of PCL obtained from the initiators in Table 3.1 measured by SEC (4 757 – 858 Da) are very small compared to those of PCL synthesized using [Al(O^{i}Pr)$_3$] and [Sn(Oct)$_2$] as initiators, giving molecular weights of 41 800 and 5 700 Da respectively.[40,103] But the high molecular weight of PCL obtained from [Al(O^{i}Pr)$_3$] initiator system has a PDI of 1.66,[29] while PDI of PCL from this project is as low as 1.36 (Table 3.2). Despite the low molecular weight of PCL synthesized during this project, the molecular weight distribution is comparable to the [Al(O^{i}Pr)$_3$] initiator system.

To get some insight into the active species, complex **10** was chosen to study the NMR spectrum of the polymerization mixture after complete conversion (Figure 3.10). This

[103] Mingotaud, A. F.; Dargelas, F.; Cansell, F. *Macromol. Symp*. **2000**, *153*, 77.

spectrum was run before the polymer was cleaned, thus the polymer chains were still attached to the metal complex. Peaks corresponding to the different protons of the polymer, as well as those of the initiator are seen from the spectrum. PCL end-capped with the benzoate group could be identified, supporting a coordination-insertion mechanism for the ROP of the monomer.

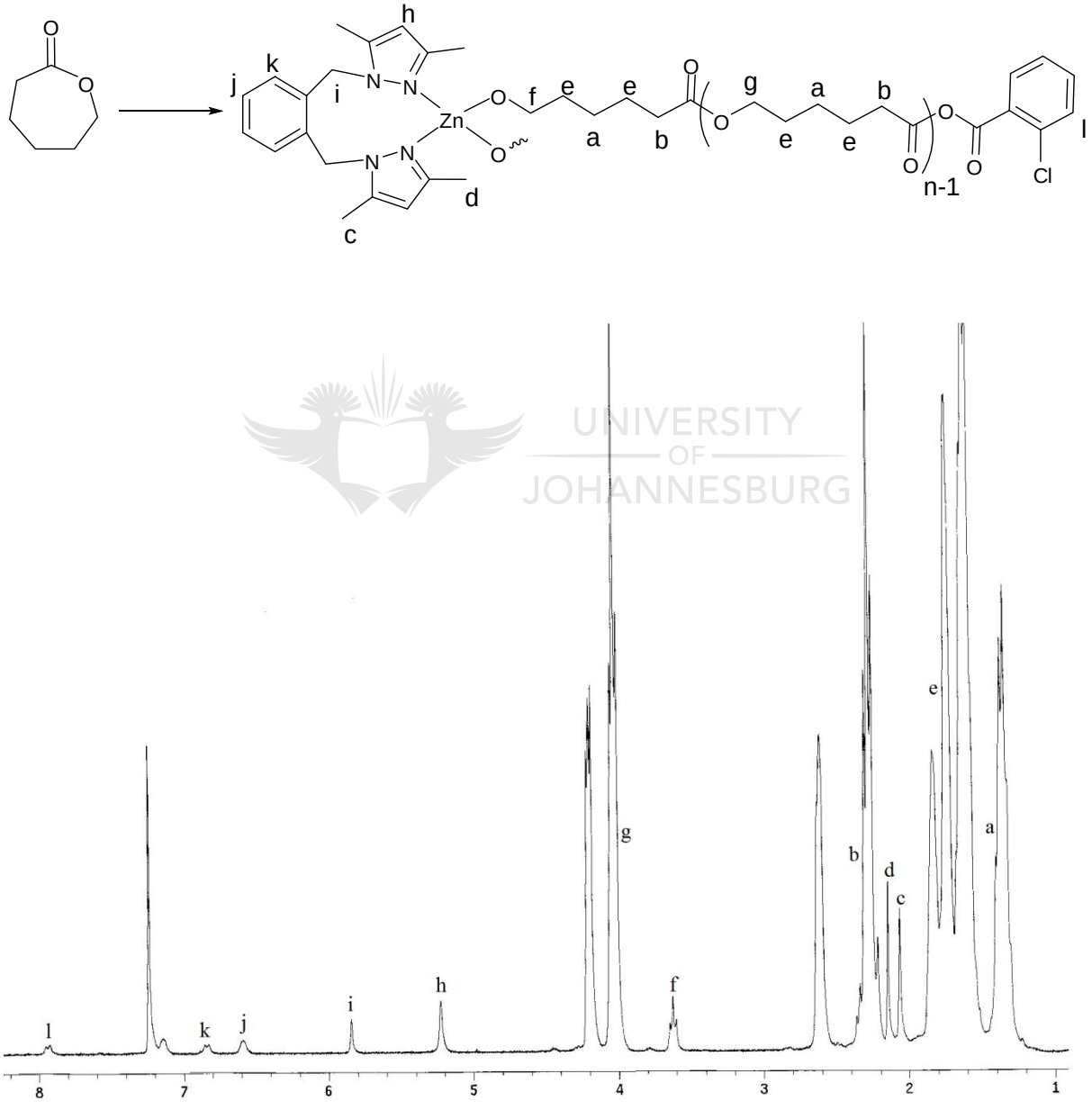

Figure 3.10. ^{1}H NMR spectrum of polymerization mixture in $CDCl_3$.

Similarly, PCL produced using complexes of **L1** were characterized by ^{1}H NMR spectroscopy and the M_n values obtained are summarized in Table 3.2. Complex **15** showed the highest rate constant in this no linker system. In addition, this k_{app} value is higher than the rate constants displayed by initiators of **L4** and **L6**. Furthermore, the highest M_n was obtained for the polymer synthesized by **22** (4 742 Da) and the lowest M_n was shown by initiator system **2** (1 676 Da).

Table 3.2. Bulk ε-CL ROP using complexes of **L1**, [M]/[I] = 50:1 at 110 ^{o}C.

Complex	% Conversion	k_{app} (h^{-1})	M_n (^{1}H NMR)	M_n (SEC)[a]	PDI
1	100	0.185	4 405	4 757	1.69
2	98	0.120	1 676	3 125	1.84
4	98	0.182	1 817	-	-
3	97	0.169	2 026	-	-
14	100	0.090	4 242	4 734	1.36
15	97	0.286	2 514	3 450	1.61
16	100	0.143	4 742	-	-
17	98	0.151	2 866	-	-

[a] Using a correcting factor 0.56 for M_n.

The activities of the initiators of the different pyrazolyl ligands were compared using [Zn(3,5-NO_2-$C_6H_3COO)_2$] complexes of **L1**, **L2**, **L4** and **L6**. From the plots of $\ln([M]_o/[M]_t)$ against time, it was observed that the rate constant values decrease in the order: **6** > **12** > **9** > **2**. Alternatively, the activities of the pyrazolyl ligands can be arranged in the order: **L2** > **L6** > **L4** > **L1**. Moreover, the number of active Zn-O bonds was determined from the slope of the

graph of DP_n against time. For initiator **6**, the slope was obtained as 1.23, indicating that only one, out of the two Zn-O bonds in the complex, is active (Figure 3.11).

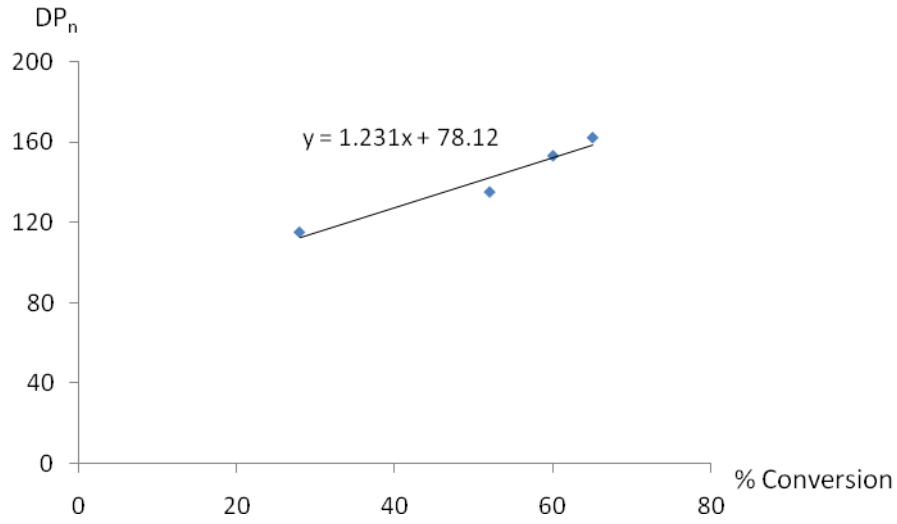

Figure 3.11. DP_n v/s % conversion plot for PLA synthesized using **6**.

3.8.2 PLA characterization

Complexes of **L6** were used for D,L-lactide polymerization and the products were characterized in a similar way as PCL. In comparison with ε-CL ROP, the rate constants for lactide ROP are lower; the highest k_{app} value is shown by initiator **25**. These values and the values of M_n for PLA, synthesized in toluene using complexes of **L4** and **L6**, are summarized in Table 3.3. The highest M_n is shown by initiator system **25** (2 953 Da), while the lowest is shown by **21** (1 420 Da). PLA obtained from the methanol systems are observed to have comparable M_n with the system without methanol, taking into account the percentage conversions. Similar to PCL, SEC molecular weights, calibrated on polystyrene standards, were multiplied by 0.58 as a correcting factor for PLA.

Table 3.3. ROP of D,L-lactide in toluene using complexes of **L4** and **L6**, [M]/[I] = 100:1 at 110 ^{o}C.

Complex	% Conversion	k_{app} (h^{-1})	M_n (^{1}H NMR)	M_n (SEC)[b]	PDI
9	90	0.018	1 537	2 218	1.57
9[a]	65	0.019	908	-	-
10	95	0.020	1 630	2 197	1.84
10[a]	62	0.011	925	-	-
11	96	0.034	2 350	-	-
12	92	0.016	2 315	-	-
13	100	0.023	1 945	3 185	1.77
21	76	0.034	1 420	-	-
23	97	0.032	1 695	602	1.64
24	91	0.011	1 877	-	-
25	100	0.044	2 953	-	-
26	96	0.019	1 812	-	-
26[a]	28	0.003	1 020	-	-

[a] Reactions were carried out using methanol as additive.

[b] Using a correcting factor 0.58 for M_n.

The no linker system was used to polymerize D,L-lactide using complexes of **L1** and the PLA obtained was also characterized using ^{1}H NMR spectroscopy and SEC to determine the M_n values (Table 3.4). PLA formed using **1** afforded highest M_n (1 900 Da), while complex **16** produced PLA of lowest M_n (1 242 Da). Contrary to the linker system, the molecular weights of the PLA produced using complexes of **L1** were affected by the addition of methanol in the reaction mixture. Thus, complex **1** produced PLA of lower M_n (818 Da)

when methanol was added, compared to the reaction where only toluene was used. Similar observations are made for the initiator **14** that produced PLA of lower M_n when methanol was used.

Table 3.4. ROP of D,L-lactide in toluene using complexes of **L1**, [M]/[I] = 100:1 at 110 ^oC.

Complex	% Conversion	k_{app} (h^{-1})	M_n (^1H NMR)	M_n (SEC)[b]	PDI
1	96	0.024	1 900	1 971	2.05
1[a]	100	0.024	818	2 484	1.42
2	96	0.025	1 645	833	2.35
3	96	0.023	1 885	-	-
4	95	0.023	1 342	-	-
14	94	0.039	1 780	1 232	1.84
15	92	0.018	1 810	1 167	1.87
16	92	0.020	1 242	-	-
17	93	0.020	1 650	-	-

[a] Reactions were carried out using methanol as additive.

[b] Using a correcting factor 0.58 for M_n.

When the values of molecular weight for the PLA synthesized are compared to the ones for PLA obtained from [$Al(O^iPr)_3$] and [$Sn(Oct)_2$] it observed that, similar to PCL, the initiator system used in this project gave lower molecular weights than the two most commonly used initiators. Thus, [$Al(O^iPr)_3$][4] and [$Sn(Oct)_2$][39] gave PLA of molecular weight 90 000 and 130 000 Da respectively compared to weights of 3 185 – 602 Da obtained for the initiators used for this study. Nevertheless, the molecular weight distributions for the polymers, synthesized by the different systems, are comparable, with PDI values of around 1.4.

From the values of M_n obtained from ^{1}H NMR spectroscopy and SEC, it can be seen that there is no correlation between the two methods. It is clear that ^{1}H NMR spectroscopy cannot be used to deduce the M_n values of polymers and the best method is SEC.

3.8.3 SEC analysis of PCL and PLA

Size exclusion chromatography is a widely used technique in the analysis of the molecular weight distribution of polymers. This method allows a good separation of the analytes depending on their size. The column, based on cross-linked polystyrene, allows the polymer chains to elute out at different rates, depending on the sizes of the chains.

Hence, SEC of polymers synthesized using **6** as initiator is used as a typical example. From the SEC of PLA and PCL, it was observed that the molecular weight of PLA was smaller than PCL, which has been seen for all the initiator systems studied. Thus, the 7-membered ε-CL ring opens more easily than the 6-membered ring D,L-lactide, resulting in higher molecular weight of the PCL than PLA. Many of the SEC of both polymers show the presence of more than one peak, one main peak and the other ones are much smaller. This indicates the occurrence of intramolecular transesterification reactions, involving back-biting leading to cyclic structures. In the case of PCL synthesized by initiator **6**, three peaks are present in the chromatogram: corrected M_w (weight molecular weight) = 7 263, 850 and 267 Da. Hence, the average corrected M_w was found to be 2 613 Da with PDI of 2.563. The SEC for PLA obtained from the same initiator system reveals two peaks of M_w (corrected) = 1 882 and 285 Da. The average corrected M_w was reported as 1 603 Da and a PDI of 1.545 was obtained. Comparing the two polymers, the polymerization is more controlled for lactide ROP, which gives polymer of narrower molecular weight distribution as well as less intermolecular transesterification occurs.

3.8.4 MALDI-TOF MS of PCL and PLA

Currently, the best technique to identify end groups of PCL and PLA is MALTI-TOF MS, which is used by most researchers in this area. Structural information from MALDI-TOF MS experiments complement traditional analytical methods such as NMR and SEC: SEC provides molecular weight distribution information, while MALDI-TOF MS spectra provide the end group information. Hence, some PCL and PLA samples were analyzed using this technique, from which the end groups of the polymers were evaluated. Okuda *et al.*[104] and Phomphrai *et al.*[105] have studied the MALDI-TOF mass spectra of PLA and PCL respectively as a means of finding the types of polymer chains formed. They reported three types of polymers: A, which is the polymer chain with an -OH end group; B, which has ligand still attached to the polymer chain and C, which is a cyclic oligomer or polymer (Figure 3.12).

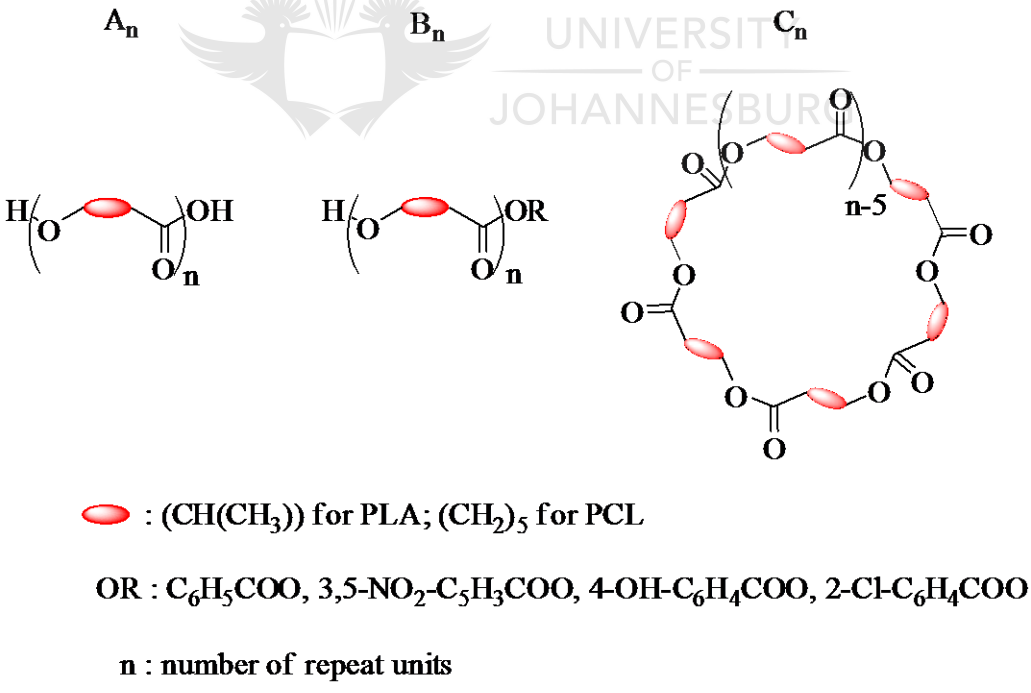

Figure 3.12. Structures of the different types of polymers obtained from MALDI-TOF MS.

[104] Okuda, J.; Haiyan, M. *Macromolecules* **2005**, *38*, 2665.

[105] Phomphrai, K.; Pongchan-o, C.; Thumrongpatanaraks, W.; Santrirutnugul, P.; Kongsaeree, P.; Pohmakotr, M. *Dalton Trans*. **2011**, *40*, 2157.

The MALDI-TOF MS for the polymers synthesized during the course of this study were separated into two groups: the zinc-based initiators and copper-based initiators used for the synthesis of PLA and PCL.

The polymers synthesized using zinc-based initiators were analyzed by MALDI-TOF MS and a typical spectrum for PCL, synthesized using **10** as initiator, is illustrated in Figure 3.13. From the spectrum, two sets of peaks are observed, indicating bimodal distribution for the polymers prepared for this initiator system. This bimodal distribution gives a sign that some transesterification reactions are taking place.

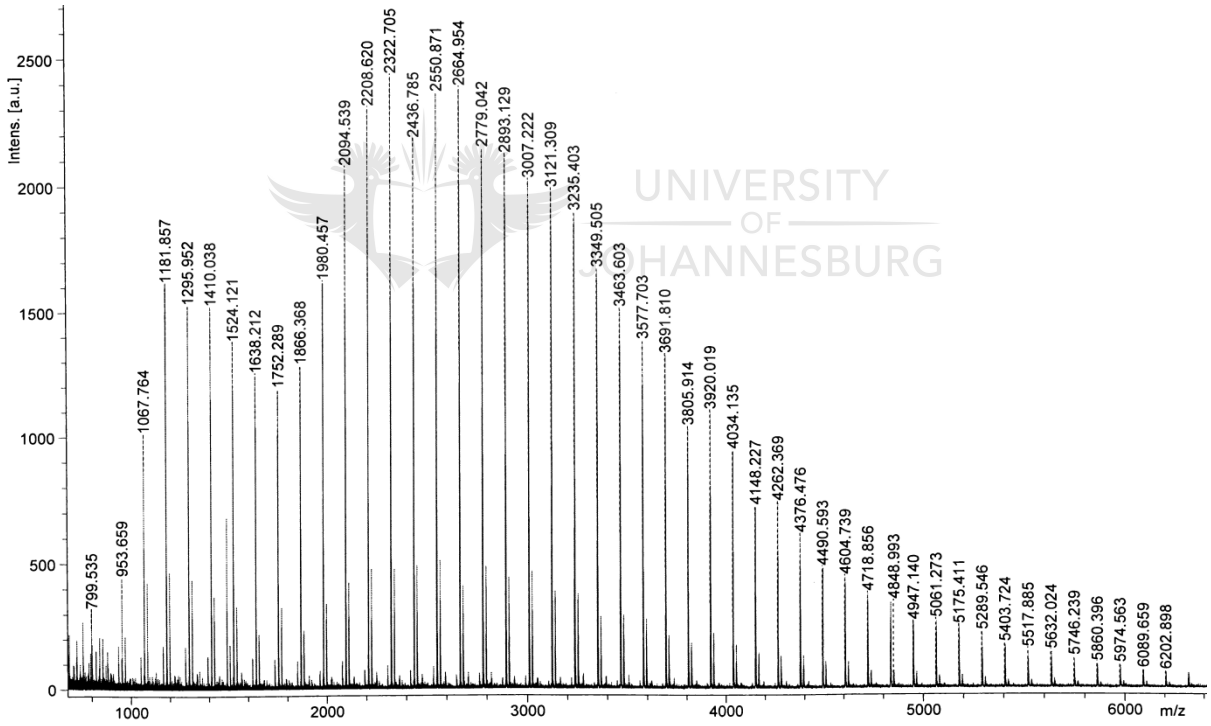

Figure 3.13. MALDI-TOF mass spectrum of PCL synthesized using **10**.

The variation in the masses is broad, from around m/z = 800 to masses higher than m/z = 6 200, indicating that the PCL chain lengths vary by a lot. Hence, some PCL chains will have 10 repeat units, while others will have 50 repeat units. But from the spectrum, it is seen that

most of the chains have masses roughly equal to m/z = 2 550 and hence around 20 repeat units in the chain. Moreover, the values of the peaks of highest intensities correspond to PCL of type A, similar to the polymers synthesized using the copper complexes of **L6**.

Results obtained from the two techniques, the SEC and MALDI-TOF MS of PCL obtained from initiator system **10**, show the average molecular weight of the PCL from the SEC is 6 984 Da, which is higher than the average value from the MALDI-TOF MS. Therefore, these two techniques have to be used independently: SEC is more accurate in determination of M_n while MALDI-TOF MS shows more accuracy in the end group analysis of the polymers than in determining the M_n and the PDI of the polymers, making them two complementary methods in characterizing polymers.

In order to compare the activity towards the synthesis of PCL and PLA, the MALDI-TOF mass spectrum of the PLA formed using **10** was studied. In this case, monomodal envelop-shaped distribution was observed (Figure 3.14), indicating the absence of transesterification during the polymerization of lactide.

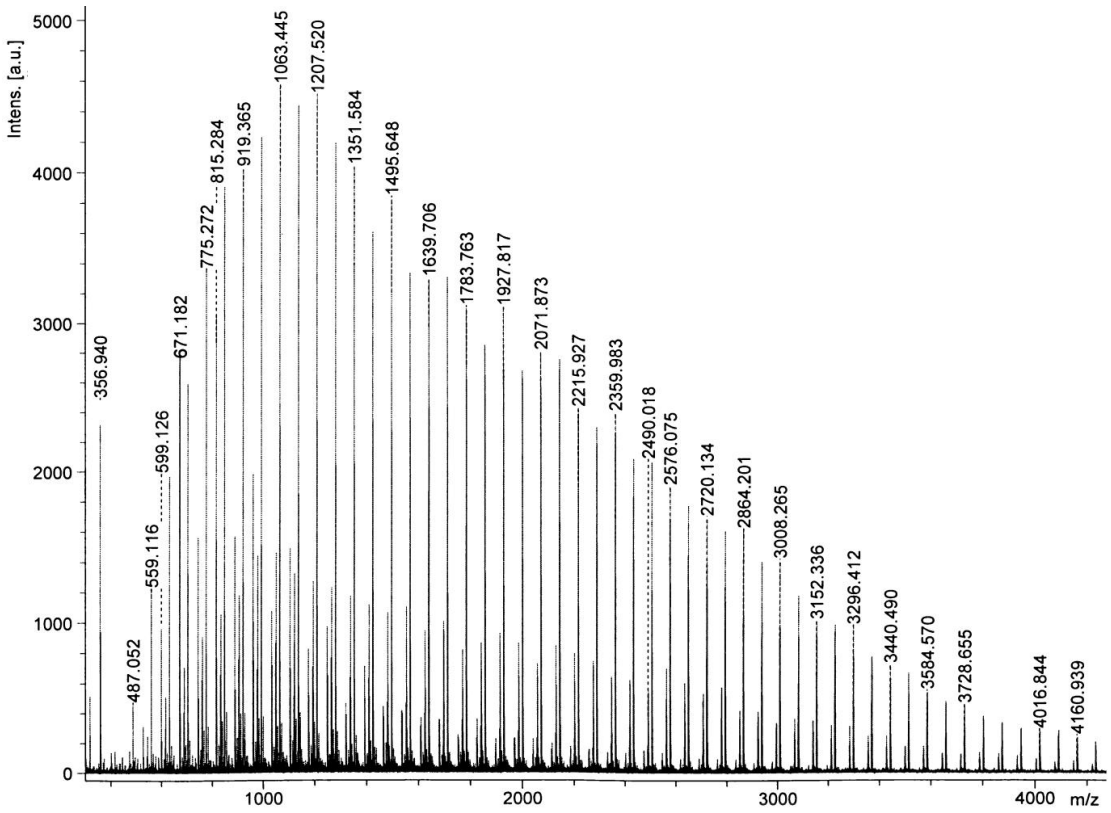

Figure 3.14. MALDI-TOF mass spectrum of PLA synthesized using **10**.

Most of the PLA chains have m/z = 1 063, showing that the PLA chains consist of about 14 repeat units. The doping ion in this case is potassium and as expected, there is a slight difference between the calculated and found values. But this initiator system is the only one to give rise to polymers that were doped with potassium; the other zinc initiators give polymers with sodium as doping ion. Another important observation made for the zinc initiator system is the synthesis of polymers of almost the same molecular weights, irrespective of the initiator used. These values are summarized in Table 3.5, with the masses of the polymers of highest abundance.

Table 3.5. Assignment of peaks for PCL and PLA synthesized by **10-13**.

PCL			PLA		
m/z (obs)	**m/z (calc)**	**Assignment**	**m/z (obs)**	**m/z (calc)**	**Assignment**
1 067	1 068	$A_9 + Na^+$	2 346	2 345	$A`_{32} + Na^+$
1 181	1 182	$A_{10} + Na^+$	2 490	2 489	$A`_{34} + Na^+$
1 295	1 296	$A_{11} + Na^+$	2 562	2 633	$A`_{36} + Na^+$
1 410	1 410	$A_{12} + Na^+$	2 706	2 777	$A`_{38} + Na^+$
2 208	2 209	$A_{19} + Na^+$	2 922	2 921	$A`_{40} + Na^+$
2 322	2 323	$A_{20} + Na^+$	3 066	3 065	$A`_{42} + Na^+$
2 436	2 337	$A_{21} + Na^+$	3 210	3 209	$A`_{44} + Na^+$
2 550	2 552	$A_{22} + Na^+$	3 354	3 353	$A`_{46} + Na^+$
2 664	2 666	$A_{23} + Na^+$	3 498	3 497	$A`_{48} + Na^+$
2 779	2 780	$A_{24} + Na^+$	3 642	3 641	$A`_{50} + Na^+$
2 893	2 894	$A_{25} + Na^+$	3 786	3 785	$A`_{52} + Na^+$

Considering the copper initiator systems, a typical envelope-shaped spectrum for PCL, synthesized using **23** as initiator, is shown in Figure 3.15a. An expansion of the region m/z = 1 150-1 550 revealed that there is a pattern that repeats itself several times (Figure 3.15b). The peaks of highest intensities were found to correspond to an open polymer chain

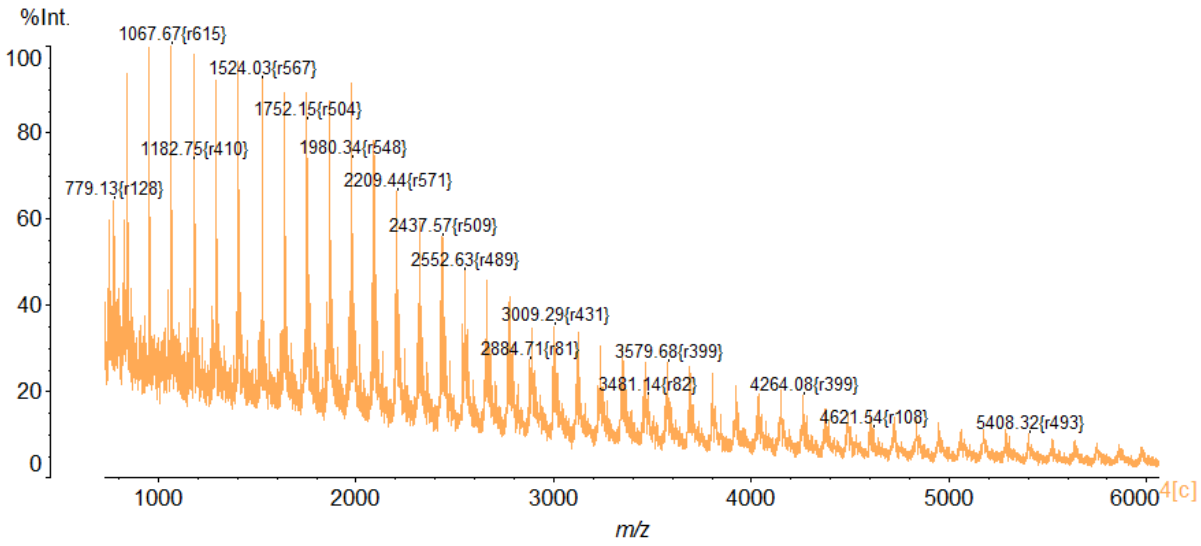

(a)

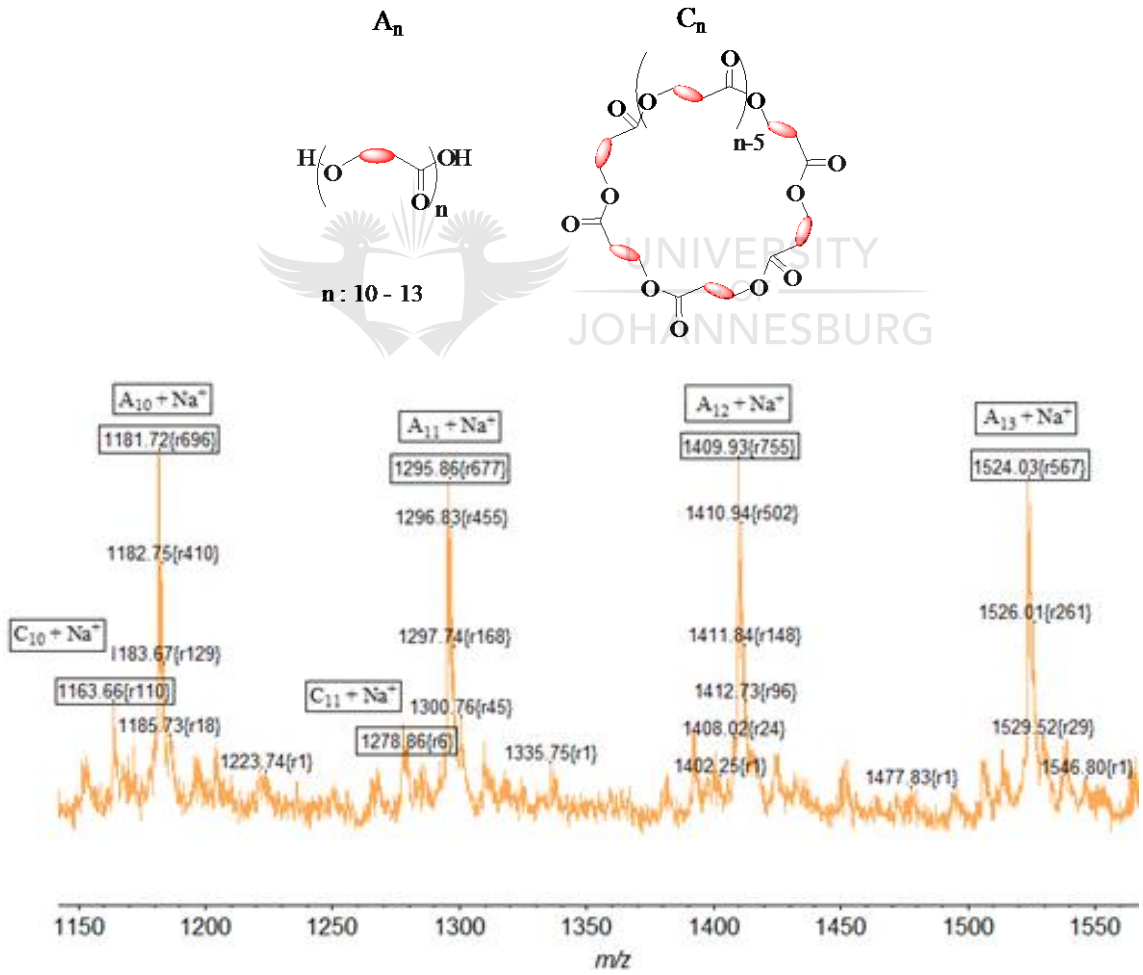

(b)

Figure 3.15. **(a)** MALDI-TOF mass spectrum of PCL made using **23**, **(b)** Expansion of **(a)** in the region m/z = 1 150-1 550.

having a hydroxyl group as end group (type A). The masses were calculated by adding sodium ion, which comes from the matrix. The next series of peaks correspond to cyclic PCL of the type C. Masses for PCL of type B could not be identified, indicating that during the cleaning process, the polymer hydrolyzed.

The MALDI-TOF mass spectrum of PLA synthesized using **23** as initiator shows that the m/z values of the polymers are higher for PLA than for PCL (Figure 3.16a). When an expansion of the spectrum of the PLA is examined carefully, it is observed that there are more peaks in the repeat segment of the spectrum than was observed in the previous case. The peaks of highest intensities are assigned to PLA of type A` because of the good correlation between the calculated value for this type of polymer (using $Na^+$ as doping ion) and the found ones. The masses matching PLA of type C` are found when Na^+ is accounted for in the calculation of the masses. In the spectrum, masses are also found for PLA of type B`, in which case the doping ion is K^+.

Apart from these peaks, an additional peak is observed. The separation between the peaks of this intensity is 72, which is similar to the separation of the other peaks. Surprisingly, the masses associated to these peaks correspond to a type of polymer that is different from the reported ones. This new polymer type, D`, is derived based on the process undergone by the polymer and is found to correspond to the polymer end group being a methoxy group. This $OCH_3$ group might be a consequence of the cleaning process, which involved the use of a methanol solution of HCl. Hence, PLA of type D` is also formed in relatively high intensity compared to PLA of type B` and C`. An expansion of a region in the MALDI-TOF mass spectrum with allocation of the peaks to the end groups of PLA is illustrated in Figure 3.16b.

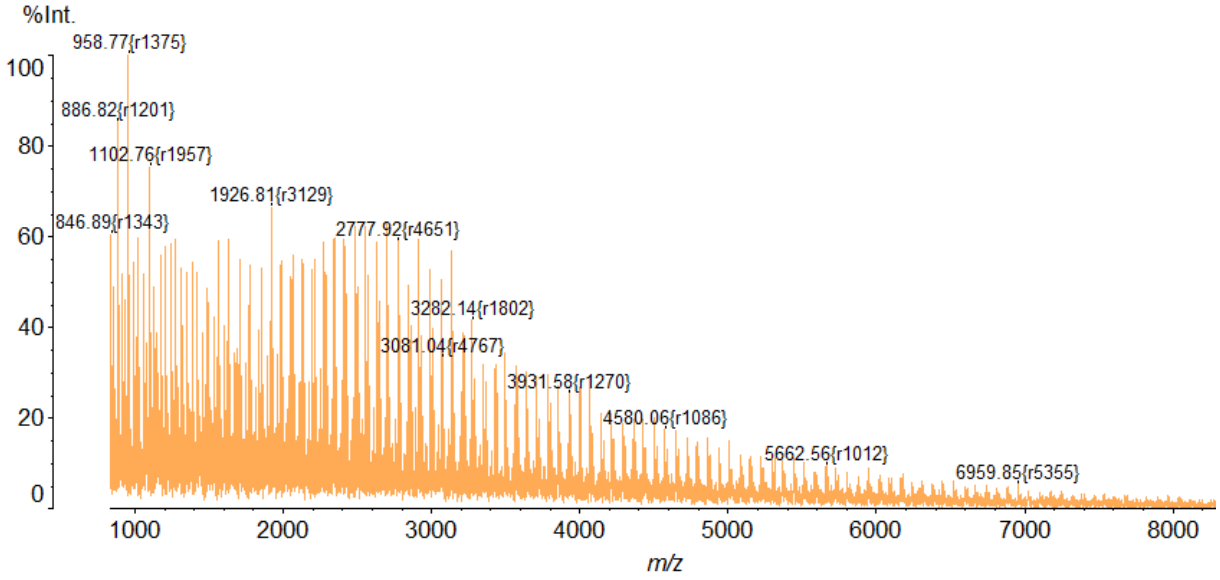

(a)

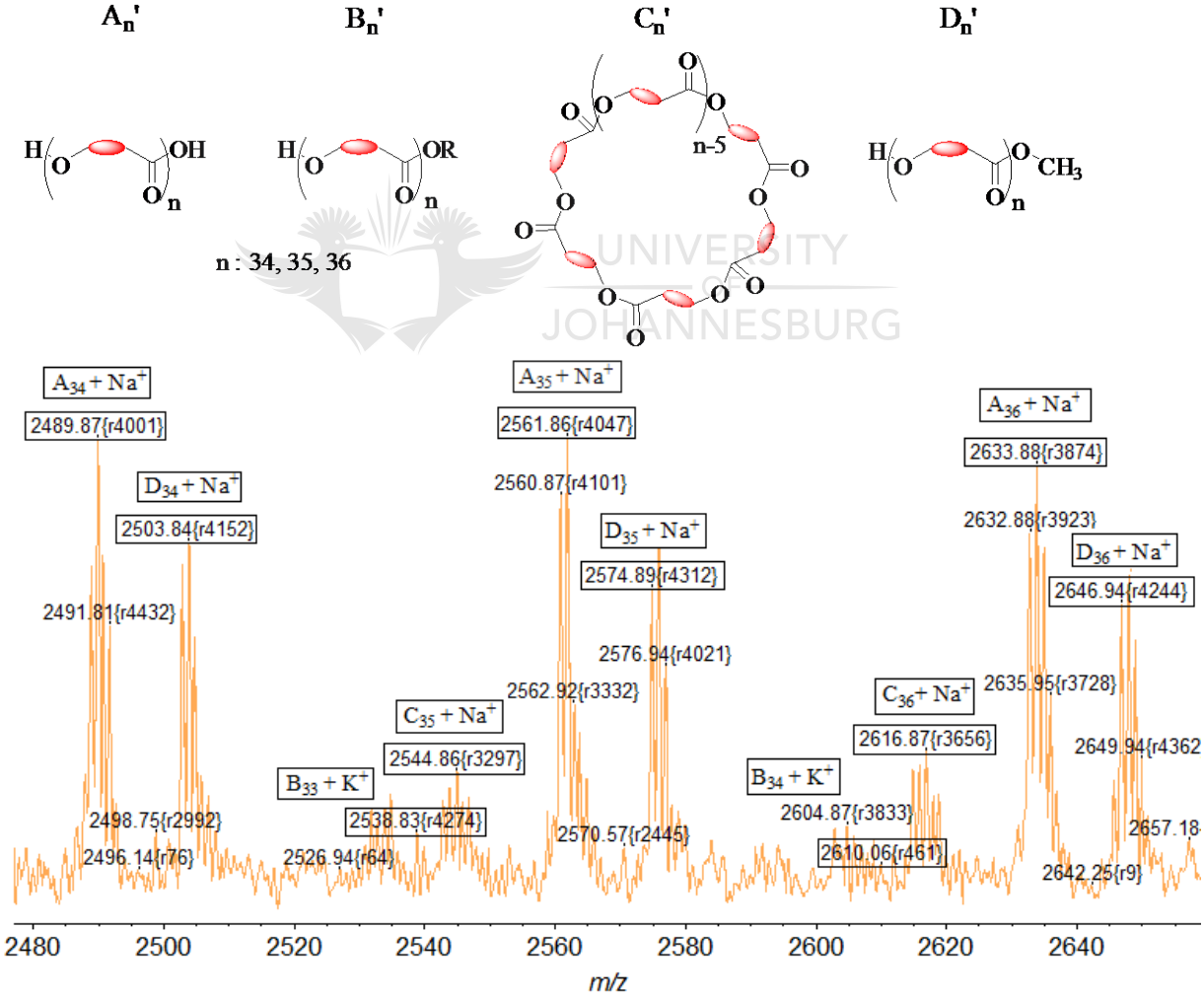

(b)

Figure 3.16. **(a)** MALDI-TOF mass spectrum of PLA from initiator **23**, **(b)** An expansion of **(a)** in the region m/z = 2 480-2 660.

Similar to the initiator system using **23**, the MALDI-TOF MS of PCL and PLA synthesized using the other copper(II) benzoates of **L6**, were also obtained.

From the different expansions of the spectra, the masses of the peaks found have been allocated to the type of end groups formed. These values are summarized in Table 3.6, with the found and calculated values almost similar to each other. It was observed that in cases where the doping ion is potassium, the calculated and the observed m/z values are not very close. Nevertheless, these values allow the comparison of the masses of the polymers formed for the different initiator systems. Thus, initiator **26** shows the highest mass of polymer, both PCL and PLA; polymers of lowest masses are formed by initiator **24**. This shows that the initiator plays a crucial role in the determination of the molecular weight of the polymer being synthesized and careful selection of the initiator allows polymers of a specific molecular weight to be produced.

Furthermore, an observation made is that the peaks of highest intensities correspond to the polymers having a hydroxyl end group. This means that the polymer chains end with an OH group, which is the result of the cleaning process, during which the bonds between the ligand and the metal are broken. Moreover, from the results obtained from this analysis, it is observed that polymer of type B, which still contains the ligand as end group, is very rare. Therefore, this illustrates that the clean polymer does not contain the complex. Hence no metal is present in the polymer according to this analysis, but traces of the metal might still be in the polymer, which is not too small to be detected by the MALDI-TOF MS.

Table 3.6. Assignment of peaks for PCL and PLA synthesized by **L6** complexes of Cu.

Initiator	PCL			PLA		
	m/z (obs)	m/z (calc)	Assignment	m/z (obs)	m/z (calc)	Assignment
25	1 867	1 867	$A_{16} + Na^+$	1 351	1 353	$A`_{18} + K^+$
25	1 981	1 981	$A_{17} + Na^+$	1 390	1 391	$A`_{19} + Na^+$
24	953	954	$A_8 + Na^+$	1 422	1 423	$D`_{19} + Na^+$
24	995	992	$B_7 + K^+$	1 464	1 463	$C`_{20} + Na^+$
26	3 008	3 008	$A_{26} + Na^+$	2 129	2 129	$A`_{29} + Na^+$
26	3 034	3 038	$D_{26} + K^+$	2 143	2 143	$D`_{29} + Na^+$
26	3 122	3 122	$A_{27} + Na^+$	2 184	2 183	$C`_{30} + Na^+$
23	1 163	1 164	$C_{10} + Na^+$	2 489	2 489	$A`_{34} + Na^+$
23	1 181	1 182	$A_{10} + Na^+$	2 503	2 503	$D`_{34} + Na^+$
23	1 278	1 278	$C_{11} + Na^+$	2 538	2 537	$B`_{33} + K^+$
23	1 295	1 296	$A_{11} + Na^+$	2 544	2 543	$C`_{35} + Na^+$

The molecular weight of a polymer is not the only factor that determines its properties; the stereochemistry of the polymer, in this case PLA, as well as the thermal properties of the polymer are crucial factors which determine the type of polymer formed.

3.8.5 Thermal analysis of PCL and PLA

Thermal analyses, using differential scanning calorimetry (DSC) and thermogravimetric analysis (TGA), were conducted to study the thermal response of the polymers. DSC is the most cited way of determining characteristic temperatures of a polymer. T_g, glass transition temperature, is the temperature of a polymer below which there is no segmental motion, resulting the polymer behaving in an increasingly brittle manner arising due to temporary

distortions of the primary valence bonds. As the temperature rises above T_g, the polymer becomes more rubber-like. So, depending on the application of the polymer, the knowledge of T_g is essential. In general, elastomers have T_g values well below room temperature (PCL has T_g ~ -64 ^oC) while rigid polymers have T_g above ambient temperature.[106]

A more important parameter is the melting point (T_m) of a polymer, above which the whole polymer chain mobility occurs and the mechanical properties are zeroed. As the melting temperature is reached, an endothermal peak appears due to heat required by the sample to continue the isothermal change in state. From the DSC thermogram in Figure 3.17a, T_m of the PCL sample, synthesized by initiator **26**, can be seen to be 60.1^oC, which lies in the range of T_m values for PCL in literature (56-65 ^oC).[10] Moreover, the most commonly used thermal decomposition test is TGA. In TGA experiments, the sample is brought quickly up to the desired temperature and the weight of the sample is monitored during the course of the thermal decomposition. The decomposition curve for PCL synthesized by **26** shows that PCL decomposes at 390 ^oC (Figure 3.17b). Similarly, the other PCL synthesized were analyzed by DSC and TGA and the same T_m and decomposition temperatures were observed, irrespective of the molecular weight of the polymer formed.

PLA samples were also analyzed similar to PCL, but no melting was observed for PLA. The TGA plot for PLA shows that the polymer starts decomposing at 60 ^oC, implying that PLA decomposes before melting, which is reported to be around 170 ^oC.[107] This explains why no melting point is observed in the DSC thermogram of PLA.

[106] Van de Velde, K.; Kiekens, P. *Polym. Test.* **2002**, *21*, 433.

[107] Williams, C. K.; Hillmyer, M. A. *Polym. Rev.* **2008**, *48*, 1.

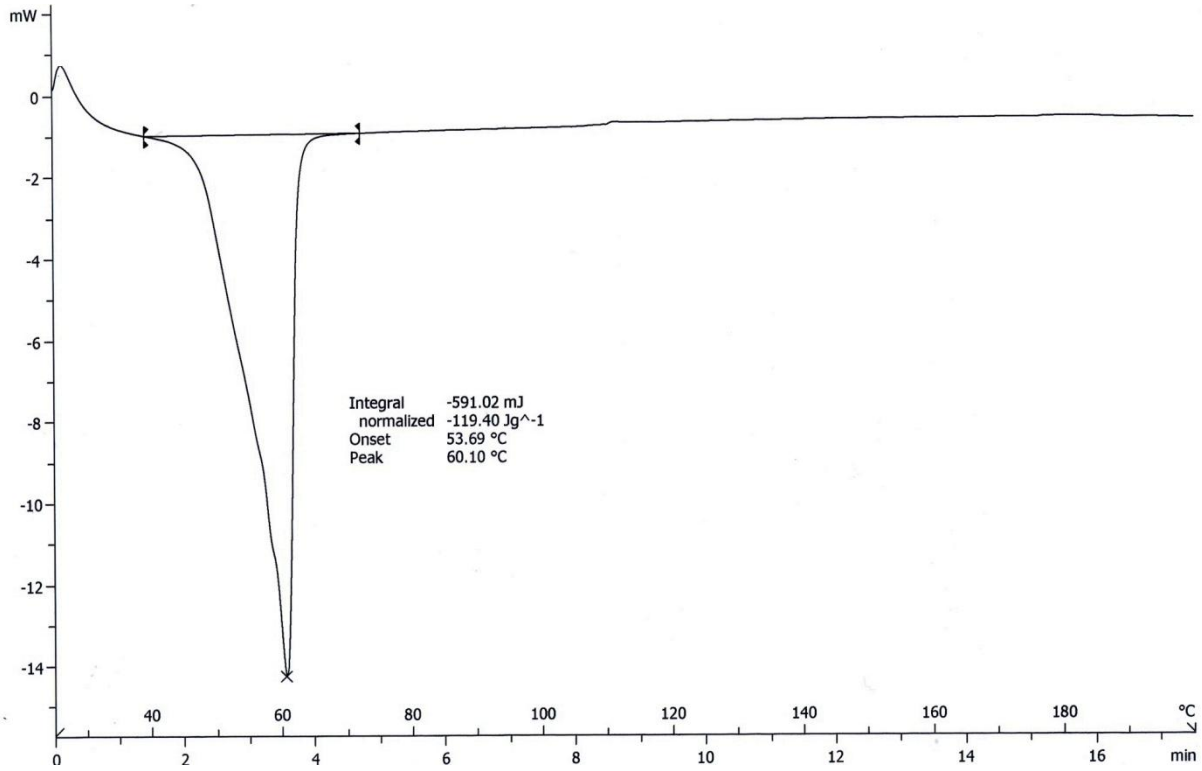

(a)

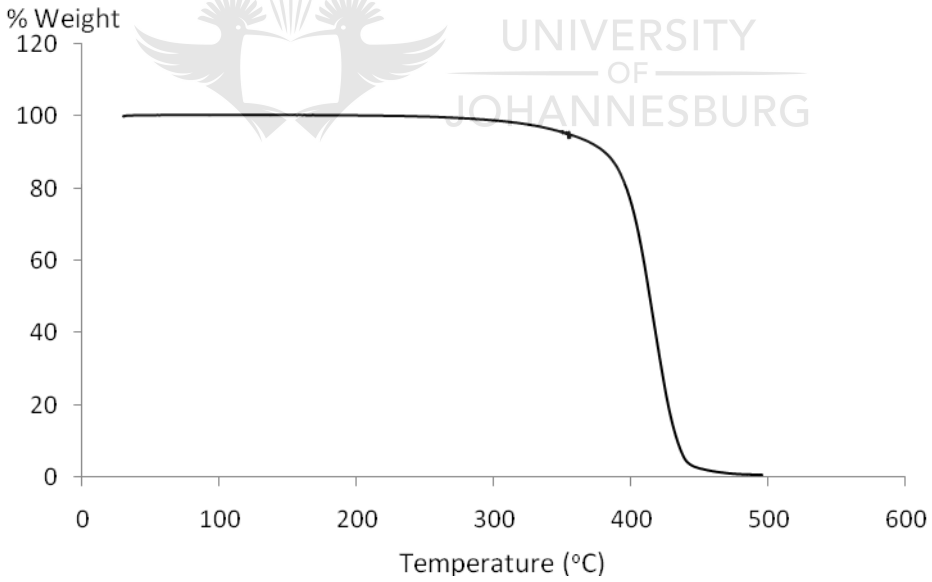

(b)

Figure 3.17. **(a)** DSC of PCL from **26**, **(b)** TGA of PCL from **26**.

3.8.6 Determination of microstructures of polymers by NMR analysis

The microstructure of a polymer depends on the distribution of the configurational repeat units in the polymer chains. The tacticity of a polymer chain is thus determined by the regularity of the configuration at successive chiral centres. An *isotactic* polymer is one where the asymmetric carbons of all the repeat units have the same configuration. When there is a regular alternating configuration in the repeat units, the polymer adopts a *syndiotactic* structure. Finally, for an *atactic* polymer, there is no order in the configuration at the chiral carbon (Figure 3.18). The sequence of the repeat units may give indications about the type of propagation of the polymer chains. If the propagation is independent on ultimate dilactoyl unit in the polymer chain, it is of Bernouillian type and if it depends on ultimate dilactoyl unit in the polymer chain, it is of Markovian type.[108]

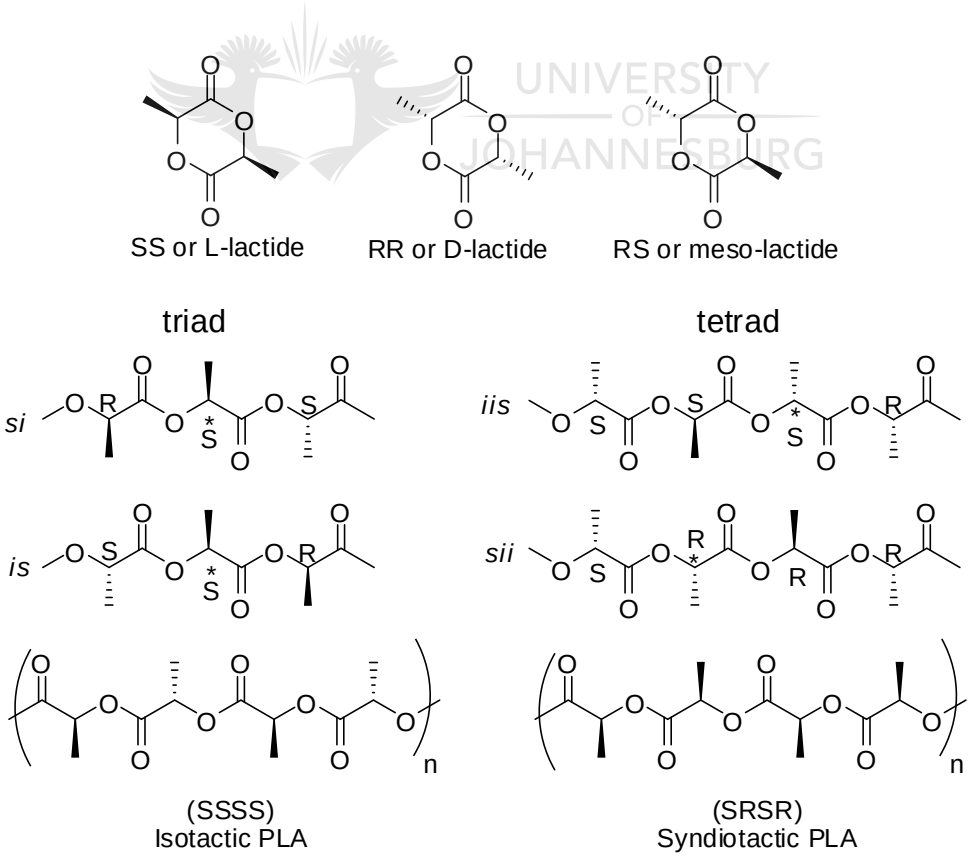

Figure 3.18. Tacticities of PLA.[11]

[108] Le Borge, A.; Spassky, N.; Jun, C. L.; Momtaz, A. *Macromol. Chem.* **1988**, *189*, 637.

The microstructure of the polymers and consequently their properties are modified by racemization and transesterification side reactions. $^{13}C\{^{1}H\}$ NMR is one of the most powerful methods to study the microstructure of polymers as the chemical shift of a particular atom depends on its chemical environment and stereochemistry. Chabot *et al.* reported that in the case of polylactides, the addition of repeat units occurs in pairs of configurational units RR or SS, depending upon the diastereoisomer used.[109] The different successive configurational units containing one, two or three molecules of lactides are shown in Scheme 3.2 below.

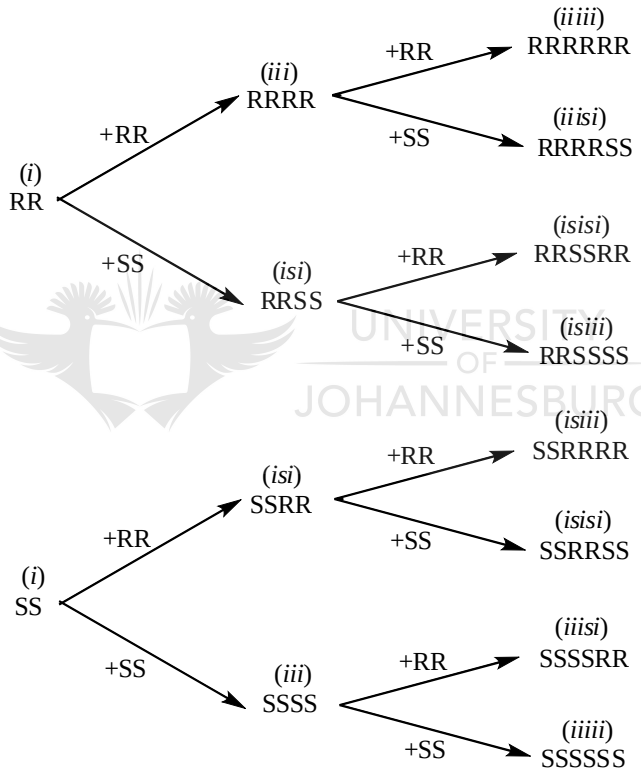

Scheme 3.2. Possible configurations of the repeat units.

The asymmetric carbon present in each repeat unit of the polymer chain can be stereosensible to diad, triad, tetrad, pentad and hexad effects. The observations of the different types of n-

[109] Chabot, F.; Vert, M.; Chapelle, S.; Granger, P. *Polymer* **1983**, *24*, 53.

ads depend on the resolution of the NMR spectrometer used and the nature of the group being considered (methyl and carbonyl) (Figure 3.19).

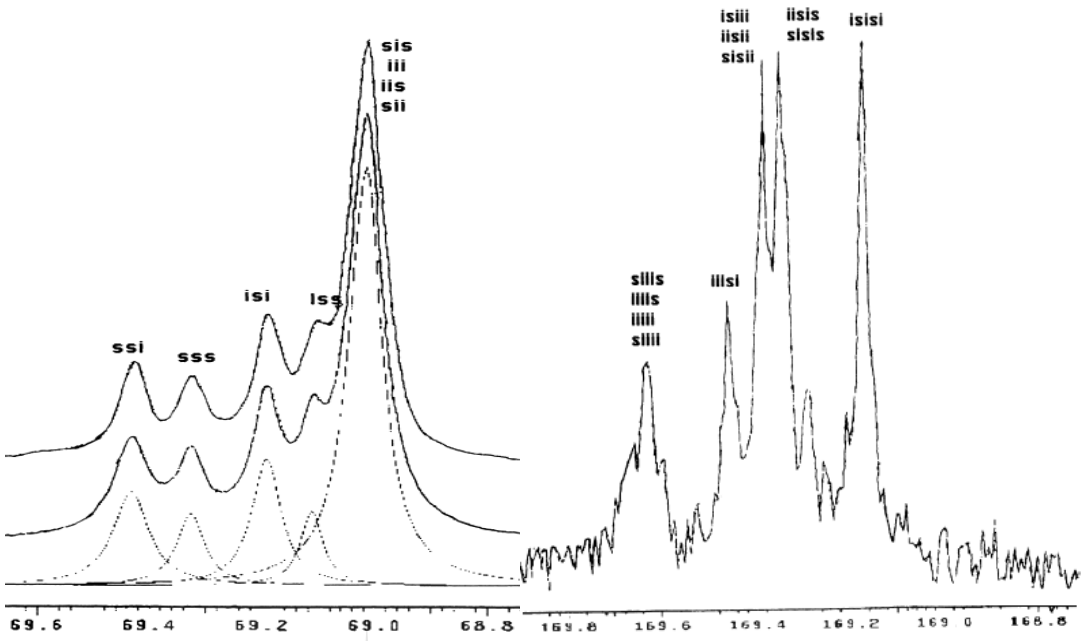

Figure 3.19. $^{13}C\{^{1}H\}$ NMR spectrum of PLA with assignments of **(a)** the methine peaks and **(b)** the carbonyl peaks.[110]

Table 3.7[11] below gives the tetrad and hexad intensities and hence the determination of the tacticity of the polymer obtained based on a Bernoullian statistics, which was found for PLA prepared by $[Al(acac)_2]$ as initiator.[111]

[110] Kasperczyk, J.; Bero, M. *Polymer* **2000**, *41*, 391.

[111] Bero, M.; Kasperczyk, J.; Jedlinski, Z. *Makromol. Chem.* **1990**, *191*, 2287.

Table 3.7.Theoretical values of tetrads and hexads for the different possible structure of PLA.

$^{13}C\{^{1}H\}$ NMR Characterization						
Tetrad intensities (%)				**Hexad intensities(%)**		
iii,iis,sii, sis,ssi	**isi**	**sss**	**iss**	**iiiii, iiiis, siiii, siiis**	**iiisi, isiii, sisii, iisis, iisii,sisis**	**Isisi**
Predominantly isotactic						
75	25	0	0	37.5	50	12.5
Disyndiotactic						
50	50	0	0	12.5	18.75	3.12
Atactic						
50	12.5	12.5	12.5	0	50	50

Hence, based on this spectrum in Figure 3.19, it can be concluded that carbonyl and methine carbon atoms are the most stereosensitive groups leading to hexad and tetrad sequences respectively. The assignments of the different signals are in agreement with literature results.[28] Thus, close inspection of the $^{13}C\{^{1}H\}$ NMR spectra in the methine region of the PLA synthesized by complexes **10** and **13** revealed that when carried out in toluene, these two initiators of **L6** afforded predominantly isotactic PLAs (Figure 3.20a & c). For both PLAs, the methine peaks integrate to approximately 25:75% corresponding to isi:(iii,iis,sii,sis,ssi)%; this is supported by the hexad intensities that corresponds to the predominantly isotactic PLA. Moreover, the carbonyl peaks, corresponding to the hexad pattern, are shown in Figure 3.20b and Figure 3.20d.

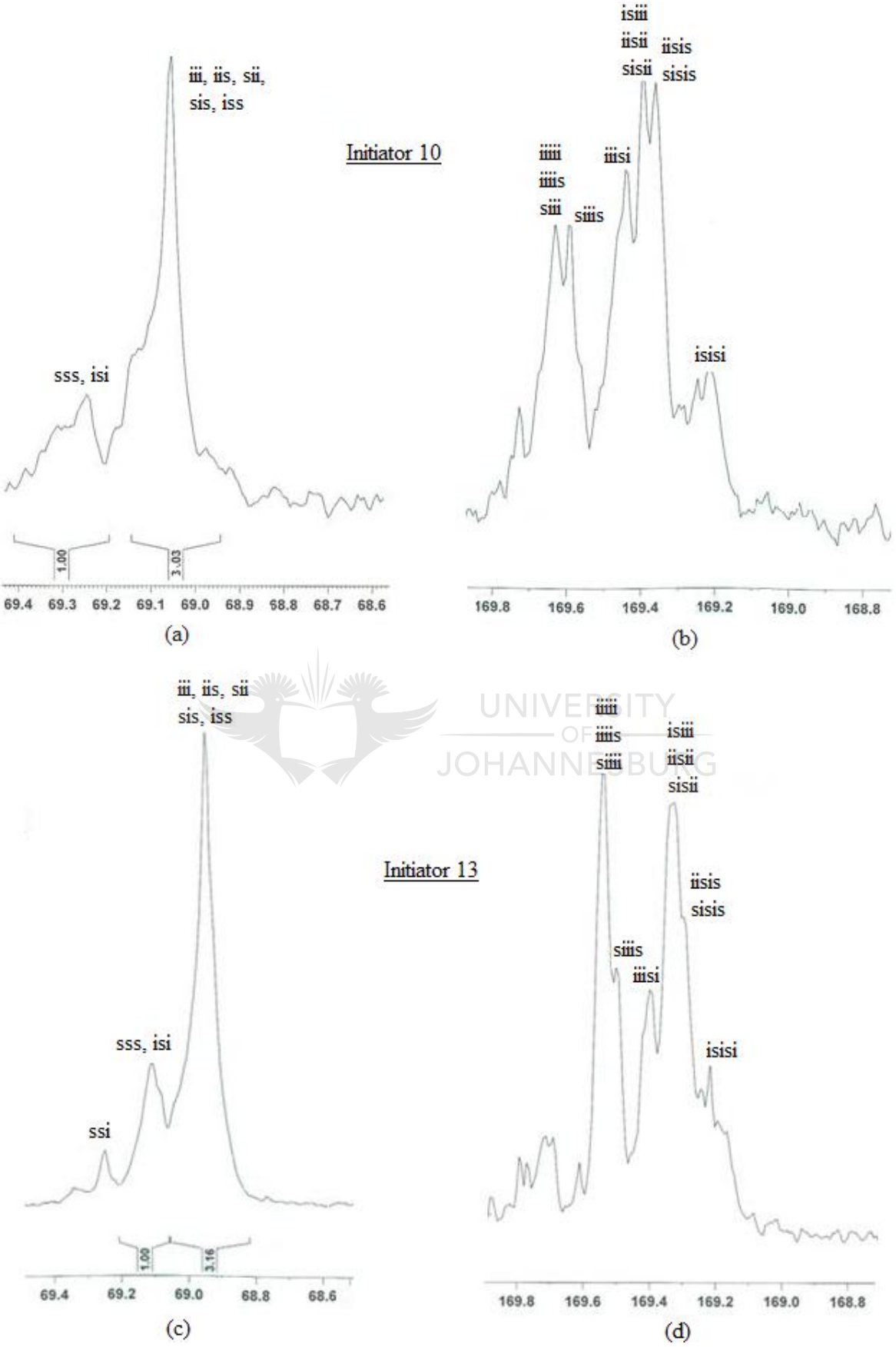

Figure 3.20. Expanded regions of methine and carbonyl carbon atoms in $^{13}C\{^{1}H\}$ NMR spectra

of two different PLA samples.

Furthermore, in order to study the effect of the alcohol additive on the microstructure of the PLA formed, the polymer formed using initiator system **13** was analyzed. Thus, Figure 3.21a shows the methine expansion for PLA prepared in toluene as the only solvent. Figure 3.21b gives the same signal for the PLA synthesized in toluene with the addition of methanol in the reaction mixture. A loss of stereocontrol is obvious from the $^{13}C\{^{1}H\}$ NMR spectra of the polymers, such that the PLA obtained is no longer isotactic.

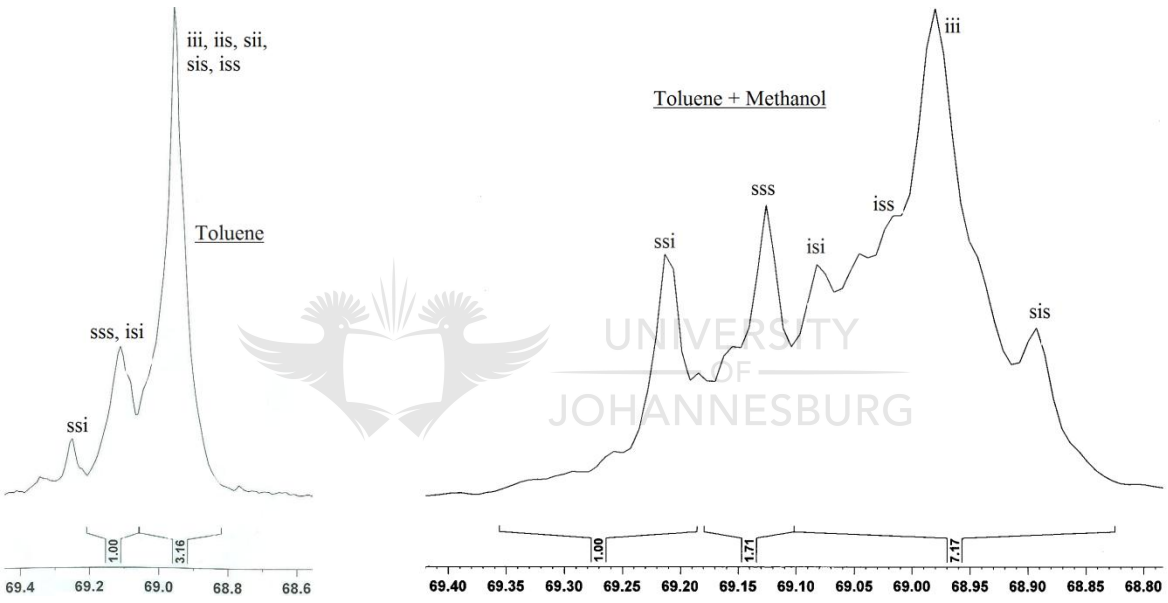

(a) (b)

Figure 3.21. Expansion of signals in methane region for PLA prepared by **13** in two different solvent mixtures.

3.9 Conclusion

All the initiators have shown activity towards the ROP of both ε-CL and D,L-lactide. Results show that the performance of the initiators was dependent on the metal centre, the N donor ligand, as well as the substituents on the phenyl ring of the benzoate. This confirms the influence of the initiator structure, and hence the ancillary ligand, on the ability of the cyclic

ester to ring-open. Depending on the monomer being polymerized the performance of the initiator changes. For instance, ε-CL polymerization occurs at a higher rate when zinc complexes are used as initiators compared to copper complexes. In contrast, copper complexes show higher activities than their zinc analogues towards lactide polymerization. The effect of the structure of the initiator on polymerization was also found to depend on the monomer being used. But, in both cases, there is a marked difference in the activities of the monometallic, bimetallic and polymeric initiators. Moreover, the presence of a linker on the pyrazolyl ligand was shown to influence the performance of the initiator, such that complexes of **L6**, which has a benzyl ring in the linker, shows better activities than their **L4** analogues, which has a methyl linker. Also, substituents on the pyrazole ring have an influence on the effectiveness of the initiator in terms of the rate of polymerization, the molecular weight and stereocontrol of the polymers formed. Molecular weight and PDI of the polymers were determined by SEC and MALDI-TOF MS, showing that different initiator systems gave different molecular weight and polydispersity of polymers. Evidence for the occurrence of inter- and intramolecular ester exchange using $^{13}C\{^{1}H\}$ NMR, SEC and MALDI-TOF MS was found.

SUMMARY

A series of pyrazole and pyrazolyl compounds (**L2**-**L6**) have been successfully synthesized following literature procedures for **L2**, **L4**-**L6**. Compound **L3** was made using a new method that is greener and requires a shorter period of time as compared to the conventional method. Zinc(II) and copper(II) benzoates of these compounds were then synthesized. The benzoic acids used had different substituents on the aromatic ring, which were found to affect the final product of the reaction. Analytical characterization techniques helped in determining whether the expected products were formed. The techniques used were NMR (^{1}H and ^{13}C{^{1}H}), IR, elemental analysis and mass spectrometry in some cases.

For further confirmation of the structures of the products made, the crystal structures of some of the compounds formed were determined. The X-ray structures of the complexes showed that monometallic, bimetallic as well as polymeric structures were obtained, with the geometries at the metal centre varying between tetrahedral and octahedral. In the case of compounds **6**, there are two different zinc(II) centres in the structure: tetrahedral and square pyramidal. It was also observed that for two complexes, **11** and **23**, the structure deduced from the analytical characterization techniques did not correspond to the X-ray structures. A possible explanation might be the use of the kinetically more stable product for the analytical analyses whereas for the crystal structure determination, the thermodynamically stable products have been used. Most of the complexes formed involved the coordination of both the benzoate and the pyrazolyl compounds to the metal, except for **22** and**18**, where it was found that the N donor ligand did not coordinate to the copper(II). This might be due to the bulky structure of the N donor compound (**L2** and **L5**) due to the phenyl substituents on the pyrazole rings. Yet, when compared to the reaction of zinc(II) acetate towards **L2**, the

expected products were formed. So, a possible explanation for the inability of forming copper(II) complex of **L2** might be the lower acidity of the copper(II) centre as compared to the zinc(II) centre. But overall, the synthesis of a series of clean pyrazolyl benzoates of zinc(II) and copper(II) was successful.

When these complexes were used to initiate the ring opening polymerization of ε-caprolactone and D,L-lactide, all the compounds were found to be able to initiate the polymerization process. The activities of the complexes varied from one to the other depending on the metal, the substituents on the benzoate ring, the substituents on the pyrazoles as well as the presence or absence of a linker on the pyrazolyl ligands. For ε-caprolactone polymerization, the best initiator among the pyrazoles having a linker was **12** of formula [Zn(3,5-NO_2-$C_6H_3COO)_2$**L6**], in a solvent-free medium at 110 ^oC and using [M]/[I] ratio of 50:1. For this ligand system, the zinc complexes were more active towards ε-caprolactone polymerization. For the ligand system that does not have a linker, the compound that initiated polymerization the fastest was **15** of formula [Cu(3,5-NO_2-$C_6H_3COO)_2$(**L1**)$_2$]. A similarity between these two best performing initiators is the presence of the dinitrobenzoate in the structure, which irrespective of the metal or the ancillary ligand, tends to make the compound a better initiator. Increasing the [M]/[I] ratio to 1 500:1 or even 3 333:1, slowed down the polymerization rate, yet not much difference has been found between these two ratios.

On the other hand, the polymerization of D,L-lactide was fastest when the copper complex **25** of formula [Cu(4-OH-$C_6H_4COO)_2$**L6**]$_2$ (of the linker system) was employed as initiator using [M]/[I] = 100:1, at 110 ^oC in toluene. Complex **14**, [Cu($C_6H_5COO)_2$(**L1**)$_2$], showed the best performance in the no linker initiator system. Copper(II) initiators appear to be better

performing than their zinc(II) analogues in the polymerization of D,L-lactide. This polymerization was also repeated in the presence of methanol, which has been found to speed up the rate of the reaction. When methanol was used as additive for the initiator system with a linker, an unexpected slowing down of the polymerization rate was observed, whereas for initiators without any linker on the ancillary ligand, the addition of methanol increased the rate of polymerization.

The polymers were characterized using techniques such as NMR, SEC and MALDI-TOF MS in order to determine the molecular weights of the polymers formed as well as the tacticity of the PLA synthesized. From SEC, it was observed that moderate M_n (858-4 757 Da for PCL and 602-3 185 Da for PLA) and PDI values (1.36-2.16 for PCL and 1.42-2.35 for PLA) were obtained as compared to literature values. MALDI-TOF MS showed that different types of polymer end groups were formed, varying from cyclic to hydrolyzed chain ends. From the $^{13}C\{^1H\}$ NMR analysis, stereochemistry of the PLA formed was determined and from the spectra obtained, it was observed that the polymerization was controlled and predominantly isotactic PLA chains were obtained from D,L-lactide. From the thermal analysis of the PCL and PLA synthesized, PCL was found to melt at 60.1 ^oC and decomposes at 390 ^oC while PLA decomposes before melting and the decomposition begins at 60 ^oC.